University of Glasgow

Bathawab, Fatma Mirfat (2017) *Engineering surface mobility to direct stem cell fate.* PhD thesis.

https://theses.gla.ac.uk/8110/

Copyright and moral rights for this work are retained by the author

A copy can be downloaded for personal non-commercial research or study, without prior permission or charge

This work cannot be reproduced or quoted extensively from without first obtaining permission from the author

The content must not be changed in any way or sold commercially in any format or medium without the formal permission of the author

When referring to this work, full bibliographic details including the author, title, awarding institution and date of the thesis must be given

Enlighten: Theses
https://theses.gla.ac.uk/
research-enlighten@glasgow.ac.uk

University of Glasgow | School of Engineering

ENGINEERING SURFACE MOBILITY TO DIRECT STEM CELL FATE

Fatma Mirfat Bathawab

Thesis submitted to the School of Engineering at the University of Glasgow in fulfilment of the requirements for the Degree of Doctor of Philosophy

January 2017

Table of Contents

List of Figures 4
Acknowledgements 15
Authors Declaration 16
Publications 17
Conferences 17
Abbreviations 18
Abstract 20
Chapter 1 22
Introduction - History of Tissue Engineering 22
Mesenchymal stem cells: Their Properties and Therapeutic potential 23
MSCs and their 3D environment 26
Need for bone regeneration 27
Bone repair - A historical account 28
The ECM and biomaterial design 29
Biomimetic biomaterial design and protein adsorption 32
Polymer surface mobility 33
The interfacial protein layer 35
Fibronectin structure and function 37
Cell - material interface and cell fate 42
Mobility of the protein layer 43
Focal adhesions and the interfacial protein layer 43
Integrins 44
Design of Contemporary Biomaterials 46
Hypothesis, Objectives and Outline 46
Chapter 2 48
Introduction - Polymer Substrate Characterization 48
Materials and Methods 50
Preparation of polymer surfaces: 50
Water contact angle 51
AFM nanoindentation 52
Human fibronectin purification 52
Micro BCA (bicinchoninic acid assay) 54
AFM scanning (tapping mode) 54
Direct ELISA 55

Quantification of fibronectin availability....55
Analysing fibronectin stretching using the H5 fragment....56
Determining protein mobility....57
Data Analysis:....57
Results and Discussion....58
AFM stiffness: Elastic moduli (E')....59
Water contact angle....59
Fibronectin conformation....62
Quantification of adsorbed fibronectin by BCA....66
Fibronectin domains exposure by ELISAs for the RGD and Synergy sites....68
Fibronectin mobility....69
Conclusion....70
Chapter 3....72
Introduction - Effect of Polymer Chain Mobility on Cell Behaviour....72
Materials and Methods....74
Protein coating for cell culture....74
C2C12 cell culture....75
Cell morphology and fibronectin reorganization on polymer surfaces – L929 cells....75
Focal adhesion Immunofluorescence staining....76
Integrin staining....77
C2C12 differentiation in the presence and absence of blebbistatin....78
Fixation and immunostaining of differentiated C2C12....79
Results and Discussion....79
Cell morphology and cell - mediated fibronectin reorganization....80
Adhesion of C2C12 cells on fibronectin coated polymers....82
Integrin recruitment analysis....84
C2C12 myogenic differentiation....86
Conclusions....88
Chapter 4 – hMSCs for Osteogenic differentiation....89
Introduction....89
MSC isolation and use in tissue engineering....90
Cell signalling during bone formation....91
Role of surface physical properties in MSC differentiation....95
Conjugation of biomaterials with BMP-2 for research and therapeutics....97
Aims, hypotheses and outline....97

Materials and Methods 98
hMSC cell culture and osteogenic differentiation 98
Immunostaining of osteogenic markers osteocalcin and osteopontin 99
Mechanistic studies using inhibitors of Erk1/2, ROCK and myosin II 99
Preparation of samples with surface bound BMP-2 100
Growth factor binding site exposure on fibronectin coatings - direct ELISA 100
Density of bound BMP-2 on fibronectin coatings - sandwich ELISA 101
MSC differentiation in the presence of BMP – 2 stimulation 101
Analysis of the phosphorylation of Smad 1/5/8, Erk1/2 and Runx-2 using the In-Cell Western™ Assay 102
Calcium Assay 103
Results and Discussion 103
Behaviour of mesenchymal stem cells on biomaterials 103
Osteogenic differentiation of MSCs in the absence of differentiating stimuli 104
Surface analysis 109
Presentation of BMP-2 on fibronectin-coated surfaces enhances osteocalcin expression 112
Phosphorylation of Erk1/2, pSmad 1/5/8 and Runx-2 114
Conclusion 116
Chapter 5 – Discussion 119
Future Research Avenues 125
Appendix A 126
Table: Immunostaining reagents used in this work. 126
Appendix B 127
Integrin Ratio Analysis Matlab code 127
Main Function 127
Data file (excel) generator function 130
References 132

List of Figures

Figure 1: Timeline showing the discoveries leading to the current understanding of the non-hematopoietic stem cells (MSCs) and their regulatory role on hematopoietic stem cells. Illustrating the work of early 19th and 20th century scientists who discovered the bone marrow origin of regenerative cells found at wound sites (Cohnheim, 1867)) and helped form the understanding that there exists a population of bone marrow stem cells distinct from hematopoietic stem cells which may contribute to their regulation. Initially bone marrow MSCs were described as colony-forming unit-fibroblasts (CFU-F) due to their tendency to form colonies of fibroblast-like cells which were then shown to possess self-renewal capabilities and multipotency (Friedenstein et al., 1970), Till and McCulloch (Becker, 1963). Characterization of the CFU-Fs was carried out by Castro-Malaspna (Castro-Malaspina, 1980). These breakthroughs were followed by further characterization of MSCs, establishment of their culture in vitro and deeper understanding of their role in the hematopoietic stem cell niche. Figure adapted from Kfoury and Scadden (2015) (Kfoury and Scadden, 2015).....24

Figure 2: The mesengenic process. This schematic illustrates the capability of self - renewal and multipotency behind the rejuvenation and repair of mesenchymal tissues. Adult stem cells have the ability to differentiate into osteocytes/ bone cells, cartilage, muscle, marrow stromal cells, tendon/ligament cells and other connective tissue cells via sequential lineage transitions. (The information in this figure is reviewed in (Caplan, 1991; Wei et al., 2013)..25

Figure 3 - Schematic of a cell interacting with ECM components. Cells secrete components of the extracellular matrix which they then assemble into fibrils. Most of the secreted structural proteins, proteoglycans and glycoproteins for example fibronectin, contain structural motifs which once exposed can be bound by integrins. Integrins are transmembrane

receptors of cells, they go on to form adhesions which may mature and contribute to signalling processes (58).....31

Figure 4 Glass transition temperature, polymer mobility and poly(alkyl acrylates) polymer systems of interest to this study. (A) Changes in polymer volume and thus mobility with increasing temperature, showing the effect of glass transition temperature. (B) Graph highlighting the difference between the specific Tg of a polymer and the cell culture working temperature of 37°C; a gap which in polymers with low Tg will be larger than in polymers with high Tg, thus representing higher mobility of that polymer at that temperature. (C) Glass transition temperatures of the 4 poly(alkyl acrylates) used in this study, showing the difference between them and 37°C. (D) Schematic of how polymer side chain length affects polymer chain mobility by increasing free volume (white area). 34

Figure 5: Schematic of how polymer side chain length affects polymer chain mobility by increasing free volume (white area) and the resulting conformation of adsorbed fibronectin. 1C-6C represent the number of carbons in the side chains. 2C - 6C induce fibrillogenesis of adsorbed fibronectin. Apart from their underlying difference in polymer surface mobility, the fibronectin fibrils on 2C-6C were observed to be very similar in conformation as shown by the images in the bottom panels (AFM). 37

Figure 6 - Fibronectin dimer. Schematic showing two fibronectin molecules linked with a disulphide bond at the C-termini, illustrating its modular (bead on a string) structure (86). The binding sites for integrin heterodimers αvβ3 and α5β1 are located within the 9th and 10th fibronectin type 3 repeats.....38

Figure 7 – The 9th and 10th FNIII repeats. Showing the distance at (A) 32Å when unstretched, extending to (B) 52Å upon mechanical stretching. This change due to mechanical forces has been implicated in differential integrin recruitment, and has been termed the “integrin switch”. The figure is adapted from Krammer et al., (2002).....39

Figure 8 - Schematic of fibronectin conformation on polymers. Left, Globular fibronectin on C = 1 and Right, a more open conformation which is believed to expose sites of biological interest on C = 2, C = 4 and C = 6. 42
Figure 9 – Polymer surface preparation. (1 and 2) the polymer solution is spin coated on glass coverslips, after solvent removal by vacuum drying, the surfaces were incubated with a fibronectin solution. If required, surfaces were then incubated with a BMP-2 solution. 51
Figure 10 – Stiffness measurements by AFM nanoindentation. (A) Sketch showing AFM tip deforming a polymer surface, (B) Example force curve showing the initial 50 nm indentation (δ) on which the Hertz model was applied to calculate the Young's moduli. (C) Graph of Young's moduli of polymer films, each point representing an average derived from individual measurements (n = 64) carried out on each surface. There were no statistical differences in young's moduli of the polymer films. The large variation in the measurements on C = 6 were attributed to the highly adhesive nature of this polymer. 59
Figure 11 - Polymer surface wettability. Hysteresis was calculated from dynamic measurements on the polymer surfaces before and after coating with a 20 μg/ml fibronectin solution. (A) Static water contact angle schematic. (B) Static water contact angles for polymers. (C) And (D) Advancing and receding contact angle schematics respectively. (E) Dynamic contact angles and hysteresis on bare polymers and polymers coated with either fibronectin or labelled fibronectin. Bars indicating standard deviations are overlapped when too small. Each point is an average of readings from 9 measurements. 61
Figure 12 - Atomic force microscopy scans of adsorbed fibronectin. Fibronectin conformation on polymer surfaces shown by AFM scans (AC mode/ Tapping mode used to probe the topography) after adsorption from a fibronectin solution of 20 μg/ml concentration. Fbronectin undergoes fibrillogenesis forming nanofibrils on PEA (C = 2), PBA (C = 4) and PHA (C = 6). The top and bottom 1 μm by 1 μm images show the similarities between the

distribution of unlabeled and labelled fibronectin (fibronectin-FITC) on the polymers. Values shown underneath the images of nanofibrils relate to the fractal dimension; a descriptor of pattern complexity which here is used to represent connectivity. The FN-FITC scans in (B) were performed in collaboration with Mark Bennet as part of his Masters project (Bathawab et al., 2015). Images are representative of three taken from each triplicate. 62

Figure 13 - AFM AC mode scans. Left to right: Scans of fibronectin on polymers with increasing number of carbons in the side chain. Top to bottom: AFM scans on the same polymer incubated with different initial fibronectin concentrations. Images are representative of three taken from each triplicate. 64

Figure 14 - fibronectin Immunofluorescence staining. A polyclonal antibody against fibronectin on the four polymer surfaces. fibronectin deposits can be seen on (A) C = 1 and fibronectin networks were observed on (B - D) C = 2, 4 and 6. Images are representative of three taken from each triplicate.....65

Figure 15 - Density of fibronectin adsorbed on the polymer surfaces. As quantified by the micro - bicinchoninic acid assay kit (BCA) by Thermo Scientific. Starting concentrations of incubation solutions are indicated on the x-axis. Each bar represents an average of 9 readings (3 from each triplicate). Standard deviations are indicated by black error bars. 66

Figure 16 – Fibronectin stretching. ELISA quantification of fibronectin stretching using an antibody fragment which preferentially binds stretched over non – stretched fibronectin (Cao et al., 2012). The highest signal was observed on C = 2. The absorbance readings were normalised with respect to fibronectin availability (See Figure 17 B). Each bar represents an average of 9 readings (3 from each triplicate). Standard deviations are indicated by black error bars. One way Anova analysis revealed statistically significant difference: *$p \leq 0.05$ (GraphPad software, La Jolla, CA).....67

Figure 17 - Indirect analysis of fibronectin conformation using ELISAs. Analyses of the exposure of specific fibronectin structural sites upon adsorption of fibronectin on polymers using 20 μg/ml. (A) A 3D model of 7^{th} – 10^{th} FNIII with Yellow arrows pointing to the binding sites for mAb1937 (Synergy) and HFN 7.1 (RGD). Image adapted from the RCSB PDB (www.rcsb.org) (Leahy et al., 1996) PDB ID 1FNF. (B) Overall availability of fibronectin using a polyclonal antibody. (C) Exposure of cell binding site; RGD using the HFN 7.1 antibody. (D) Synergy site exposure (mAb 1937Ab). Graphs C and D were normalised with respect to fibronectin availability (B). Each bar in the graphs represents an average of 9 readings (3 from each triplicate) and standard deviations are indicated by black error bars. One way Anova analysis revealed statistically significant differences: *$p \leq 0.05$, **$p \leq 0.01$, ***$p \leq 0.001$, and ****$p \leq 0.0001$ (GraphPad software, La Jolla, CA). 68

Figure 18 - Interfacial/Protein mobility. A measurement of the rate of change in fluorescence intensity profile indicating protein mobility. (A) Bleach border region, showing a manually area selected for analysis (dotted red box), the fluorescence intensity of the bleached area was compared to the unbleached area which was assumed to be 100% fluorescent. Images were taken every 24 hours for 120 hours. (B) The gradient of the linear region of the bleach border changed over time for each polymer surface. This experiment was carried out in collaboration with Mark Bennet as part of his Masters project (Bathawab et al., 2015). Each bar in the graphs represents an average of 9 readings (3 from each triplicate) and standard deviations are indicated by black error bars. One way Anova analysis revealed statistically significant differences: ****$p \leq 0.0001$ (GraphPad software, La Jolla, CA).....70

Figure 19 – Cell anchorage and signalling via integrins. Focal adhesions are dynamic complexes made up of several cytosolic proteins including talin, Src family kinases (SFK) and vinculin which interact directly or indirectly with integrins. Integrin heads have been shown to protrude from the plasma membrane by approximately 20 nm (Nermut 1988) and to

anchor cells by interacting with structural peptide sequences within ECM proteins such as fibronectin. Activated integrins may also cluster to produce amplified signalling and it has been shown that integrin interaction with fibronectin fibrils stimulate cytoskeletal contractility through a Rho-dependent mechanism (Hocking et al., 2000). Integrin signalling is reviewed in (Harburger and Calderwood 2009).....73

Figure 20: Focal adhesion analysis steps. Major axis lengths of the focal adhesions were analysed by first generating a binary image (B) from (A) the vinculin stain (Red). (C) A histogram of this data was then plotted, showing a major axis length profile. The actin staining (Green, image A) was used as a mask within which vinculin staining was analysed. 77

Figure 21: Characteristic cell morphology on the four polymer surfaces. (A) Cell area, (B) cell perimeter and (C) aspect ratio. This demonstrates that L929 cells have no significant morphological differences on each surface. This experiment was carried out in collaboration with Mark Bennet as part of his Masters project (Bathawab et al., 2015). Each bar in the graphs represents values derived from 9 images (3 from each triplicate), the standard deviations are indicated by black error bars. 80

Figure 22 - Cell – mediated reorganisation of fibronectin-FITC on a glass control and four polymers of interest. (A) Cell area (Top panel) and corresponding fibronectin layer (Bottom panel). Scale bar; 25 µm), (B) Relative differences in fluorescence within the area of the cell (Actin mask) compared to outside the cell. This experiment was carried out in collaboration with Mark Bennet as part of his Masters project (Bathawab et al., 2015). Each bar in the graph represents values derived from 9 images (3 from each triplicate), the standard deviations are indicated by black error bars. One way Anova analysis revealed statistically significant differences: *$p \leq 0.05$ and ****$p \leq 0.0001$ (GraphPad software, La Jolla, CA)...81

Figure 23 – Adhesion analyses of C2C12 cells (3 hours). (A) Immunostaining, top panel: vinculin (Red), actin (Green) and Dapi (Blue) and bottom panel: inverted focal adhesion images. (B) Distributions of focal adhesion major axis lengths with their corresponding frequency, finally (C) normalised focal adhesions (in percentage) in relation to major axis length categories. (Bathawab et al., 2015). Each bar in the graph represents values derived from 9 images (3 from each triplicate), the standard deviations are indicated by black error bars. Focal contacts (major axis < 1μm) were filtered out. One way Anova analysis revealed statistically significant differences: *p ≤ 0.05, **p ≤ 0.01 (GraphPad software, La Jolla, CA). 83

Figure 24 – Integrin recruitment analysis in human foreskin fibroblasts cultured for 3 hours on fibronectin-coated polymers. As example, images of the analysis on PEA are shown here, where a Matlab programme was used to calculate the ratio between the size of staining for (A) β_1 and β_3 integrin subunits within a paxillin stain which was used as a mask for focal adhesions. (B) A heat map of the ratios and (C) A graph of the intensity ratios. Each bar in the graphs represents an average of 9 readings (3 from each triplicate) and standard deviations are indicated by black error bars. 85

Figure 25 – C2C12 myogenic differentiation. In (C – Top panel) absence and (C – bottom panel) presence of the myosin II inhibitor; Blebbistatin. Myogenic differentiation as quantified by myosin II staining (RED) shows high differentiation on C = 2 and C = 4, however, in the presence of Blebbistatin this increase is abolished on C = 4 and maintained on C = 2. Therefore, suggesting that myogenic differentiation on mobile polymers is contractility dependent. Each bar in the graph represents values derived from 9 images (3 from each triplicate), the standard deviations are indicated by black error bars. One way Anova analysis revealed statistically significant differences: *p ≤ 0.05, **p ≤ 0.01, ***p ≤ 0.001, and ****p ≤ 0.0001 (GraphPad software, La Jolla, CA). 86

Figure 26 – The classical process of tissue engineering (grafts). Where MSCs are harvested from the body (autologous cells are preferred), cultured and proliferated in vitro then placed onto biomaterials with inductive features for the differentiation of hMSCs to the desired cell type. The setup is then implanted into the patient's injury site to start the regenerative process. Figure sourced with permission (Oseni et al., 2011). 90

Figure 27 – The TGF-β pathway. Canonical and non-canonical signalling pathways for osteogenic differentiation. Showing the BMP-2 growth factor presented on the fibronectin growth factor binding site. In the canonical TGF-β/BMP signalling, receptor regulated smads are phosphorylated by activated receptors, they then form a complex with smad4 (a co-smad). This complex is translocated to the nucleus where it induces the expression and phosphorylation of Runx-2. Runx-2 binds a promoter region in several osteoblast specific genes, thus regulating the expression of alkaline phosphatase, osteopontin and osteocalcin. The canonical and non - canonical pathways converge in the nucleus both resulting in increased Runx-2 expression with Erk1/2 activation (non - canonical) enhancing Runx-2 stabilization and transcriptional activity. The adhesion signal from integrin receptors also activates Erk. 92

Figure 28- Agonist and antagonist of the BMP receptor. Upon BMP-2 binding the type I and type II BMP receptors dimerise. The growth factor BMP-2 activates the canonical and non-canonical TGF-β pathways. Noggin is able to bind the BMP-2 receptor binding site, therefore effectively blocking BMP-2 activation. 94

Figure 29 – Schematic showing pathways activated by Physical cues. Such as stiffness and topography, affecting differentiation of hMSCs. Inhibitors used in this work to study these pathways are highlighted in purple boxes. RhoA signalling in implicated in Actomyosin contractility via ROCK and myosin light - chain kinase and the activation of Erk1/2. This

figure illustrates how mechanical cues can induce Runx-2 expression and phosphorylation via ROCK and Erk1/2 signalling. 96

Figure 30 – Osteocalcin expression on the polymer surfaces in the absence of differentiating stimuli. (A) Images showing fluorescently labelled OCN and OPN in a 21-day culture on fibronectin coated polymers, (B) Schematic showing the relationship between polymer mobility, Tg, free volume and the fibronectin conformation formed and (C) Graph of quantification of OCN and OPN nodule sizes. Each bar in the graphs represents results from 9 images (3 from each triplicate) and standard deviations are indicated by black error bars. One way Anova analysis revealed statistically significant differences: *$p \leq 0.05$ and **$p \leq 0.01$ (GraphPad software, La Jolla, CA). 105

Figure 31 – Calcium deposition by hMSCs cultured without differentiating stimuli. Graph showing the quantification of the deposited calcium as measured by the O-cresolphthalein complexone method. Calcium ions were found to be higher on C = 2 compared with the rest of the polymers. The optical density was read at 577 nm and values were normalised with respect to the cell growth area (1.13 cm^2). Each cluster in the graph represents an average of 9 readings (3 from each triplicate) and standard deviations are indicated by black error bars. One way Anova analysis revealed statistically significant differences: ***$p \leq 0.001$ (GraphPad software, La Jolla, CA). 106

Figure 32 – Mechanistic study to deduce pathways involved in the increased osteogenic differentiation observed for C = 2. (A) A flow diagram of how mechanical signals are transduced through contractility (Arnsdorf et al., 2009) or Erk1/2 (Kanno et al., 2007) to lead to increased osteogenic differentiation. (B) Inhibition of Erk1/2 resulting in the disappearance of the increase previously observed in osteocalcin expression on C = 2, (C) and (D) show graphs of OCN quantification for samples cultured in the presence of the inhibitors of ROCK and Myosin II respectively, both of which do not inhibit the increase in osteocalcin levels on

C = 2. Each cluster in the graphs represents results from analysis of images from each sample triplicate and standard deviations are indicated by black error bars. One way Anova analysis revealed statistically significant differences: *p ≤ 0.05 and **p ≤ 0.01 (GraphPad software, La Jolla, CA).....107

Figure 33 – ELISA analyses for the exposure of the growth factor site on fibronectin also known as the heparin II domain. Fibronectin fibrils on polymers C = 2, C = 4 and C = 6 were bound by the specific antibody to higher levels than the globular fibronectin on C = 1. (A) A schematic of fibronectin bound at the growth factor site during the ELISA analysis of its exposure. (B) Plotted are the results of analysis of n = 6, standard deviations are indicated by black error bars. One way Anova analysis revealed statistically significant differences: *p ≤ 0.05, **p ≤ 0.01, ***p ≤ 0.001, and ****p ≤ 0.0001 (GraphPad software, La Jolla, CA). ..109

Figure 34 – Bound BMP-2 density. Sandwich ELISAs used to quantify bound BMP-2 on fibronectin – coated polymers incubated with 100 ng/ml solution of BMP-2. Schematics illustrate (A) a freely accessible growth factor binding site (Martino and Hubbell, 2010a) and (B) a growth factor binding site blocked with a specific antibody. (C) Graph comparing BMP-2 surface density on fibronectin-coated polymers with and without blocking the growth factor site. Plotted are the results of analysis of n = 6, standard deviations are indicated by black error bars. One way Anova analysis revealed statistically significant differences: *p ≤ 0.05 (GraphPad software, La Jolla, CA).....111

Figure 35 – Osteogenic differentiation of BMP-2 stimulated hMSCs. Representative images of MSCs cultured for 21 days using three different conditions (A) 1st row - BMP-2 in medium, 2nd row - BMP-2 bound onto fibronectin and 3rd row - fibronectin bound BMP-2 and the presence of soluble Noggin. The image in the 4th row is representative for the osteogenic control. (B) Quantification of the osteocalcin in the fluorescent images. Osteocalcin – Red, Actin – Green and Dapi – Blue. The graph shows the highest osteocalcin expression on the C

= 2 polymer with surface - bound BMP-2 in contrast with when BMP-2 is added in the medium, there is also a marked decrease in osteocalcin expression upon BMP-2 inhibition with noggin. Plotted are the results of analysis of ~17 images from triplicate samples, standard deviations are indicated by black error bars. One way Anova analysis revealed statistically significant differences: **p ≤ 0.01 and ***p ≤ 0.001 (GraphPad software, La Jolla, CA). 113

Figure 36 – Quantification of phosphorylation of Erk1/2, Smad1/5/8 and Runx2 in cells adhered to BMP-2 bound to fibronectin coated surfaces. InCell Western analysis of phosphorylated; smad1/5/8 and Erk1/2 and the osteogenic transcription factor Runx2 in hMSCs immediately post adhesion. No significant differences were observed for Erk1/2 phosphorylation, while smad1/5/8 phosphorylation was significantly higher on C = 2. hMSCs on C = 2 samples also exhibited significantly higher Runx2 phosphorylation compared with those on C = 6 samples. Quantification of each phosphorylated protein was normalised with the total protein. Plotted are results from 6 reading (3 from duplicate samples), the standard deviations are indicated by black error bars. One way Anova analysis revealed statistically significant differences: *p ≤ 0.1 and ***p ≤ 0.001 (GraphPad software, La Jolla, CA). 115

Acknowledgements

Firstly, alhamdulilah, I have come a long way and I thank God for giving me all that I need in my personal and professional life to become the person that I am. My deepest appreciation is to my husband Nawaf Al Maery, my elder brother Hayder Bathawab and my sister Wafaa Bathawab without whom I could not have completed my PhD. I would also like to express my deepest appreciation to my parents, my younger brother Muhammad and my unborn child from whom I derived strength, determination and reassurance. I also thank my husband's family especially his mother who always supported and motivated me and made sure I never went without good food.

I would like to express my deepest appreciation for my supervisors Professor Manuel Salmeron - Sanchez, Professor Matthew J Dalby and Dr Marco Cantini who provided me with their unwavering support, guidance and encouragement throughout my project. And Matt's advice and guidance since my final year of my undergraduate degree.

I would also like to express my sincere thanks to my colleagues from the Microenvironments for Medicine group for being such great company, for their help and support and for maintaining one of the most organised laboratories I have come across.

I also want to thank my close relatives and friends, who received many excuses from me for not being able to attend their functions. Furthermore, I thank my colleagues and instructors from the DTC for being there right from the start and everyone at the Centre of Cell Engineering, MVLS. I also thank everyone at the School of Engineering for their help and for the opportunities they have put in place for graduate students.

Authors Declaration

"I declare that, except where explicit reference is made to the contribution of others, this thesis is the result of my own work and has not been submitted for any other degree at the University of Glasgow or any other institution"

Fatma Mirfat Bathawab

Publications

- Bathawab F, Bennett M, Cantini M, Reboud J, Dalby M, Salmerón-Sánchez M. Lateral Chain Length in Polyalkyl Acrylates Determines the Mobility of Fibronectin at the Cell/Material Interface. Langmuir. 2016 (32):800-9.
- **In preparation**: Bathawab F, Bennett M, Cantini M, Dalby M, Salmerón-Sánchez M. Mobility of ECM proteins to enhance growth factor potency. Target journal; Biomaterials.

Conferences

- Bathawab F, Cantini M, Dalby M, Salmerón-Sánchez M. Mobility of ECM proteins to enhance growth factor potency. Poster presentation at the British Orthopaedic Research Society (BORS) Conference, Glasgow, UK. September, 2016.
- Bathawab F, Cantini M, Dalby M, Salmerón-Sánchez. Engineering surface mobility to direct stem cell fate. Podium presentation at the Tissue Engineering and Regenerative Medicine (TERMIS) conference, EU Chapter. June - July, 2016 Sweden.
- Bathawab F, Cantini M, Dalby M, Salmerón-Sánchez. The effect of polymer surface mobility on cell behaviour. Podium presentation at the Glasgow Orthopaedic Research Initiative (GLORI) Conference. November, 2015 Glasgow

Abbreviations

wt. %: weight-weight percentage.

w/v %: mass/volume percent.

ELISA: enzyme-linked immunosorbent assay.

ICW: In-Cell Western.

ECM: extracellular matrix.

FRAP: fluorescence recovery after photobleaching.

DPBS: Dulbecco's phosphate buffer saline.

DPBS++: with 0.5mM magnesium and 1mM calcium ions.

DPBS--: without magnesium and calcium ions.

MSC: mesenchymal stem cells.

RGD: arginine glycine aspartic acid amino acid motif.

PHSRN: proline histidine serine asparagine motif.

HFN 7.1: anti-Fibronectin antibody specific for the cell attachment site.

Rho A: Ras homolog gene family, member A.

ROCK: Rho-associated protein kinase, acts downstream of Rho A.

BMP: bone morphogenetic protein.

BCA: the bicinchoninic acid assay used for determining total protein concentration.

MEK: mitogen-activated protein kinase kinase, phosphorylates Erk/MAPK proteins.

Erk: extracellular signal–regulated kinase also known as MAPK.

Smad: protein homologs of both the drosophila protein, mothers against decapentaplegic (MAD) and the C. elegans protein SMA.

TGF-β: transforming growth factor beta 1, a polypeptide member of the transforming growth factor beta superfamily of cytokines.

CD markers: cluster of differentiation markers are cell surface protein markers. Stem cells are characterised by expression of CD105, CD73 and CD90, and lack expression of CD45, CD34, CD14 or CD11b, CD79alpha or CD19 and HLA-DR surface molecules.

CD73: 5'-nucleotidase.

CD90: a cell surface glycoprotein originally identified on mouse thymocytes.

CD34: a highly glycosylated and phosphorylated single – pass membrane protein, thought to play a role in the attachment of stem cells to the bone marrow extracellular matrix or to stromal cells.

CD14: monocyte differentiation antigen.

CD11b: a member of the integrin family which pairs with CD18, it is expressed in ~44% of bone marrow cells.

CD79alpha: a subunit of an intracytoplasmic protein also known as immunoglobulin-associated alpha.

CD19: a protein which assembles with the antigen receptor of B-lymphocytes in order to decrease the threshold for antigen receptor-dependent stimulation.

HLA-DR: human leukocyte antigen - antigen D Related, an MHC class II cell surface receptor.

CD44: a cell-surface glycoprotein involved in cell–cell interactions.

CD105: Endoglin.

CD31: platelet endothelial cell adhesion molecule (PECAM-1).

CD45: lymphocyte common antigen is a receptor-linked protein tyrosine phosphatase.

OCN: osteocalcin.

OPN: osteopontin

Abstract

Since the first contact and fusion of an egg and sperm and throughout development, a cell lives a life of constant communication with its environment. Cells interact with the external environment via a layer of proteins and respond to not only biochemical cues but also physical properties including stiffness and topography of adjacent surfaces. However, even though polymeric biomaterials have been described as one of the cornerstones of tissue engineering, the effect of an intrinsic polymer property known as mobility on cell behaviour is poorly characterised. Mobility is a physical property of polymers inversely proportional to the glass transition temperature (Tg); the temperature at which polymers undergo a transition between a rubbery viscous state to a glassy brittle solid. Therefore, films of four poly(alkyl acrylates) with similar surface chemistry but different glass transition temperatures achieved by varying branch chain lengths (1, 2, 4 or 6 methyl groups) were used in this work to investigate the role of polymer mobility on cell behaviour. I verified using atomic force microscopy the similarity in topography and stiffness between the four substrate surfaces and ascertained that fibronectin molecules adsorb in a globular conformation on the polymer with the shortest side chain (1 methyl group) compared with a more extended conformation on the rest of the polymers. My study of the fibronectin coatings using fluorescence recovery after photobleaching (FRAP) on the different polymer surfaces suggested that the mobility of the polymer substrate is translated to the interfacial protein layer. This interesting finding highlighted a possible pathway for cells cultured on fibronectin coated polymer surfaces to detect the underlying polymer mobility via the fibronectin coating. The interaction of cells with surfaces occurs via membrane proteins which interact with specific structural sites within extracellular matrix proteins; these include the cell binding site (RGD: Arginine Glycine Aspartic acid amino acid motif) and the Synergy site (PHSRN: Proline Histidine Serine Asparagine amino acid motif). My ELISA analyses indicated a higher exposure of these important cell-binding sites on the more extended fibronectin compared with the globular one however, this did not correlate to the mobility of polymers or the mobility of the fibronectin layer. This was also the case for myogenic cell differentiation, which was indiscriminately higher on polymers with extended fibronectin, however, cytoskeletal contractility was found to play an essential role in the myogenic differentiation of cells on these polymers in a mobility dependent manner. We then sought to understand the role of

mobility in modulating osteogenic differentiation of human MSCs in the presence and absence of stimulation with BMP-2. The Fibronectin network-forming polymer with the lowest mobility (side chain of 2 methyl groups) induced the highest expression of osteogenic markers in the absence of BMP-2 stimulation. My mechanistic studies using specific inhibitors also revealed that the Erk1/2 pathway was required for this increase in osteogenic markers, while contractility, unlike in myogenesis produced only minimal effects on osteogenic differentiation. In this set of polymers, mobility increases with side chain length, while all the polymers with more than one methyl group in their side chain induced the independent formation fibronectin networks upon adsorption. The polymer with two methyl groups in its side chain is characterised with the lowest mobility among the three fibrillogenesis - inducing polymers, and the highest expression of osteogenic markers in the absence of BMP-2. In the presence of BMP-2, smad phosphorylation was also higher on this polymer suggesting a combined synergistic effect towards osteogenic differentiation provided by the simultaneous activation of the Erk1/2 pathway and high phosphorylation of smad1/5/8. My observations suggest that fibronectin fibrils coating a polymer with low mobility may be most suited for osteogenic differentiation of hMSCs by simultaneously exposing cell-binding sites to a higher degree. Thus, inducing Erk1/2 signalling and presenting BMP-2 in a manner that stimulates the highest phosphorylation of smad1/5/8 hence achieving a stronger synergistic effect on the overall expression of osteogenic markers. The findings from this work strongly support previous studies suggesting that polymer mobility is a subtle change in the substrate with significant downstream biological significance and is crucial to understand to improve the application of polymeric biomaterials.

Chapter 1

Introduction - History of Tissue Engineering

The discovery of a 5500-year-old artificial human tooth made of shell carving from Egypt was published in 2004 (Irish, 2004). The literature is full of other discoveries of artificial archaeological items designed to improve human dental health, as reviewed in (Abraham, 2014). Through experimentation, it has been realised over time that some materials are better than others at interacting and integrating with the human biology. Conventionally, it was thought that chemical and biological inertness translated to better biocompatibility, this approach has worked relatively well for the design of implantable devices. However, in the field of tissue engineering or where tissue integration is preferred (Nuss and von Rechenberg, 2008) and applications in biotechnology such as gene/ cell/ drug delivery, biomaterials must participate more intimately with the surrounding tissue (Williams, 2008).

Our pressing need for the use of artificial materials as prosthetics and for research is therefore now heavily dependent on my knowledge of the material - cell interaction. In addition, there is little doubt among researchers that a deeper understanding of the effects of surface properties of artificial materials on cells is required to aid research efforts to modulate cell behaviour.

The discovery of multipotency, which began with Cohnheim (Cohnheim, 1867) and Till and McCulloch (Becker, 1963), underlies the whole concept of tissue engineering. With multipotent cells, tissues could be grown and used in therapeutic and research applications, however, as it was later discovered these cells require intricate signals within a conducive environment for them to form largely uniform populations of the desired cell type (Montarras et al., 2005) and (Sacco et al., 2008).

As the origin of stem cells is directly associated with the processes that begin with fertilisation of the ovum by a sperm, knowledge gathered over years of research from embryology and developmental biology is ultimately crucial in tissue engineering and thus biomaterial design. Post fertilisation, totipotent embryonic stem cells (ESCs) divide, differentiate and undergo irreversible lineage commitment; forming a foetus with sparse multipotent (foetal) stem cells left within tissues for natural regenerative use throughout the life of the adult individual (adult stem cells) (Jiang et al., 2002).

Stem cells were first extracted from the bone marrow, however, they were soon identified in almost every tissue for example; muscle and adipose as reviewed in (da Silva et al., 2006).

Stem cells in the adult organism are also referred to as tissue - specific stem cells, these differentiate only to form cells characteristic of the tissue they reside in. For example, there are epidermal, epithelial and recently discovered bronchoalveolar stem cells. There are two major multipotent stem cell types in the bone marrow; the hematopoietic stem cells (HSCs) which form all the types of blood cells and the bone marrow stromal stem cells or MSCs which form all the types of cells of mesodermal origin. The mesenchymal tissues, which are also known generally as the soft/connective tissues, make up the bulk of the body of an organism. Consequently, MSC self-renewal capabilities and their ability to differentiate into different mesenchymal lineages *in vitro* (Gimble et al., 2008) have made them popular in the fields of tissue engineering, regenerative therapy and biomaterial research.

Mesenchymal stem cells: Their Properties and Therapeutic potential

The tendency of MSCs to migrate to a wound site led to their discovery in the early 1880s (Cohnheim, 1867). Cohnheim inserted an insoluble analine dye into the veins of animals; this led to the observation of not only dye-containing immune cells but also cells with a fibroblast-like morphology at a topical wound site. Cohnheim concluded that since these non-hematopoietic cells came from the blood stream, they must have originated in the bone marrow; therefore creating the hypothesis that the bone marrow is an important source of cells needed for natural wound repair.

Till and McCulloch who were working on the effects of radiation and bone marrow transplantation in mice, first observed the dual properties of stem cells; self-renewal and differentiation to multiple lineages (Becker, 1963) .

Figure 1 shows a timeline illustrating the discoveries, which led to my current understanding of bone marrow MSCs. Breakthroughs underlying current knowledge in bone tissue engineering, were first appreciated in experimental hematology, and bone marrow MSCs were discovered within the stroma which supports haematopoiesis.

The establishment of long term *in vitro* culture of bone marrow stem cells by Gartner and Kaplan (1980) (Gartner, 1980) has since enabled researchers to further explore the use of the self-renewing and multipotent cells in tissue engineering.

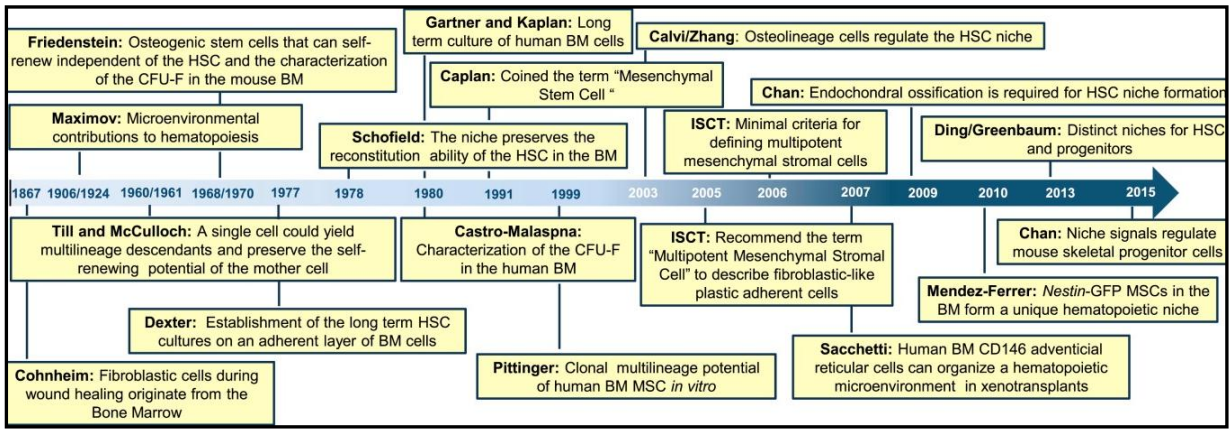

Figure 1: Timeline showing the discoveries leading to the current understanding of the non-hematopoietic stem cells (MSCs) and their regulatory role on hematopoietic stem cells. Illustrating the work of early 19th and 20th century scientists who discovered the bone marrow origin of regenerative cells found at wound sites (Cohnheim, 1867)) and helped form the understanding that there exists a population of bone marrow stem cells distinct from hematopoietic stem cells which may contribute to their regulation. Initially bone marrow MSCs were described as colony-forming unit-fibroblasts (CFU-F) due to their tendency to form colonies of fibroblast-like cells which were then shown to possess self-renewal capabilities and multipotency (Friedenstein et al., 1970), Till and McCulloch (Becker, 1963). Characterization of the CFU-Fs was carried out by Castro-Malaspna (Castro-Malaspina, 1980). These breakthroughs were followed by further characterization of MSCs, establishment of their culture *in vitro* and deeper understanding of their role in the hematopoietic stem cell niche. Figure adapted from Kfoury and Scadden (2015) (Kfoury and Scadden, 2015).

MSCs are multipotent cells; able to differentiate into multiple mesenchymal lineages (Pittenger, 1999) including adipocytes (McBeath et al., 2004a) (Fink and Zachar, 2011), chondrocytes (Solchaga 2011), osteoblasts (Dalby et al., 2007), myocytes (AC et al., 2009),

and ß-pancreatic islets cells (Milanesi 2012) as illustrated in Figure 2. Their multipotency and their ability to be cultured and differentiated *in vitro* (Gimble et al., 2008) make them a very attractive cell type for tissue engineering. These cells reside within several tissues including the bone marrow (Friedenstein et al., 1976),

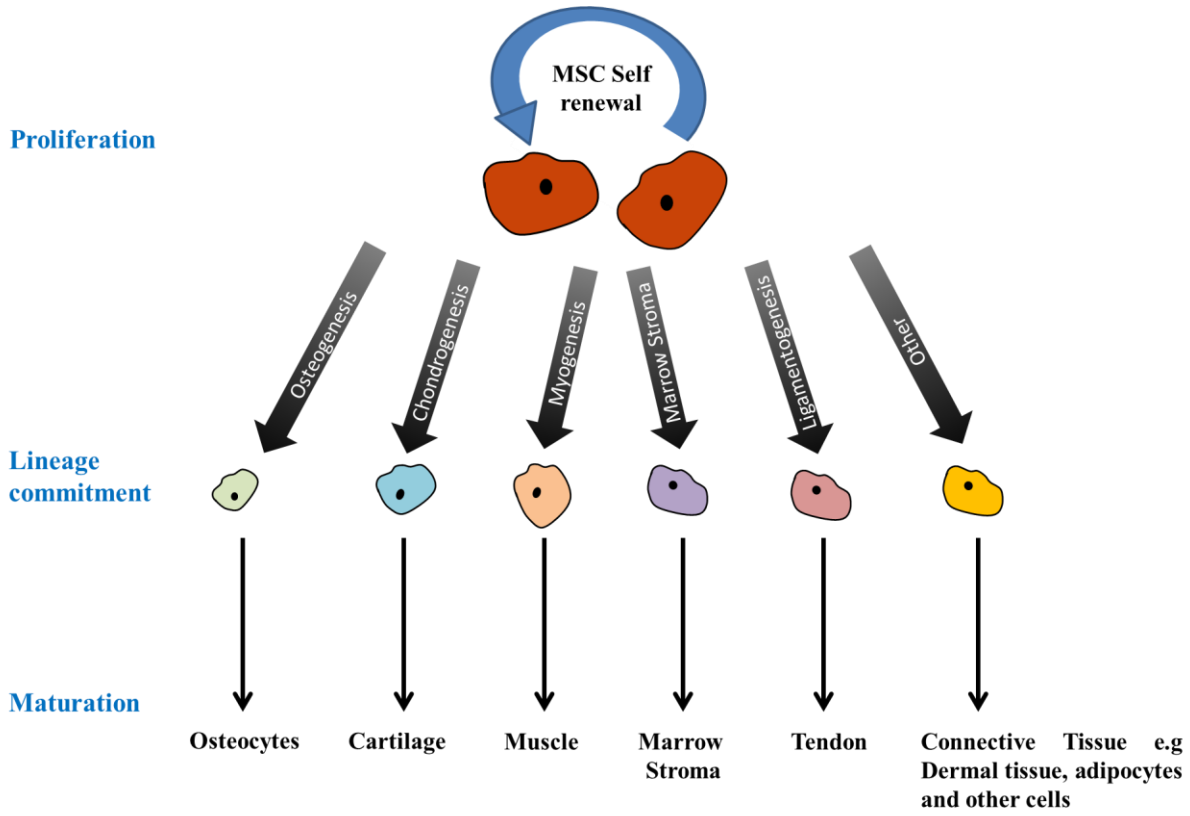

Figure 2: The mesengenic process. This schematic illustrates the capability of self - renewal and multipotency behind the rejuvenation and repair of mesenchymal tissues. Adult stem cells have the ability to differentiate into osteocytes/ bone cells, cartilage, muscle, marrow stromal cells, tendon/ligament cells and other connective tissue cells via sequential lineage transitions. (The information in this figure is reviewed in (Caplan, 1991; *Wei* et al., 2013).

periosteum (22) (23), muscle (24), adipose tissue and peripheral circulation (Hass et al., 2011). Bone marrow is still considered to be the most important source of stem cells (Caplan, 1991), due to ease of isolation compared with the isolation of MSCs found in other tissues for

example muscle. The most commonly used procedure for the isolation of MSCs from bone marrow is density gradient centrifugation (Juopperia et al., 2007) coupled with adherence to cell culture plastic.

MSCs and their 3D environment

More recent studies have indicated the reliance and contribution of MSCs to the bone marrow niche (Méndez-Ferrer et al., 2010) and their immunomodulatory abilities (Gao and Fu, 2016). A stem cell niche is defined as the cellular and molecular microenvironment which regulates stem cell function, including quiescence, self- renewal, differentiation and their response to external cues. This anatomical location provides stem cells with appropriate extrinsic cues including biochemical signals, topographical and ECM interactions which regulate stem cell behaviour, most crucial of which is the balance between self - renewal and differentiation (Jones and Wagers, 2008). However, studying mammalian stem cell niches is difficult due to the lack of knowledge on the precise location of tissue stem cells; this is the case even for the best-characterised niche – the mouse HSC niche in the bone marrow. The role of MSCs as regulators HSCs in the bone marrow niche is well established (Méndez-Ferrer et al., 2010).

Cells exist within a 3D extracellular matrix (ECM) with defined physicochemical properties determined by their composition. Apart from one cell type regulating another via paracrine signalling, the 3D cellular microenvironment varies between the different tissues and provides cells with unique sets of biochemical and mechanical cues.

The constant bilateral communication between the inside and outside of the cell in this niche plays a major role in modulating stem cells in terms of their quiescence, self-renewal, differentiation and other crucial life processes, through the activation of several important pathways (Watt and Huck, 2013). This renders studies on how stem cells perceive and respond to cues from the ECM crucial for more intelligent biomaterial design. As a result when cultured *ex vivo* for example on standard tissue culture plastic this fine control/ balance over the behaviour and fate of these cells is lost and the stem cells spontaneously differentiate to heterogeneous populations mainly made up of fibroblasts (Montarras et al., 2005) (Sacco et al., 2008).

Key material properties have now been shown to modulate MSC fate; these include topography (Dalby et al., 2007) (McNamara et al., 2010), stiffness (Engler et al., 2006) and cell shape/ geometry of adhesive area (McBeath et al., 2004a). Elaborate and delicate techniques to decorate surfaces with these properties have been developed, some of these require access to complex engineering e.g. for nanofabrication and/or chemical surface modification; making the use of these materials mechanically unfit for industrial processing. The aim of this project is to study the effect of polymer mobility (an innate property of polymers; materials already widely used as biomaterials) as a tool to direct stem cell fate.

MSCs are an attractive cell type due to their multipotency *in vitro* (Gimble et al., 2008), protocols for their isolation from different tissues have continued to be developed and a minimal criteria to define MSCs has been outlined by the International Society for Cellular Therapy (Dominici et al., 2006). This criterion details that MSCs should be plastic adherent in standard culture conditions, express surface cell markers; CD105, CD73 and CD90, and lack expression of CD45, CD34, CD14 or CD11b, CD79alpha or CD19 and HLA-DR surface molecules. Moreover, they must retain the potential to differentiate to osteoblasts, adipocytes and chondroblasts *in vitro*. Efforts to engineer better biomaterial surfaces are on-going, and rely heavily on better understanding the cell – material interaction. Researchers are aware of the importance of surface properties of substrate and research efforts are focussed on understanding them.

Need for bone regeneration

One tissue that has been in focus of the efforts to devise regenerative therapies is bone. An ageing population (Humby, 2016) and increase in popularity and access to high impact sports are behind the high number and complexity of bone injuries (Johnell and Kanis, 2006), thus creating an increasing need for better strategies for bone repair. For small and simple fractures, bone tissue naturally regenerates upon injury, following similar molecular and cellular processes as in embryonic development where skeletal and vascular components develop in a soft cartilage callus environment.

Upon such a fracture, the damaged bone ends bleed and a clot or a hematoma (solid swelling of clotted blood) is formed. This is followed by acute inflammation characterized by vasodilation within the soft regions and accompanied by the exudation of plasma and leukocytes (Wray, 1964). Mast cells and granulocytes start to arrive at the injury site and the process of clearing up debris is begun (Lindholm et al., 1969). Next cell division peaks initially all over the injured bone and later is localised to the areas adjacent to the injury site (Tonna and Cronkite, 1961). Fibroblasts then migrate into the fracture site and create a fibrin meshwork by transforming the hematoma into a granulation tissue; this is followed by the arrival of MSCs from adjacent tissues e.g. the periosteum (Young, 1962) , their proliferation and differentiation into chondrogenic and osteogenic lineages.

These cells start to lay down the bone matrix, first forming the "woven bone" of the soft callus with a cartilaginous phase (3 – 4 weeks); this is followed by mineralisation forming a hard callus (3 – 4 months). The soft callus and hard callus are resorbed as lamellar bone is laid down by osteoblasts. Then the normal process of bone resorption and deposition by osteoclasts and osteoblasts respectively is re-established. Complete bone repair can take several months or even years. Bone fracture healing reviewed in Calmar, et al. (Calmar, 2002). However, bone fractures above a critical size e.g. 50 mm in dog mandibles and 5 mm in rabbit mandibles , are unable to undergo this natural healing process (Jin-Young and Jae-Hyung, 2005).

Bone repair - A historical account

Historically, the human effort to repair/regenerate bone dates as far back as the Neolithic period, with manuscripts describing practises including trepanation of the cranial bone (7000 - 3000 B.C). The descriptions of the Roman medical writer Celsus (c. 3 A.D to 64 A.D), the medical compendium of Paul of Aegina (625-690 A.D), Al-Zahrawi/ Albucasis (936-1013 A.D.) and Ibn Sinna/ Avicenna (980-1037 A.D) who describe in detail, the treatment of fractures, Ibn Sinna's Canon of Medicine remained in use up until 1650 A.D (Nasser et al., 2009). In 1668 the first bone (xeno) graft procedure was described by the Dutch surgeon Job van Meekeren and performed by a Russian surgeon (Meekeren, 1668). Successful autografts and allografts were demonstrated in the 1800s including the first successful reconstruction of

a large osseous defect of the humerus using an untreated allograft carried out by the University of Glasgow graduate William Macewen (Macewen, 1881) and in 1950 the first bone bank was established.

The constant need for advancement of technologies throughout history comes from the fact that while solutions were created, more questions were being raised. For example, it was only in the 1950s when it was realised that untreated/"live" allografts caused strong immune responses (Bonfiglio et al., 1955), however, surgeons still used allografts (treated) due to limited harvestable autologous bone. The risk of infection increased with multiple surgeries and size of required bone material.

The 1960s saw a key discovery by Dr Urist of the ability of decalcified bone matrix to induce ectopic bone formation when implanted in rabbit muscle tissue (Urist, 1965). This experiment changed the future of bone regeneration strategies and in 1971 he suggested the name bone morphogenetic protein (BMP) for the protein responsible for this effect. Henceforth several BMPs have been described and their use to enhance biomaterials for bone regeneration has greatly increased (Martino et al., 2011) (Schwab et al., 2015).

Therefore, it is now widely recognised that to encourage the natural healing processes, materials intended for intimate interaction with the human biology, need to not only cause no harm but also carry inductive cues for better outcomes. This approach may benefit both implants when used as coatings and scaffolds to encourage tissue regeneration.

The ECM and biomaterial design

X-Ray radiographs of sea shells used in the Mayan culture as dental implants showed significant osteointegration. Therefore the Mayan people may have been the first in history (600AD) to use an osteoinductive (osteogenesis inducing) dental implant (Abraham, 2014). The need for biomaterials in tissue engineering is increasing; at the research level, established biomaterial preparation technologies include surface modifications using e.g. topographies, chemistries, fragments of biological molecules to create biomimetic surfaces, and growth factors to activate regenerative pathways. Proteins used on surfaces to create a biomimetic effect are mainly derived from the ECM (Shin et al., 2003).

The ECM comprises of proteins secreted, assembled, remodelled and degraded by cells (Frantz et al., 2010). Cells in tissues are encapsulated inside the ECM and interact with the outside environment via ion channels and membrane receptor proteins e.g. integrins which bind specifically to sites (specific amino acid sequences) present in the structure of ECM proteins, or via growth factor (GF) receptors which are bound by soluble factors such as the BMP-2 protein.

Actin and myosin fibres are highly dynamic cytoskeletal components which maintain cell shape, are essential for contractility, migration of cells and are directly linked to the ECM via focal adhesions and integrins. It is therefore of no surprise that the cytoskeleton is crucial in the ability of cells to perceive and respond to physical properties of surfaces (Dalby et al., 2003) (McBeath et al., 2004a) (McNamara et al., 2010). The ECM is the non-cellular component (protein-rich) and highly dynamic structure surrounding cells in all tissue types except blood. The ECM functions more than mere scaffolding for support and elasticity within tissues; resident cells achieve a homeostatic balance of physical and biochemical environmental cues for healthy cellular processes by maintaining the ECM. For this reason, organs have unique ECMs which differ in their compositions and physical properties, and ECM health is required for tissue health (Humphrey et al., 2014). For example, ECM rigidity and changes in its composition have been linked to several pathological conditions including cancer (Chaudhuri et al., 2014) (Lu et al., 2012) and age - related complications (Eun Yang et al., 2011) (Coppé et al., 2014) . Moreover, the requirement for a healthy ECM has been shown by mutation studies, some of which have proven embryonic lethal (George et al., 1993). The role of the ECM has also been illustrated by loss of function studies, reviewed in (Rozario and DeSimone, 2010). The ECM constituents (Figure 3) are secreted and deposited by cells starting during embryogenesis.

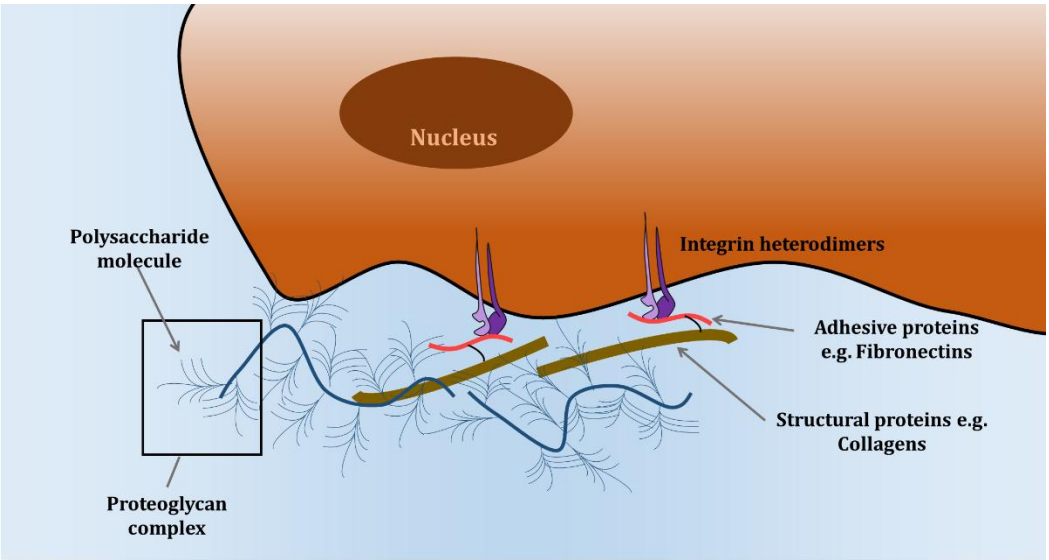

Figure 3 - Schematic of a cell interacting with ECM components. Cells secrete components of the extracellular matrix which they then assemble into fibrils. Most of the secreted structural proteins, proteoglycans and glycoproteins for example fibronectin, contain structural motifs which once exposed can be bound by integrins. Integrins are transmembrane receptors of cells, they go on to form adhesions which may mature and contribute to signalling processes (58).

In mammals, the ECM is made up of ~300 proteins also known as the matrisome (Reviewed in (Hynes and Naba, 2012). These can be divided into 3 main classes;

- Structural proteins (collagens and elastins)
- Proteoglycans; protein-polysaccharide complexes that embed the structural proteins.
- Adhesive glycoproteins; Fibronectins and laminins whose structure consists of cell binding sites for cell attachment.

In this study, I utilised a coating of fibronectin, a major extracellular matrix protein, to create a biomimetic surface for cells on the polymers, complete with an ECM - like topography and functional structure.

Biomimetic biomaterial design and protein adsorption

Upon implantation into the body, biomaterials are immediately coated in biological fluids consisting mostly of serum proteins which then adsorb to the implant surface, providing cells with binding sites with which to interact with the biomaterial. However, this adsorption of proteins to the biomaterial surface is dependent on physical properties of the surface including nanotopography (Raffaini, 2013), chemistry (Arima and Iwata, 2007), hydrophobicity (Ouberai et al., 2014) and, as has been shown in several studies (Guerra et al., 2010) (Berglin et al., 2004) (Sabater i Serra et al., 2016), polymer mobility affects protein adsorption. The protein layer adsorbed onto the biomaterial will from now on be referred to as the interfacial protein layer.

Proteins from biological fluids adsorb non-specifically on foreign materials. The biomimetic approach is an attempt to design biomaterials to elicit specific cellular responses by engineering the interfacial protein layer to interact with cells by biomolecular recognition (Martino et al., 2011) (Hubbell, 1999) (Healy, 1999). One approach is to coat cell substrates with native ECM proteins/ protein fragments thus eliciting required responses including cell adhesion and activation of specific signalling pathways. It has now become apparent from several observations that the behaviour of cells is affected by the conformation (Rico et al., 2009), density (Koo et al., 2002) and anchorage (Pompe et al., 2009) of these ligands to the underlying surface. These ECM components adsorbed onto materials can be coupled with growth factors which further tunes the cellular response (Martino et al., 2011) (Virginia Llopis-Hernández et al., 2016).

As discussed above, several physical surface properties have been explored with regards to biological interactions, however, an intrinsic property of polymers known as mobility is poorly understood. In this study, I look past the influence of protein conformation and density and focus on the effect of polymer surface mobility on the interfacial protein layer and how this affects cell behaviour. To vary mobility at the surface level I chose four polymers with increasing molecular mobility.

Polymer surface mobility

Polymers undergo physical changes as the temperature increases/decreases and at a distinct temperature for each polymer a more drastic change is observed. This temperature is known as the glass transition temperature (Tg), which is the temperature at which the physical state of a polymer transitions between a glassy state and a rubbery state (Figure 4A). Within the polymer, a change in the mobility of the polymer macromolecules occurs; this change is indirectly proportional to the Tg. However, even though polymeric biomaterials have been described as one of the cornerstones of tissue engineering, the influence of this property on the interfacial protein layer and cell behaviour is not well understood. This is in contrast to physical properties e.g. stiffness and topography which have been widely studied. This work sought to understand the effect of this poorly understood material property; the mobility of polymer chains at the surface of polymeric biomaterials on both the interfacial protein layer and cell behaviour including cell differentiation.

Mobility is related to polymer chain dynamics, polymer chains are large macromolecules of repeating units whose dynamics are dependent on several factors including pressure and temperature. The concepts of free volume (Cohen and Turnbull, 1959) and cooperative motion (Adam and Gibbs, 1965) are useful in the explanation of the existence of a specific Tg. Figure 4A, B and D illustrate the thermal expansion of polymers as the temperature is increased which results in an increase in the volume occupied by each molecule (Figure 4D). This reduces the activation energy barrier and increases the probability of molecular motion per unit time ($E/kT = B'/f$). When the temperature is gradually decreased, molecules lose their cooperative/ collective movement as they are frozen out.

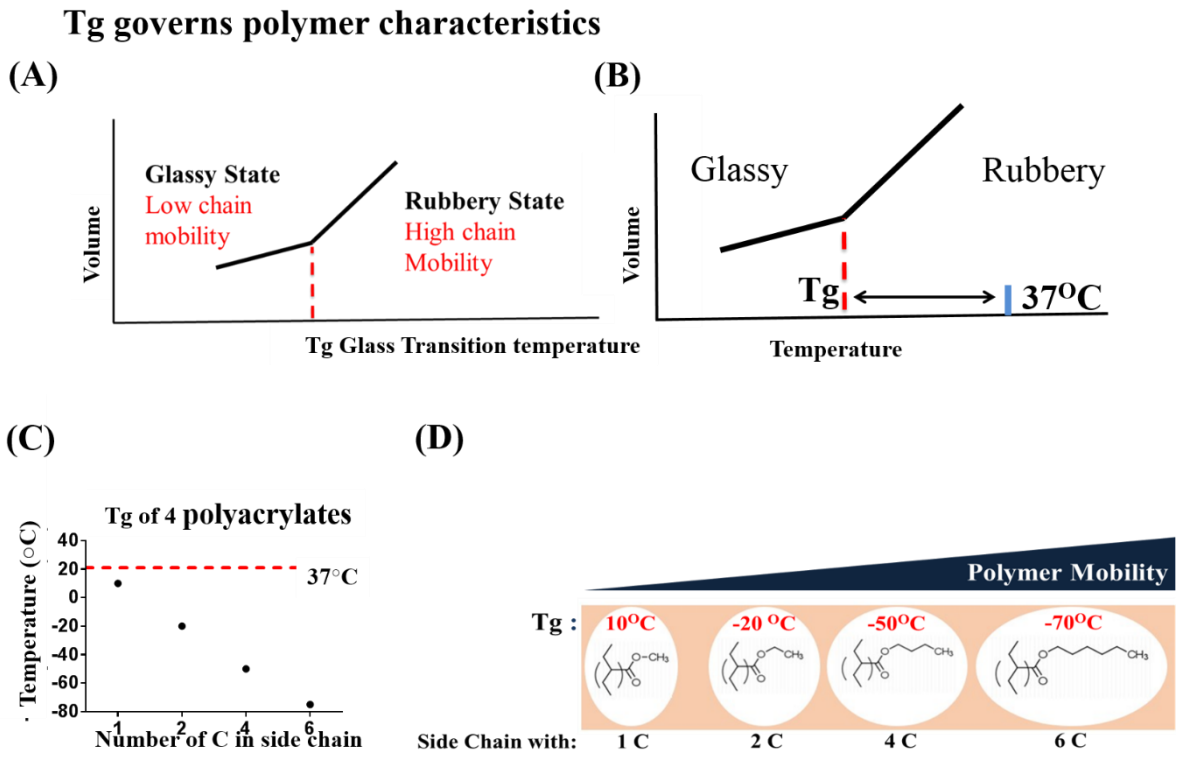

Figure 4 Glass transition temperature, polymer mobility and poly(alkyl acrylates) polymer systems of interest to this study. (A) Changes in polymer volume and thus mobility with increasing temperature, showing the effect of glass transition temperature. (B) Graph highlighting the difference between the specific Tg of a polymer and the cell culture working temperature of 37°C; a gap which in polymers with low Tg will be larger than in polymers with high Tg, thus representing higher mobility of that polymer at that temperature. (C) Glass transition temperatures of the 4 poly(alkyl acrylates) used in this study, showing the difference between them and 37°C. (D) Schematic of how polymer side chain length affects polymer chain mobility by increasing free volume (white area).

T_g varies with film thickness (Roth and Dutcher, 2005a), therefore films with a constant thickness (~740nm) were used in this study. Such that polymers exhibit rubbery surfaces (lower Tg and higher mobility) compared to the bulk, this phenomenon is attributed to the cooperative motion of the enriched chain ends at the surface (Jiang et al., 2001). I therefore,

hypothesized that this heightened mobility on the polymer surface is translated to the protein layer and ultimately influences cell behaviour.

Surface properties such as stiffness, topography and wettability are known to affect cell behaviour (Chaudhuri et al., 2014) (Resende et al., 2014) (Cantini et al., 2013). In this work, I demonstrate the similarity of my polymers in these three surface properties to eliminate the possibility of their confounding effects on cell behaviour (Bathawab et al., 2015).

The interfacial protein layer

The adsorption of ECM proteins on substrates has been widely used to mimic the natural environment of the cell. Solubilised matrix proteins, purified protein solutions and chemically bound ECM protein fragments have been used (Shin et al., 2003). However, proteins are complex polymers of amino acids and thus the chemical properties e.g. hydrophobicity of their different regions play a major role in their folding/structure/conformation. Consequently, the conformation of proteins upon adsorption is influenced by the properties of their environment; in this case the biomaterial surface and the ionic properties of the solvent. There is a deep interest in understanding protein adsorption due to its importance in the blood coagulation cascade (Hirsh, 1991), vascularization of tissue scaffolds as reviewed in (Vogel and Baneyx, 2003) and thrombosis due to implants (Rabe et al., 2011).

Despite countless efforts, this process remains as described almost two decades ago as “a common but very complicated phenomenon” (Nakanishi et al., 2001). Protein adsorption studies indicate that proteins in solution preferably aggregate into existing surface bound protein clusters rather than coating an empty surface (Minton, 2000) (Minton, 2001). The conformation of adsorbed proteins may differ from that attained in solution, as their structure re-organizes due to entropy gain and new favourable surface - protein interactions are formed. The work by Rankl et al., (2006) shows, using a structurally flexible ("soft") protein, (goat anti-rabbit immunoglobulin G) that initially proteins bind loosely where the conformational re-orientations are slow, with time their affinity to the surface increases creating an irreversibly bound protein layer.

The aggregation of proteins is implicated in several diseases e.g. Alzheimer's and Diabetes Type 2 where the aggregated proteins lose function (Aguzzi, 2010). However, non-specifically adsorbed proteins can maintain function e.g. they can form lateral protein-protein interactions, retain enzymatic activity (Brockman et al., 1973) and as shown in this work and several others; present amino acid sequences relevant for interactions with cellular receptors (Bathawab et al., 2015). The importance of protein adsorption to several fields has led to the construction of a number of models to explain aspects of protein adsorption including the rate and conformation (reviewed in (Rabe et al., 2011).

The ECM provides much needed structural support to cells within tissues; however, the folding of ECM proteins is crucial to their function. Hence the effective use of ECM proteins as biomimetic coatings for biomaterials is heavily dependent on the conformational structure achieved upon adsorption onto that particular biomaterial. Three out of the four polymer surfaces selected for this study have been shown to independently induce the adsorption and assembly of fibronectin into an ECM - like nano-network conformation (Figure 5) (Bathawab et al., 2015) (Guerra et al., 2010). In this study, this ECM-like fibronectin layer was characterised to analyse its density, topography/conformation and mobility. Functional studies on the fibronectin layer were performed by analysing the exposure of cell binding sites and cell response studies. Moreover, since cells interact with surfaces via a layer of ECM proteins, I utilised labelled fibronectin coupled with fluorescence recovery after photobleaching (FRAP) to analyse the mobility of the interfacial layer adsorbed onto the polymer surfaces.

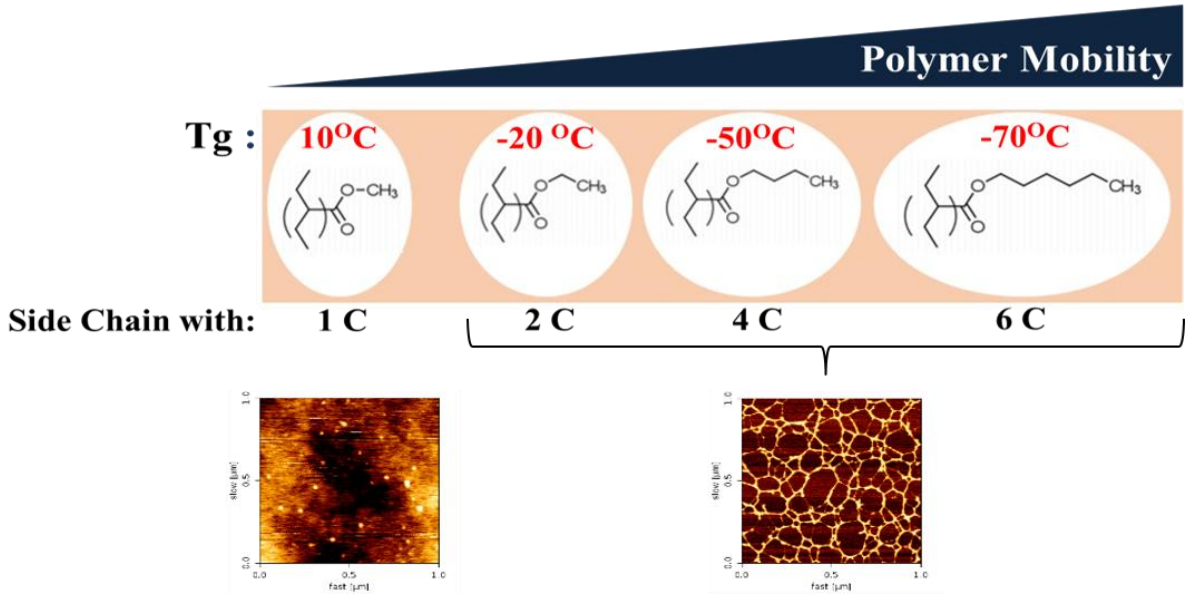

Figure 5: Schematic of how polymer side chain length affects polymer chain mobility by increasing free volume (white area) and the resulting conformation of adsorbed fibronectin. 1C-6C represent the number of carbons in the side chains. 2C - 6C induce fibrillogenesis of adsorbed fibronectin. Apart from their underlying difference in polymer surface mobility, the fibronectin fibrils on 2C-6C were observed to be very similar in conformation as shown by the images in the bottom panels (AFM).

Fibronectin structure and function

Fibronectin is a disulphide linked secreted glycoprotein homodimer (440 kDa) (Figure 6) which exists as either an insoluble ECM linker protein produced predominantly by fibroblasts, or as soluble plasma fibronectin which is secreted by hepatocytes (Roumen, 2002); the form used in this study. The modular beads-on-a-string structure of fibronectin consists of 3 repeating units; with twelve type I (FNI) and two type II (FNII) repeats both of which are bound internally by disulphide bonds and a hydrophobic core making their structure stable at physiological pH.

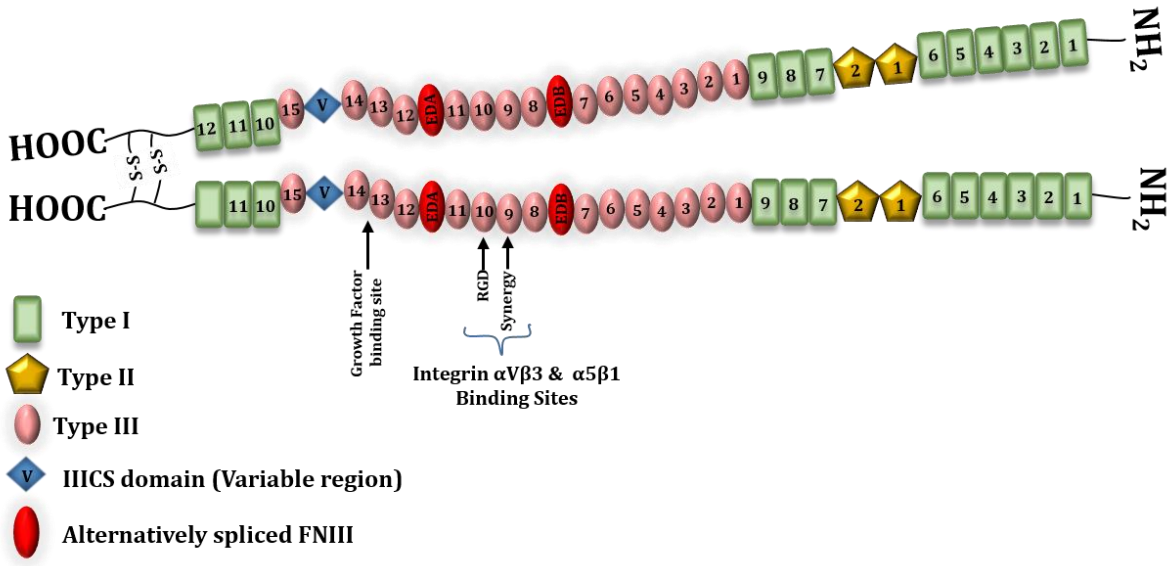

Figure 6 - Fibronectin dimer. Schematic showing two fibronectin molecules linked with a disulphide bond at the C-termini, illustrating its modular (bead on a string) structure (86). The binding sites for integrin heterodimers αvβ3 and α5β1 are located within the 9th and 10th fibronectin type 3 repeats.

These two modules are also relatively small with 45 and 65 amino acids respectively compared with the type III module (15-17 modules and 95 amino acids long) which is large and bears no internal disulphide bonds. The lack of stabilising forces in FNIII renders the module flexible and mechanoresponsive.

Moreover, the amino acid sequence Arg-Gly-Asp (RGD also known as the cell binding site) within the 10th FNIII repeat is a key integrin binding site (Pytela, 1987) and is aided by a sequence of Proline, Histidine, Serine, Arginine and Asparagine (PHSRN known as the Synergy site) in the nearby 9th FNIII repeat (Aota et al., 1994). Figure 7 shows a mechanism where mechanical stretching modulates the function of fibronectin domain (FNIII). Since stretching fibronectin may influence its function, I investigated this parameter using an antibody fragment which preferentially binds stretched fibronectin molecules.

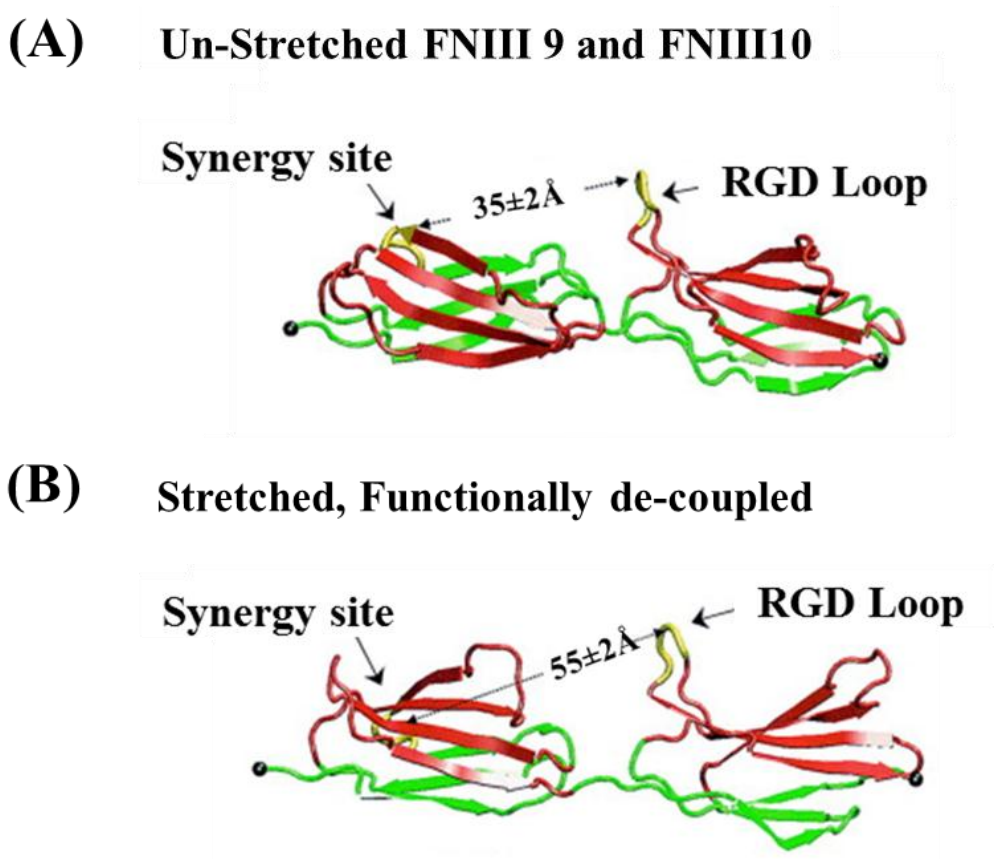

Figure 7 – The 9th and 10th FNIII repeats. Showing the distance at (A) 32Å when unstretched, extending to (B) 52Å upon mechanical stretching. This change due to mechanical forces has been implicated in differential integrin recruitment, and has been termed the "integrin switch". The figure is adapted from Krammer et al., (2002).

A simulation study (steered molecular dynamics) to understand the early unfolding pathway of the 7th, 8th, 9th and 10th FNIII modules revealed that the 10th FNIII is the weakest module. Its RGD site is at a distance of 32 Å from the Synergy site (PHSRN), and upon force - induced unfolding (where the conformations of both the two binding sites are maintained), this distance increases to 55 Å (Krammer et al., 2002). The original proximity of the synergy site to the RGD site has been shown to enhance integrin $\alpha_5\beta_1$ binding (Aota et al., 1994) (Mould et al., 1997) and increasing the distance between these two sites by inserting a linker has been shown to reduce the synergistic effects of PHSRN on $\alpha_5\beta_1$ binding (Martino et al., 2009), thus the suggested existence of a mechanosensitive conformational switch within the fibronectin structure. Fibronectin is pliable and cells are known to use integrins to

mechanically reorganise and assemble fibronectin and other ECM proteins, a review by Bradshaw and Smith (2014) (Bradshaw and Smith, 2014) discusses the relationship between the structure and function of fibronectin. Since my polymers spontaneously induce the assembly of ECM-like fibronectin nanofibrils, I investigated whether the fibronectin in these fibrils are stretched using an antibody fragment known to preferentially bind stretched fibronectin (Cao et al., 2012) and I performed immunostainings to determine whether cells seeded on these fibrils showed differential integrin recruitment.

In the ECM, proteins interact with themselves and other proteins to become supramolecular structures providing the cells with the topography and functionally active 3D structures suited to regulate development (Reviewed by Rozario T, DeSimone DW (2010) (Rozario and DeSimone, 2010), function and homoeostasis of tissues (Reviewed by Mecham R (2012) (Mecham, 2012). Different regions of the fibronectin molecule play crucial roles in the functioning of the ECM; the FNI repeats surrounding the two FNII repeats assist FNII in binding collagen, while the 1^{st}-5^{th} FNI repeats are required for the participation of fibronectin in the ECM assembly and fibronectin - fibronectin interactions (Hocking et al., 1994) (Aguirre, 1994). The ECM also functions as a reservoir of growth factors which are presented to cell receptors; the region between the 12^{th} and 14^{th} repeat has been shown to contribute to this, as it binds several growth factors including BMP-2 with high affinity (K_D values in the nanomolar range) without inhibiting growth factor activity (Martino and Hubbell, 2010a). Plasma fibronectin on the other hand interacts with fibrin to aid the formation of blood clots while FNI repeats 4-5 and 10-12 interact with fibrin during clot formation.

FNIII make up most of the protein and it is the most flexible region due to its size and lack of stabilising disulphide bonds, the RGD sequence is flexible and solvent exposed as shown by NMR (Main et al., 1992). FNIII like the other modules is made up of anti-parallel beta sheets, however, apart from its mechanosensitive flexibility another unique and intriguing feature of FNIII is that its structure and therefore function is modulated using alternative pre-mRNA splicing. This modulation plays a major role in development and differentiation.

In humans, there are ~20 different forms of fibronectin, mostly arising from differential tissue-specific splicing of the IIICS module (Figure 6). The IIICS module contains a heparin binding site and 2 integrin binding sites, thus by alternative splicing the structure and function of the fibronectin molecules and thus the ECM is modulated. Differential splicing plays a major role in the regulation of development, one such example is the expression of

cellular fibronectin with the EIIIA in pre-cartilaginous MSCs and the expression of FNIII without this region in mature chondrocytes (Kuo et al., 2002).

Fibronectin is known to interact with heparin and integrins as previously mentioned, including the following integrin α/β heterodimers; αIIbβ3, αVβ3, αVβ6, αVβ1, α5β1, and α8β1. Studies of the function of integrins are reviewed in (Humphries et al., 2006). Receptor-ligand interactions, however, are not always only based on the major interaction site but some are influenced by neighbouring interactions; a classic example is the α5β1 heterodimer whose specificity upon interaction with the RGD sequence (in the 10th FNIII repeat) is aided by the PHRSN or Synergy sequence (in the 9th FNIII repeat) (Mardon and Grant, 1994) (Mould et al., 1997). Therefore, fibronectin not only offers flexibility in integrin recruitment via site availability but also by cooperative binding.

Steered molecular dynamics (SMD) simulations show that forces of ~ 10 pN are sufficient to partially unfold the 10th FNIII repeat, thus extending the distance between the RGD and synergy domain from 32 Å to ~55 Å (Krammer et al., 2002). Therefore, the fibronectin molecule offers flexibility in function not only due to differential splicing (reviewed in (Kosmehl et al., 1996), but also due to changes induced by mechanical forces and as previously mentioned by cooperative selectivity of ligands.

At the C-termini, disulphide bonds link two monomers of fibronectin together while the corresponding FNIII modules at the N-termini of each molecule interact via ionic bonds achieving a folded conformation. In vivo, the folded molecule is then deformed mechanically by cells via integrins and assembled together with other proteins to form the extracellular matrix.

The exposure of fibronectin domains is crucial for accessibility, and cells assemble, stretch and manipulate ECM proteins such as fibronectin to access cryptic sites. Figure 8 is an illustration of the conformations on the 4 polymers used in this study; the bioactive sites in the fibrillar conformation were hypothesised to be more available than in the globular conformation found upon adsorption of fibronectin on the polymer with 1 carbon in its side chain. Fibronectin molecules assemble into fibrils when upon exposure of the fibronectin - fibronectin binding sites found in 1st-5th FNI (Hocking et al., 1994) (Aguirre, 1994). The reorientation of key hydrophobic residues within the fibronectin molecule to interact with the polymer backbone is believed to lead to the exposure of the fibronectin - fibronectin binding

sites and thus drive the conformational change and from globular to fibrillar (Salmeron-Sanchez et al., 2011).

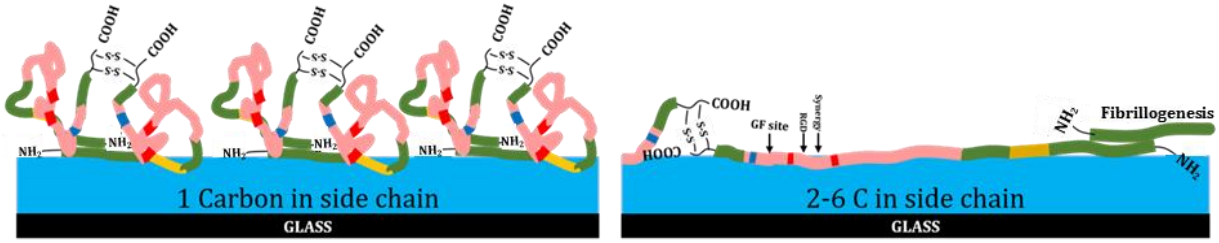

Figure 8 - Schematic of fibronectin conformation on polymers. Left, Globular fibronectin on C = 1 and Right, a more open conformation which is believed to expose sites of biological interest on C = 2, C = 4 and C = 6.

Cell - material interface and cell fate

The dynamic and complex interaction between cells and their environment is known to influence cell behaviour in important ways playing a role in healthy development and several malignancies. This study focuses mainly on MSCs, which have also been shown to respond to physical cues as reviewed by (Murphy et al., 2014). The complex nature of intracellular signalling has made it difficult to design material cues able to activate distinct pathways, however, some factors in this relationship have been established. Efforts are being exerted by the tissue engineering community to achieve functional biomaterials for stem cell culture as an alternative to the conventional use of biochemical supplements which include nucleic acids, recombinant growth factors and other animal products. Therefore material properties including stiffness (Engler et al., 2006), nano-scale topography (Dalby et al., 2007) (McNamara et al., 2010) (Resende et al., 2014) , surface chemistry (Benoit 2008) and cell adhesiveness/ cell geometry due to surface modification (McBeath et al., 2004a) have been shown to influence stem cell fate. Consequently, there is a need to understand the underlying signalling processes to enable the efficient and effective design of biomaterials for specific uses in stem cell culture.

Mobility of the protein layer

Cells interact with surface features via adsorbed proteins. However, surface adsorbed protein molecules are known to undergo lateral diffusion; this random crawl of protein molecules on the surface is thought to be due to the thermal fluctuations of the polypeptide chains. Moreover, the underlying mobility of the surface is translated to mobility of the protein layer; this has been demonstrated using FRAP analyses of BSA coated on lipid monolayers and solid substrates (Yonghui, 2003). This phenomenon is important for this study, since the translation of polymer surface mobility to the interfacial protein layer would underlie any changes in cell behaviour due to polymer mobility. FRAP analyses of polymer surfaces coated with fluorescently labelled fibronectin were carried out over 120 hours to determine the mobility of this interfacial protein layer. FRAP has been used to investigate diffusion of lipids within lipid monolayers and the mobility of protein molecules on protein - coated solid substrates.

Focal adhesions and the interfacial protein layer

Cells interact with the external environment via focal adhesions. With the exception of hematopoietic cells, the majority of cells derived from vertebrates are anchorage dependent. This means that these cells require interaction with surfaces to perform vital life processes including cell division, migration and differentiation. Focal adhesions are membrane-associated adhesive organelles made up of multiple proteins, with dual functions in force transduction/anchorage via actin filaments and signalling via multiple cytoplasmic proteins. Within focal adhesions, integrins which are transmembrane heterodimeric proteins and as their name imply, play the integral role of anchoring actin filaments via focal plaques consisting of several cytoplasmic proteins, to integrin-specific binding sites found in the ECM. It has been suggested that the array of signalling pathways activated by FAs is dependent on their compositional differences (Kuo et al., 2012). Upon binding of cell adhesion receptors to their ECM ligands, nascent focal adhesions which are sub-micron sized begin to assemble. Some of these disassemble while others attach to actin stress fibres and

increased tension of these fibres leads to the maturation and growth of the focal adhesions (Walcott S, 2011) (Zaidel-Bar et al., 2004). Due to this correlation between focal adhesion sizes and stiffness, I set out to analyse the size of focal adhesions in cells cultured on our setup, to determine if mobility played any role at this level of cell response.

The cells ability to perceive and respond (in behaviour) to mechanical properties of substrates indicate the role of forces at the cell-material interface in intracellular signalling (Han et al., 2012). The ECM is a mesh of fibrils of proteins in different conformations revealing cell binding sites and sites that sequester growth factors from the tissue fluid. As discussed, the ECM therefore provides not only structural support to cells within tissues but also cues for cellular processes (Frantz et al., 2010). Cells interacting with the ECM *in vivo* or with ECM - derived protein coatings, perceive these biological cues contrary to cells growing on uncoated or chemically treated surfaces e.g. Polydimethylsiloxane (PDMS – a commonly used cell culture substrate) which are met with a plain continuous surface. The similarity in scale between the fibrils and focal adhesion complexes (hundreds of nanometres) means that an entire focal adhesion complex will likely be associated with a single ECM fibril. Noteworthy for this study is the established ability of cells to perceive the mechanical properties of these fibrils (Schwarzbauer and DeSimone, 2011) (Kim et al., 2011). Integrins play a key role within focal adhesions in the perception and transmission of signals due to physical cues and the assembly and remodelling of the ECM.

Integrins

Integrins are transmembrane glycoproteins that function as heterodimers to link the interior of the cell with specific structural amino acid sequences within proteins adsorbed on cell culture substrates *in vitro*, within the ECM in vivo or on the surfaces of adjacent cells. They were first identified by Hynes in the 1970s as recounted in (Hynes, 2004). However, they do not merely act as (specific) structural anchors or pegs for the cell but also transmit biochemical signals bi-directionally into and out of the cell (Hynes, 2002) (Harburger and Calderwood 2009). Their selectivity in ligand binding, role in signal transduction and ability to switch between active and inactive states lead to the modulation of crucial life processes including

cell attachment, development (Damsky et al., 1994), migration/metastasis (Ganguly et al., 2013) (Truong et al., 2014) (Hoshino et al., 2015) and differentiation (Pierre, 2013).

Genetically engineered integrin mutations provide insight into their key roles, as reviewed in (Bouvard and 2001). The mammalian genome encodes 18 α subunit and 8 β subunits, 24 α-β combinations have been identified at the protein level. Integrin heterodimers bind ligands specifically, however, binding specificity overlaps for certain ligand-integrin pairs. Distinct integrin subunits are also known to be tissue specific, this indicates functional differences; for instance, the $\alpha_6\beta_4$ integrin is the major component of the hemidesmosomes and β_4 subunit's unique large cytoplasmic domain link to the intermediate filaments compared with the conventional linkage to actin cytoskeleton by β subunits (Walko et al., 2015).

The integrin ligand of interest to this work is fibronectin, as polymer surfaces were first coated with fibronectin prior to cell adhesion. 12 integrin heterodimers (Table 1) including $\alpha_v\beta_3$ (RGD binding (Pytela, 1987)) and $\alpha_5\beta_1$ (RGD and PHSRN - Synergistic binding (Aota et al., 1994)) have been shown to interact with fibronectin sites (Figure 6) (Reviewed in (Plow et al., 2000).

Table 1: Integrin heterodimers, of α and β subunits which interact with binding sites within the fibronectin molecule (Plow et al., 2000).

α subunits	β subunits
$\alpha_{2,}\ \alpha_{3,}\ \alpha_{4,}\ \alpha_{8,}\ \alpha_{v}$	β_1
$\alpha_v\ \alpha_{IIb}$	β_3
α_v	β_5
α_v	β_6
α_v	β_8

Design of Contemporary Biomaterials

It is now apparent that cells do not only respond to biochemical signals (growth factors, ECM binding sites etc.) but they also respond to physical cues from their environment (Riveline et al., 2001). As previously discussed the role of stiffness (Engler et al., 2006) (Discher et al., 2005), chemistry (Keselowsky et al., 2003) and topography (Tsimbouri et al., 2014) has been widely studied. The mechanistic analyses of these cellular responses to physical cues have revealed that the cytoskeletal components function in a dynamic fashion, and are directly connected to the extracellular environment via focal adhesion proteins (Geiger et al., 2001), this allows for cells to sense environmental cues (mechanosensing).

Several biological molecules have been described to be sensitive to mechanical force, these include ECM proteins for example fibronectin (Krammer et al., 2002), focal adhesion proteins within the membrane and in the cytoplasm for example integrin and vinculin (Atherton, 2016). This indicates that molecules from the three domains; intracellular, plasma membrane and extracellular, play important roles in mechanotransduction. Therefore, better understanding of how cells perceive and respond to mechanical cues is a prerequisite for improvement in biomaterial design.

Hypothesis, Objectives and Outline

In this work, I set out to analyse whether subtle variations in molecular mobility affects the interfacial protein layer and ultimately cell behaviour. The overriding aim was to investigate whether polymer chain mobility could be used as an inductive physical property to drive stem cell differentiation towards the osteogenic lineage (Chapter 4). This PhD describes the steps I took towards these aims, firstly I prepared and characterized my four poly(alkyl acrylate) films, I then coated them with fibronectin. I further characterised the layer of fibronectin by analysing its conformation, density, mobility and the exposure of integrin binding sites and the BMP – 2 binding site (Chapter 2). The fibronectin conformation was studied using the AFM and indirectly using ELISAs for integrin binding site exposure, FRAP analyses of

fluorescently labelled fibronectin bound to the surfaces was used to deduce the interfacial protein mobility, and this was related to the underlying mobility of the polymer surface.

Next, functional analyses were carried out to study cell behaviour in response to these different polymers in conjunction with coatings of fibronectin -/+ BMP-2. To start with, I cultured model cell lines on my fibronectin coated surfaces to study cellular parameters which may be influenced by the mobility of the polymer surface or that of the interfacial protein layer. I therefore analysed the adhesion, cell morphology, matrix reorganization, integrin recruitment and cell differentiation in mouse premyoblasts and human and mouse fibroblasts (Chapter 3). The differentiation of premyoblasts was carried out in the presence and absence of cytoskeletal contractility inhibition to investigate whether polymer chain mobility driven cell response would be dependent on contractility; which is known to disrupt cellular perception of other physical properties such as stiffness. An overall discussion of experimental results is provided in Chapter 5.

Chapter 2

Introduction - Polymer Substrate Characterization

Four poly(alkyl acrylates) with similar surface chemistry but decreasing Tg and thus increasing polymer chain mobility (Figure 4) were selected to study the effect of polymer mobility on cell response. Each polymer comprised of a vinyl backbone with a side group $-COO(CH_2)_xH$, where x is the number of methyl groups in the side chain. The decreasing Tg was achieved by increasing x; the number of carbons in the side chain thus effectively increasing its length. As a simple descriptor, the number of carbons in the side chain will be represented in this report as the number of C, such that e.g. poly(ethyl acrylate) would be C = 2.

Prior to evaluating cell response, the polymers were characterised to ensure that differences in cell response results would likely be due differences in polymer chain mobility and not due to other physical properties e.g. substrate stiffness, hydrophobicity and substrate topography, all of which have been shown to influence cell behaviour. (Dalby et al., 2003) (Dalby et al., 2007) (Wang et al., 2012) (Engler et al., 2006).

Cells interact with surfaces via the interfacial protein layer made up of proteins which adsorb to the biomaterial surface upon the initial interaction; this fact is unfortunately mostly not considered when analysing the influence of physical surface properties on cell behaviour. In this study, fibronectin was adsorbed on the surface to provide cells with a definitive interfacial protein layer and specific binding sites for cellular interaction. The conformation of the proteins adsorbed on substrates has been shown to play a major role in modulating cell behaviour (Garcia et al., 1999). I, therefore, characterised the conformation of the fibronectin layer directly using AFM and indirectly by analysing the exposure of specific structural domains using epitope specific ELISAs.

Polymers chosen for this study vary in mobility, an intrinsic property of polymers whose role in the biological response to polymeric biomaterials is poorly characterised. Emerging evidence points towards the importance of this property in modulating cell response (Curran et al., 2011) (Liu et al., 2012) (Seo and Yui, 2013) (Seo et al., 2013). Moreover, chain mobility at the polymer surface has been shown to be higher than in the bulk (Wallace et al.,

2000). Moreover, film thickness affects Tg (Ellison and Torkelson, 2003) (Roth and Dutcher, 2005b), for this reason, polymer films of constant thickness were prepared for this study.

Polymer chains within a material are dynamic structures whose mobility is dependent on temperature, at low temperatures both the backbone chains and the side chains are frozen out, as the temperature increases the side chains start to become mobile followed by the backbone chains at temperatures above the Tg. Tg, therefore, gives a good indication of mobility (the two parameters are inversely proportional). This relationship is explained best by two models; accessible free volume and cooperative motion where increasing temperatures (from < Tg to > Tg) are accompanied by the gradual increase in accessible free volume for molecular motion and the progressive gain of motion by the branches within a polymer and ultimately the backbone itself (Roth and Dutcher, 2005a).

In this study, fibronectin was used to create an interfacial protein layer on the substrates, this protein has been shown to interact very intimately and robustly with the polymer surfaces of interest (C = 1, 2, 4 and 6) (Rico et al., 2009). It was thus hypothesised that the enhanced mobility at the polymer surface would translate to the intimately bound protein layer, which would then potentially play a role in cell response. To do this, FITC labelled fibronectin was adsorbed onto the surfaces and analysed by FRAP, this method was selected as it was easily accessible and has successfully been used to analyse surface protein mobility (Axelrod et al., 1976). The recovery of fluorescence after photobleaching of the fibronectin-FITC coated polymer surfaces could only be due to the movement of unbleached fibronectin-FITC molecules into the bleached area. Analysis of this phenomenon over time led to the discovery that the underlying polymer surface mobility is translated to the protein layer.

Materials and Methods

Preparation of polymer surfaces:

Bulk polymers were synthesised at room temperature by radical polymerization of acrylate monomers using 1 w/t % benzoin (a photo initiator), these were supplied by a collaborator from the Materials Engineering Institute, Universitat Politècnica de València, Spain. Weight/Volume Percentage solutions were prepared by dissolving bulk polymers w/v % in toluene (Sigma, Cat No: 89680). The solution was typically ready (clear) after 12 – 48 hours on the stirrer. Coverslips were cleaned by sonication in 100% ethanol and dried in the oven. 100 µl of polymer solution was pipetted onto coverslips of 12 mm diameter (volumes were scaled up for larger coverslips) and spun for 30 seconds at 3000 rpm. Samples were then dried at 60°C under vacuum to remove any residual solvent.

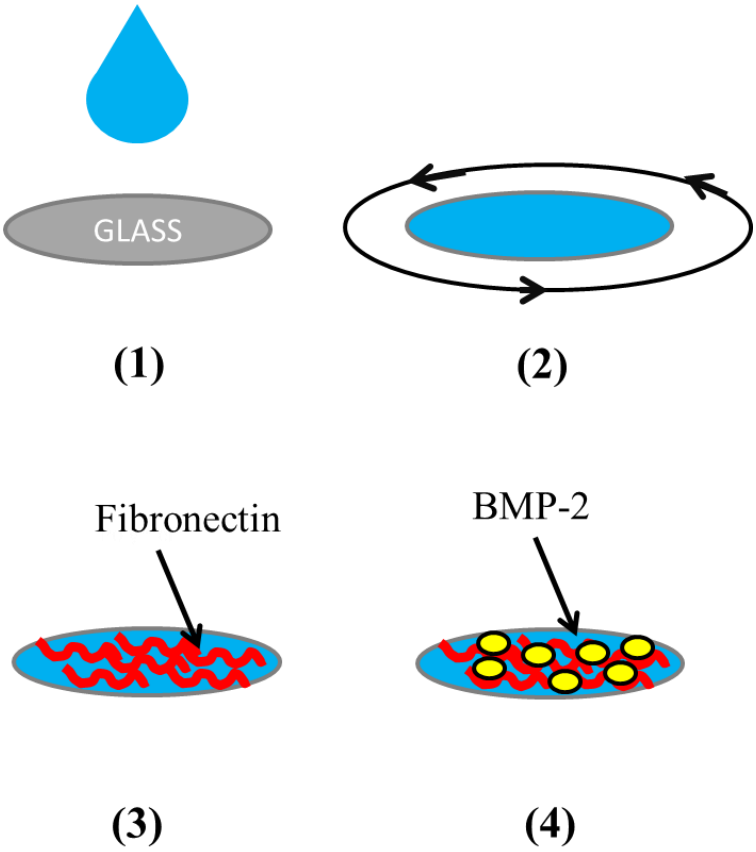

Figure 9 – Polymer surface preparation. (1 and 2) the polymer solution is spin coated on glass coverslips, after solvent removal by vacuum drying, the surfaces were incubated with a fibronectin solution. If required, surfaces were then incubated with a BMP-2 solution.

Water contact angle

Water contact angle readings of 6 µl droplets were taken 100 milliseconds after the droplet was placed on the surfaces to allow it to settle. Sample areas were only used once per reading to eliminate the effects of swelling on the measurements.

To measure the static water contact angle on the polymer films the sessile drop method was used. Using the Theta optical tensiometer (Biolin Scientific) at 21°C, 6 µl drops of ultrapure water were placed on spin-coated polymer surfaces and pictures of the drops taken after a 100 seconds delay were analysed. The drops had radii shorter than the capillary length of ultrapure water and air, at 21°C and standard pressure (1 x 10^5 Pa); therefore the gravitational effects on the drops were considered negligible (Young, 1805). The advancing and receding contact angles were assessed by slowly adding ultrapure water to the original static volume

and removing water from it and recording the contact angle when the three phase boundary between water, air and substrate moves.

AFM nanoindentation

The stiffness of polymer coatings was analysed by nanoindentation using a JPK NanoWizard® 3 BioScience Atomic Force Microscope. A cantilever with ~2.5N/m, ~75kHz resonance frequency and silicone pyramidal tip 20.8º half angle to face (FMV, Bruker) Prior to obtaining force spectroscopy curves, the calibration of tip sensitivity and spring constant was carried out at room temperature with the following JPK settings: set-point of 10nN, zeta length of 10µm and 1 second constant duaration. The "set point" setting on the JPK software gives the user control of the maximum force exerted on the sample. Sample triplicates were scanned three times each and each time force curves from a grid of 64 points (10 µm X 10 µm) were recorded. Analysis was performed using the JPK processing software (v4.3.21), and force curves were fitted with the Hertz model at 50 nm indentation (~10% of polymer film thickness).

Human fibronectin purification

Purification of full-length fibronectin from human plasma for *in vitro* experiments, using gel filtration and gelatin chromatography columns (Brew, 1994). This purified fibronectin was used for the analysis of fibronectin stretching using the H5 single chain variable antibody fragment (described below) and the integrin recruitment analysis in human foreskin fibroblasts (Chapter 3). This fibronectin was shown by AFM to adsorb in similar conformation to the fibronectin used in the rest of the experiments (Sigma - Aldrich).

Materials

200mM PMSF in Ethanol, 1M NaCl in dH2O, 10M Urea in PBS, 6M Urea in PBS.

Regeneration Buffers:

Sepharose Regeneration: (30 ml) 0.5M NaOH, 0.1% TritonX-100 in dH2O.

Gelatin Regeneration: 0.1M Tris-HCl, 0.5M NaCl at pH 8.5, 0.1M Sodium acetate,0.5M NaCl at pH4.5.

Column Preparation

10mL of Sepharose 4B (Sigma, Cat No: 4B-200) and 10 ml of gelatin sepharose (Sigma, Cat No: 17095 601) were poured into separate 50 ml tubes, capped with a No. 6 stopper and vacuum was applied for 10 - 20 minutes until any bubbles that appeared were scrapped out. Two columns were fitted with a filter (slightly curved side down), and then the degassed slurry was poured into the column using a glass rod to avoid bubbles. The column was then packed with 20% ethanol in water and stored (stoppered and upright at 4C).

Affinity Purification

Columns were assembled such that Sepharose4B column dripped into Gelatin-Sepharose column. 5 column volumes (CVs) of 2mM EDTA were run through the columns. 80 ml fresh frozen human plasma obtained from the American Red Cross was thawed on ice, this was then spun at 2000rpm for 10 minutes to remove red blood cells and 0.8 ml of 200mM PMSF and 1.6 ml of 0.5M EDTA were added to the plasma. The aliquots were spun again at 10000 rpm for 15 minutes; the supernatant was pipetted into the sepharose column. Any precipitated protein adhering to surfaces was removed to avoid clogging the column. The flow rate was maintained at ~1 drop every 2 seconds. The gelatin column was then washed with 2mM EDTA in PBS and the OD of the effluent measured using a nanoDrop until it was ~0.00 mg/ml. The sepharose column was then regenerated. The gelatin column was then washed with 1CV of NaCl and two 15 ml tubes were prepared for collection. A denaturing solution of 6M urea was used to elute bound fibronectin and 2 ml fractions were collected. Samples over 0.2 mg/ml were collected; in total ~4 ml fibronectin solution was collected.

Dialysis Procedure

A packet of snake-skin tubing (10kDa pore size, ThermoFisher Scientific) containing the affinity purified fibronectin was made using clamps (least air in the pocket as possible to avoid dilution). The fibronectin was then dialysed against 1XPBS; at 4 C and the external buffer exchanged 5 times (for fresh buffer). The buffer was cooled to 4ºC prior to transfer of fibronectin packet and the exchanges were done every ~4-5 hours. Finally dialysed fibronectin was measured by NanoDrop, aliquoted and stored at 80 ºC.

Micro BCA (bicinchoninic acid assay)

Polymer surfaces were adsorbed with fibronectin for 1 hour at concentrations of 20 µg/ml, 10 µg/ml or 5 µg/ml. The remaining supernatant was collected at the end of the incubation and the polymer surfaces were washed with DPBS, and this wash was then added to the collected supernatant for each sample. This solution was analysed to deduce the amount of unbound fibronectin. The assay for protein concentration was carried out using the Micro BCA™ Protein Assay Kit (Thermo Fisher Scientific), with the albumin provided being used as a standard. The micro BCA assay is a colorimetric assay for total protein, and is based on the reduction of Cu^{2+} by protein in an alkaline environment. The chelation of two molecules of the detection reagent (bicinchoninic acid) with one Cu^{+} produces a purple coloured product which exhibits a strong absorbance at 562nm that is linear with increasing protein concentrations. The assay was carried out as per the instruction manual from Thermo Fisher Scientific.

AFM scanning (tapping mode)

A JPK NanoWizard® 3 BioScience Atomic Force Microscope was used to scan polymer films coated with 2, 5, 10 and 20 ug/ml of fibronectin. Phase images were acquired via tapping (AC) mode in air using a pyramidal silicon nitride tip, on a cantilever with ~3N/m spring constant and resonance frequency of 75kHZ (MPP-21120, Bruker). The fractal

dimension of phase images of fibronectin nanofibrils was computed using the ImageJ Fractal box count analysis tool, utilizing box sizes of 2, 3, 4, 6, 8, 12, 16, 32, 64 pixels.

Direct ELISA

The availability of the cell binding (RGD) and Synergy (PHSRN) domains of fibronectin adsorbed on the polymer surfaces was analysed using ELISAs.

Sample triplicates were incubated with 20 μg/ml fibronectin in DPBS++ and another 3 samples were incubated only with DPBS -- (Blanks: 0 μg/ml) for 1 hour at room temperature. They were then washed twice with DPBS ++, transferred into a 24 well plate and blocked for 30 minutes using the blocking buffer (1% BSA solution, Sigma - Aldrich). The samples were then incubated at room temperature with monoclonal mouse primary antibody (mAb1937, Sigma - Aldrich) diluted 1:20 000 in blocking buffer for the synergy (PHSRN) domain or the HFN 7.1 (Developmental Studies Hybridoma Bank) at 1: 20 000 dilution for the cell binding (RGD) domain. The samples were then washed twice with 0.5% Tween20. Goat anti-mouse HRP-tagged secondary antibody (R&D systems) used at 1:10,000 was then added and incubated for 1 hour at room temperature. Samples were washed twice with 0.5% Tween20 to remove unbound antibody and transferred into a new 24 well plate to avoid signal due to any unspecific binding of HRP-tagged secondary antibody onto well plates. The substrate solution was added to the samples in the absence of light and incubated for 20 minutes. Finally the reaction was stopped by addition of the stop solution. Absorbance was then measured at 450 nm and 540 nm (Blank reading) using a plate reader. The substrate solution and stop solution were from a kit by R&D Systems from Minneapolis, USA.

Quantification of fibronectin availability

The relative amount of fibronectin adsorbed on polymer surfaces was quantified by ELISA using a rabbit anti-rat fibronectin polyclonal antibody (Millipore) 1:400 and a biotinylated goat anti-rabbit (Millipore) at 1:1000 as the secondary antibody. All antibody and extrAvidin peroxidase were diluted in 1% BSA.

Prior to insertion of polymer coated samples into wells, all the wells were pre-blocked with 1% BSA for 30 minutes, incubated with primary antibody for 1 hour at room temperature and then washed with 0.5% Tween20 in PBS thrice. Polymer coated samples were incubated with 5 µg/ml or 20 µg/ml fibronectin for 10 minutes, blocked for 30 minutes at room temperature and incubated with secondary antibody for 1 hour at room temperature. Samples were washed 3 times with 0.5% Tween20 in PBS. Finally, samples were inserted into wells and incubated with 1:1000 solution of extravidin-peroxidase (Sigma - Aldrich,) for 1 hour at room temperature. Samples were then washed twice with 0.5% Tween20 in PBS and then once with PBS. 195ul of TMB (1-stepTM Ultra TMB-ELISA Thermo Scientific, Rockford, USA, Product no: 34028) was then added to each well and allowed to develop. The reaction was stopped by adding 120ul H_2SO_4 when positive wells had turned blue and absorbance was read at 450 nm and 650 nm (blank).

Analysing fibronectin stretching using the H5 fragment

The H5 peptide probe (unpublished data, Barker laboratory, Georgia Institute of Technology) developed from a phage display screen (Cao et al., 2012) preferentially binds to stretched fibronectin. Three out of four surfaces of interest in this study induce fibronectin fibrillogenesis to different extents (Guerra et al., 2010) (Bathawab et al., 2015) .This led to the question of how stretched are fibronectin molecules on each of these polymer surfaces and an ELISA using the fibronectin fragment was carried out to analyse the extent of fibronectin stretching. Wells were pre-blocked with 1.5 % BSA in PBS for 30 minutes at room temperature and samples were coated with 5 µg/ml fibronectin. All samples were washed 3 times with PBS++ and wells incubated with the single chain variable fragment myc labelled H5 at 10 µg/ml for 1 hour at room temperature on rotation, and then washed with 1% Tween20 in PBS thrice. Samples were then incubated with 1.5 % BSA for 30 minutes room temperature, this was followed by incubation with a monoclonal biotinylated mouse anti - myc secondary antibody (Sigma, Cat No: M4439**)** used at 1:2000 dilution for 1 hour at room temperature and on rotation. Then samples were washed 3 times with the 1% Tween20 in PBS and incubated with 1:1000 solution of extravidin-peroxidase for 1 hour at room temperature. They were then washed twice with 1% Tween20 in PBS and then once with

PBS and 195 ul of working solution was added to each well and allowed to develop, the reaction was stopped by adding 120 ul H_2SO_4 when positive wells had turned blue. Absorbance was read at 450 nm and 650 nm and results were normalised with available fibronectin.

Determining protein mobility

Fibronectin labelling with FITC: 1 mg/ml of fibronectin from human plasma (Sigma-Aldrich) was labelled using the FluoroTag FITC conjugation kit (Sigma-Aldrich) whose protocol was tailored for fibronectin labelling by adjusting the fibronectin/FITC ratio. 250µl of 1 mg/ml fibronectin was incubated with FITC in the ratio FITC to fibronectin 125:1 for 2 hours. A G-25 Sephadex column was then used to separate labelled fibronectin from unconjugated molecules. The success of this labelling procedure was determined by measuring the absorbance of the retrieval fractions at 280nm (protein) and 495nm (FITC) and calculated using the equations below.

Fluorescence recovery after photobleaching (Axelrod et al., 1976): Areas on fibronectin-FITC coated polymers and glass control were photobleached using the Olympus FV1000. The samples were then stored under cell culture conditions (37°C, 5% CO_2). The fluorescence signal was measured every 24 hours for 120 hours using the Zeiss Observer Z.1 widefield microscope. Areas of 20×50 μm^2 were manually selected across the bleach border region (Red box in Figure 18A). The bleached area was considered to be of zero intensity while the unbleached to be 100%, a line graph was then acquired by averaging each column of pixels. This gradient was obtained for each time point and the rate of change of gradient was calculated and plotted on the graph (Figure 18B).

Data Analysis: All images were analyzed using ImageJ software25 (v1.48). The data were statistically analyzed using GraphPad Prism 6. Where relevant, one-way and two-way

ANOVA tests were performed to determine any statistically significant differences: *$p \leq 0.05$, **$p \leq 0.01$, ***$p \leq 0.001$, and ****$p \leq 0.0001$ (GraphPad software, La Jolla, CA). The linear gradient of bleaching analysis was determined in OriginPro 8 (OrginLab, Northampton, MA), with this subsequently being transferred to and analyzed in GraphPad Prism 6.

Results and Discussion

Polymer preparation was first optimized by adjusting polymer concentration prior to spin coating. The prepared samples were then scanned using AFM AC mode, this process was repeated until four polymer films with similarly smooth surfaces and constant thickness were achieved.

As the aim of this study was to analyse how cells respond to mobility, it was crucial to eliminate other variables which may exert their effect on cells. Surface topography, stiffness and hydrophobicity have been shown to exert an effect on cell behaviour (Dalby et al., 2003) (Dalby et al., 2007) (Wang et al., 2012) (Engler et al., 2006), topography and hydrophobicity also affect protein adsorption to biomaterials (Raffaini, 2013) (Michael et al., 2003b).

The four surfaces were found to have negligible topographical cues, with similar root – mean - square (RMS) roughness of ~375 ± 55 pm. Their thickness was 740 ± 230 nm, regardless of composition and AFM nanoindentation experiments on polymer films on glass showed stiffnesses in the megapascal range (Figure 10) which is beyond the stiffness threshold of 40kPa detectable by cells (Riveline et al., 2001).

AFM stiffness: Elastic moduli (E')

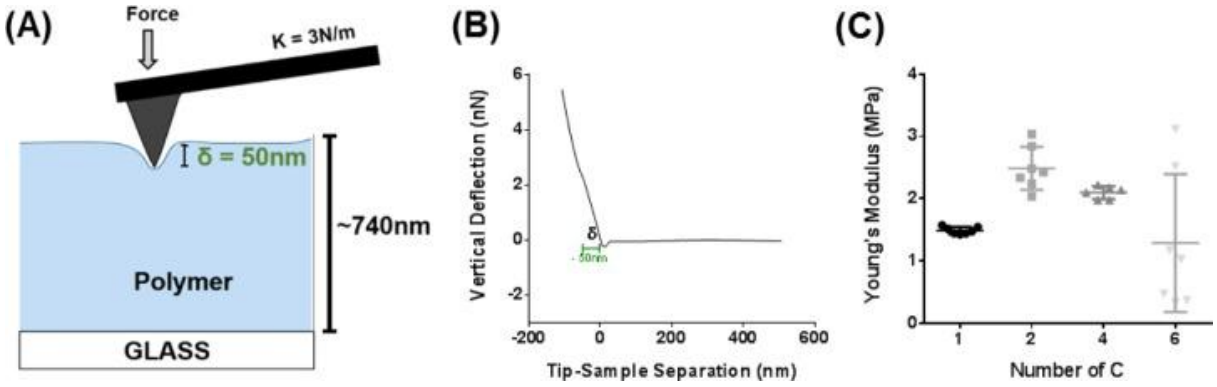

Figure 10 – Stiffness measurements by AFM nanoindentation. (A) Sketch showing AFM tip deforming a polymer surface, (B) Example force curve showing the initial 50 nm indentation (δ) on which the Hertz model was applied to calculate the Young's moduli. (C) Graph of Young's moduli of polymer films, each point representing an average derived from individual measurements (n = 64) carried out on each surface. There were no statistical differences in young's moduli of the polymer films. The large variation in the measurements on C = 6 were attributed to the highly adhesive nature of this polymer.

Water contact angle

Thomas Young proposed the treatment of the contact angle of a droplet sitting on a solid surface as a mechanical equilibrium under the action of 3 surface tensions (Young, 1805); the interface between the liquid and the solid phase (sl), the liquid and the vapour phase (lv) and the solid and vapour phase (sv). Represented by the equation: $\cos \theta = (\gamma sv - \gamma sl)/ \gamma lv$ (Figure 11A). The more non-wetting the liquid is the higher the value of theta (θ) and evidently, θ cannot be measured for non-spreading liquids. When a liquid drop falls on a solid surface it forms, a sphere sectioned by the solid surface at a distinct measurable angle, if the volume of the drop is reduced either by evaporation or if the liquid is carefully withdrawn then the droplet maintains the same contact area but the contact angle reduces, this continues until the drop recedes. The angle at which the drop recedes is known as the receding contact angle, on

the other hand, if the volume of the drop is increased and it advances (increasing the contact area) then this angle is known as the advancing contact angle.

The dynamic contact angles (advancing and receding) are characteristic of the chemistry and topography of the solid surface. Apart from these two angles, the static water contact angle was also measured in this work, however, the static contact angle is only an angle between the Advancing and receding angles, consequently, the two latter angles are more meaningful. The difference between these two angles is known as the water contact angle hysteresis and reflects the activation energy needed for a droplet to move from one stable state to another. In this work, I used multiple measurements of static, advancing and receding contact angles of deionized water droplets on several areas of each sample to study the chemical and topographical heterogeneity of the surfaces of my polymer films.

Water contact angle (WCA) analyses of polymers with and without a fibronectin coating, revealed more information on the physicochemical properties of the polymers (Figure 11B and E).

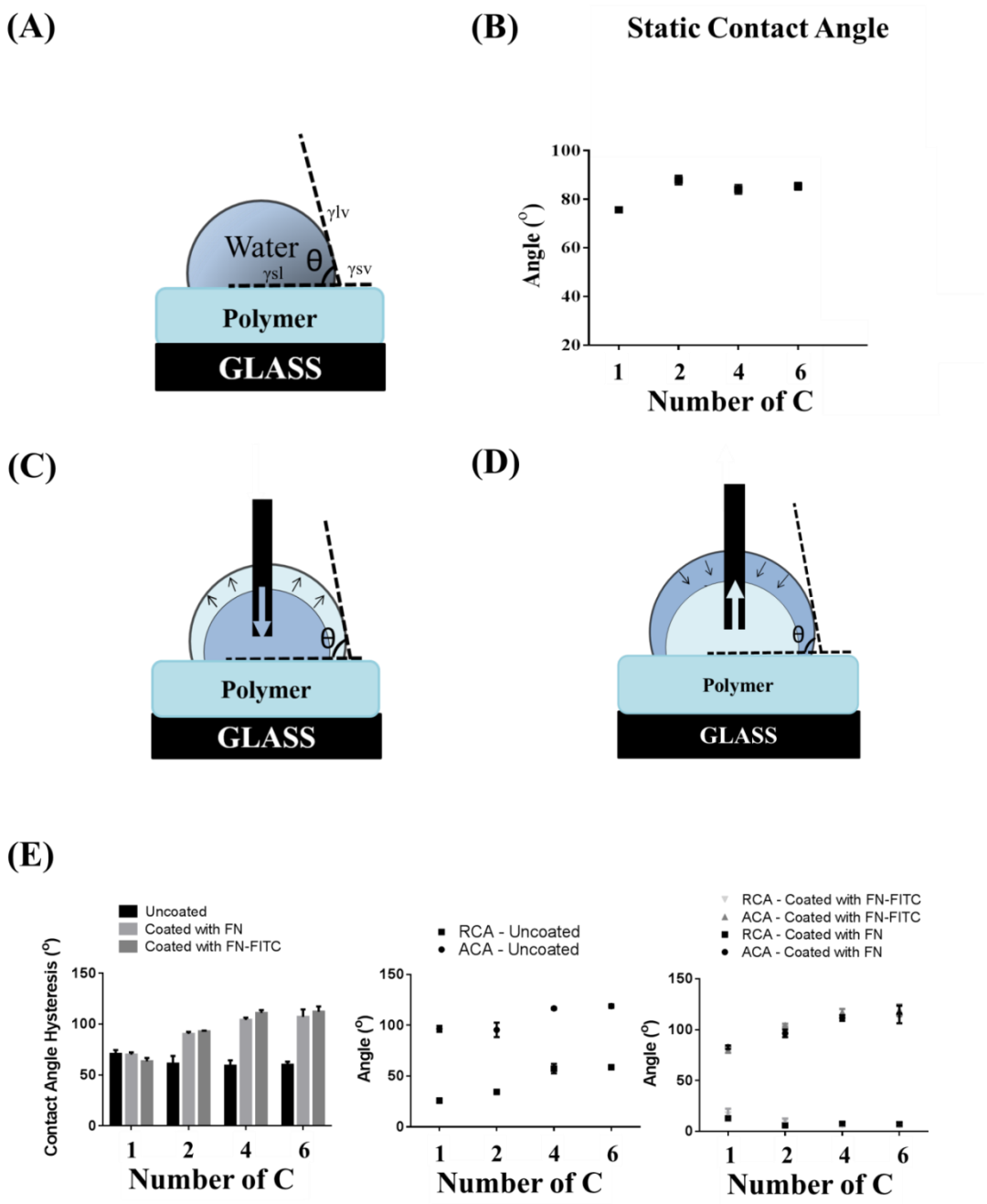

Figure 11 - Polymer surface wettability. Hysteresis was calculated from dynamic measurements on the polymer surfaces before and after coating with a 20 µg/ml fibronectin solution. (A) Static water contact angle schematic. (B) Static water contact angles for polymers. (C) And (D) Advancing and receding contact angle schematics respectively. (E) Dynamic contact angles and hysteresis on bare polymers and polymers coated with either fibronectin or labelled fibronectin. Bars indicating standard deviations are overlapped when too small. Each point is an average of readings from 9 measurements.

Minimal differences were observed on the uncoated samples for static contact angles (SCA – indicating similar hydrophobicity) and hysteresis (The difference between Advancing and Receding contact angles, which indicate surface homogeneity).

Unlike uncoated polymers, advancing contact angles of fibronectin and fibronectin-FITC coated polymers increased with the number of C in the polymer side chains while their receding contact angles decreased, as a result, the hysteresis on the fibronectin - coated polymers increased with increasing side chain length. However, hysteresis did not increase for the fibronectin - coated C = 1 polymer, reflecting the lower protein coverage due to the globular fibronectin conformation characteristic of this polymer.

The increase in hysteresis (Figure 11E) on C = 2, C = 4 and C = 6 upon either fibronectin or fibronectin -FITC adsorption may indicate an enhanced ability of the fibronectin molecules adsorbed on these polymers to undergo molecular rearrangement at the water/air interface. This suggests mobility of the interfacial protein layer.

The similarity between the results from the water contact angle analyses of the fibronectin and fibronectin-FITC coated polymers indicated that fibronectin and fibronectin-FITC are comparable; this is in agreement with the similarity in conformation between fibronectin and fibronectin-FITC as seen in the AFM AC mode scans (Figure 12).

Fibronectin conformation

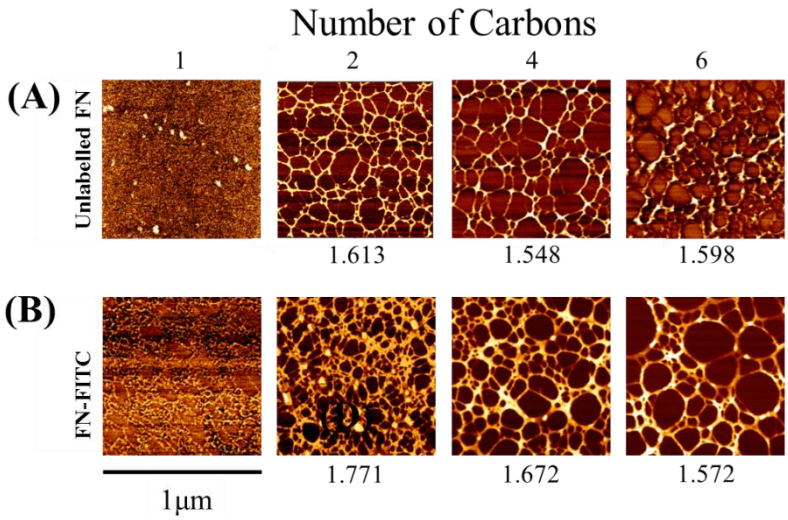

Figure 12 - Atomic force microscopy scans of adsorbed fibronectin. Fibronectin conformation on polymer surfaces shown by AFM scans (AC mode/ Tapping mode used to

probe the topography) after adsorption from a fibronectin solution of 20 μg/ml concentration. Fbronectin undergoes fibrillogenesis forming nanofibrils on PEA (C = 2), PBA (C = 4) and PHA (C = 6). The top and bottom 1 μm by 1 μm images show the similarities between the distribution of unlabeled and labelled fibronectin (fibronectin-FITC) on the polymers. Values shown underneath the images of nanofibrils relate to the fractal dimension; a descriptor of pattern complexity which here is used to represent connectivity. The FN-FITC scans in (B) were performed in collaboration with Mark Bennet as part of his Masters project (Bathawab et al., 2015). Images are representative of three taken from each triplicate.

The conformation of fibronectin on the polymers is consistently globular on C = 1 and fibrillar on C > 1 regardless of the initial coating concentration used. Moreover, the formation of fibrils is graded (Figure 13), exhibiting more connected networks both with increasing polymer mobility and increasing initial concentration. Following incubations with the highest concentration (20 μg/ml fibronectin) full networks on all the other three polymers (C >1) were observed. This material-driven fibrillogenesis is thought to be due to the reorientation of the fibronectin protein molecule to reveal hydrophobic sites which interact with the polymer backbone and lead to the exposure of fibronectin - fibronectin binding sites (1^{st}-5^{th} FNI repeats). It has been shown that blocking these sites which are found in the amino terminal of the molecule effectively inhibits fibronectin fibrillogenesis on C = 2 (Salmeron-Sanchez et al., 2011).

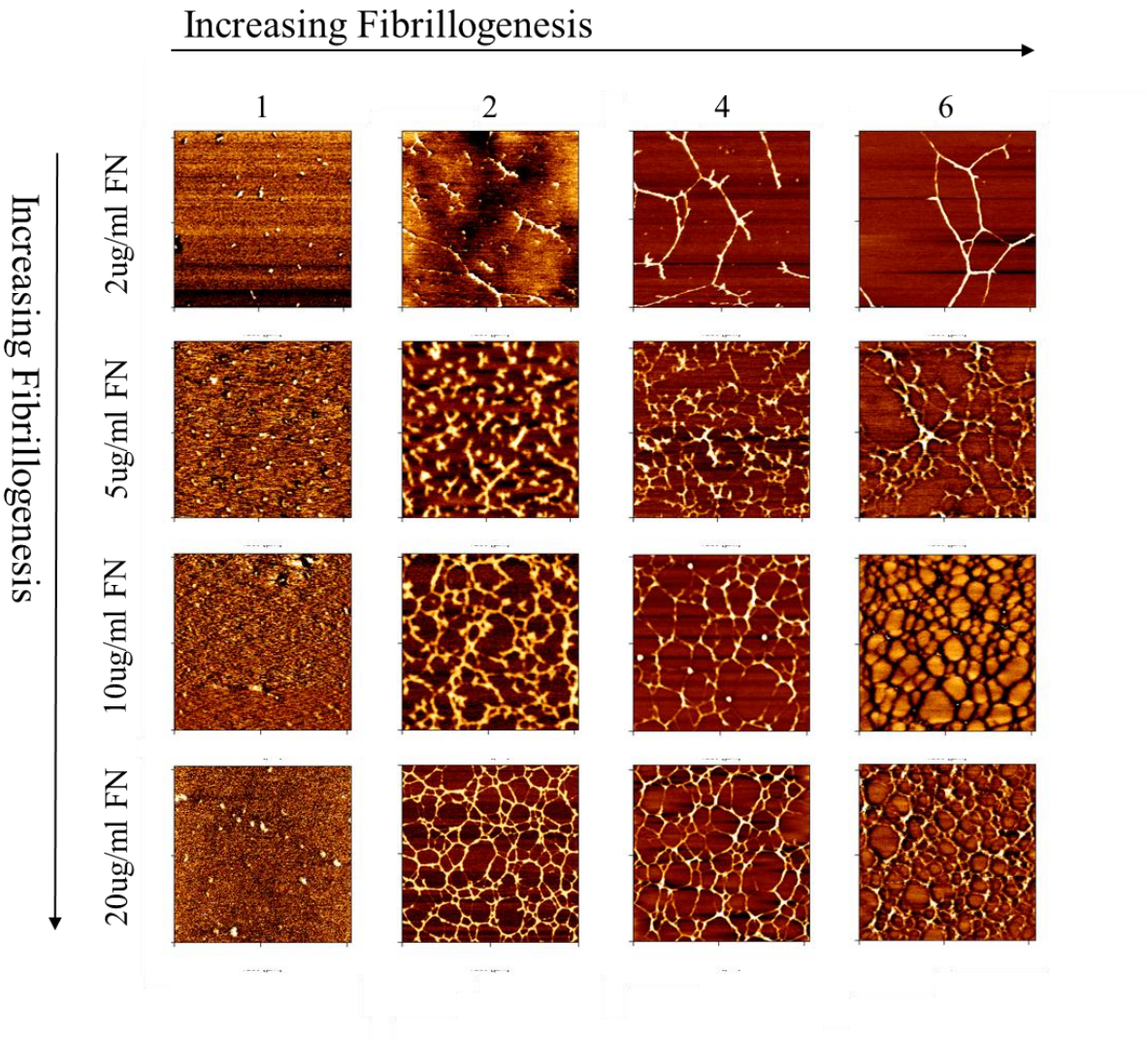

Figure 13 - AFM AC mode scans. Left to right: Scans of fibronectin on polymers with increasing number of carbons in the side chain. Top to bottom: AFM scans on the same polymer incubated with different initial fibronectin concentrations. Images are representative of three taken from each triplicate.

Immunofluorescence staining of the fibronectin coating on the polymers confirmed the AFM results, with deposits and networks observed on C = 1 and C > 1 respectively (Figure 14).

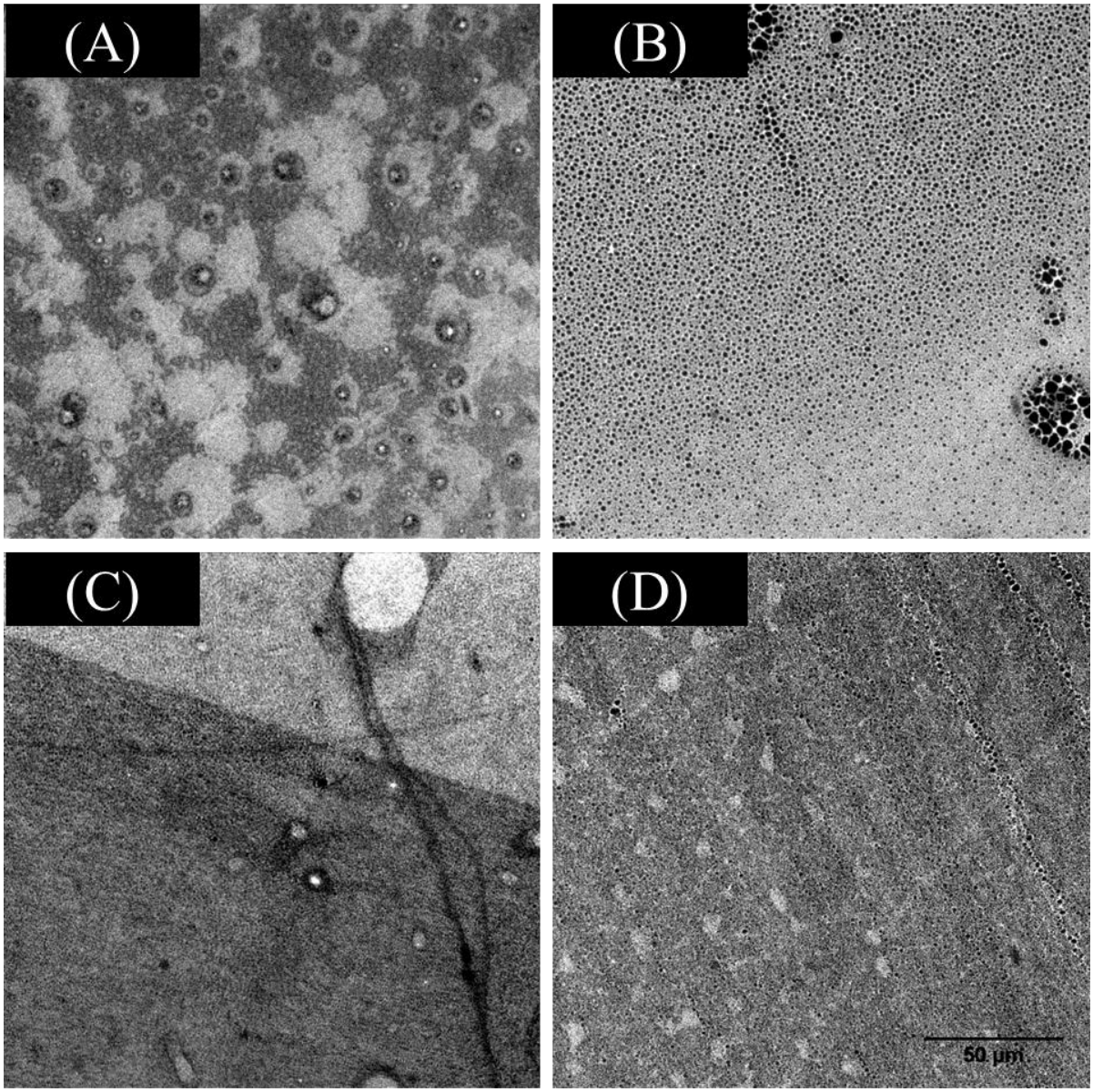

Figure 14 - fibronectin Immunofluorescence staining. A polyclonal antibody against fibronectin on the four polymer surfaces. fibronectin deposits can be seen on (A) C = 1 and fibronectin networks were observed on (B - D) C = 2, 4 and 6. Images are representative of three taken from each triplicate.

The density of adsorbed protein has also been shown to affect cell behaviour (Elias and Poloukhtine, 2013,).my analyses of fibronectin density on the polymer surfaces using the Micro BCA™ Protein Assay Kit (Thermo Fisher Scientific) revealed no significant differences between the densities on the different polymers for each initial adsorption

concentration (Figure 15). An approximate density of 400 – 600 ng/cm^2 was achieved when samples were incubated with 20 µg/ml of fibronectin solution. This is in agreement with previous analyses of the fibronectin coatings on these polymers (Guerra et al., 2010).

Quantification of adsorbed fibronectin by BCA

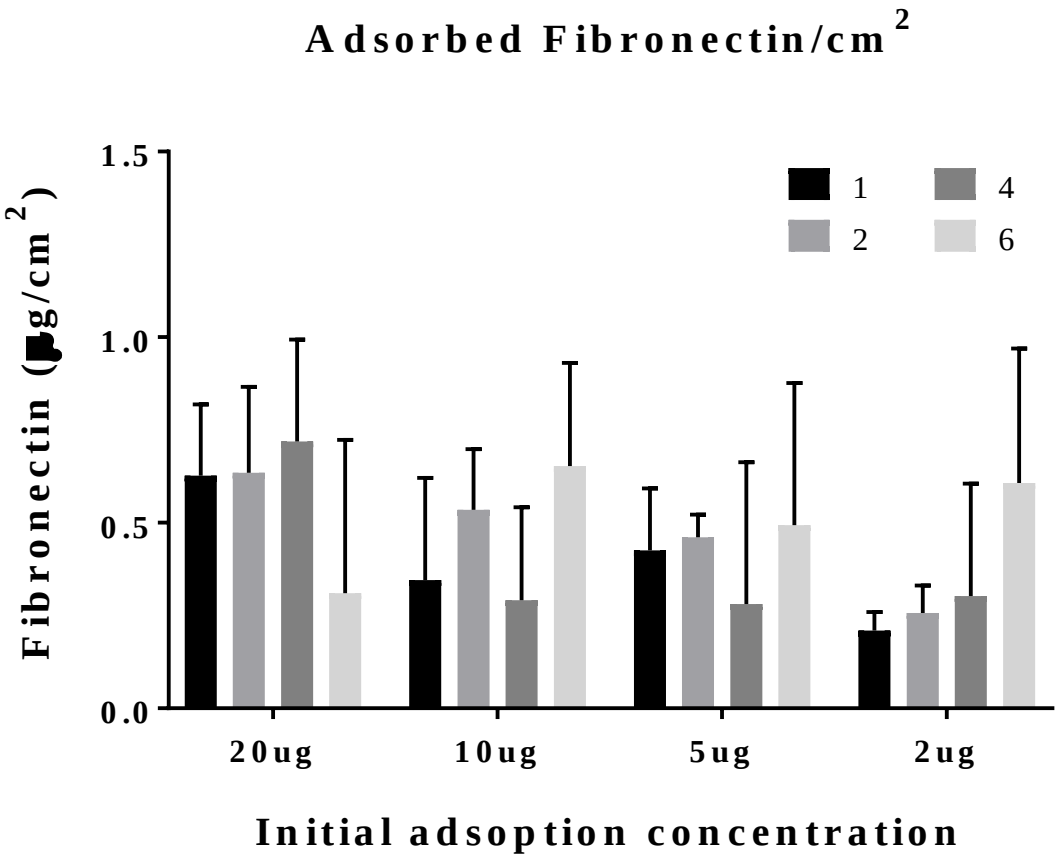

Figure 15 - Density of fibronectin adsorbed on the polymer surfaces. As quantified by the micro - bicinchoninic acid assay kit (BCA) by Thermo Scientific. Starting concentrations of incubation solutions are indicated on the x-axis. Each bar represents an average of 9 readings (3 from each triplicate). Standard deviations are indicated by black error bars.

The 20 µg/ml of fibronectin concentration was used as the initial adsorption concentration for all experiments that followed, since the networks formed were most complete and a higher surface density was achieved.

The fibronectin molecule is a mechanically stretchable molecule that contains within its structure, important sites for cellular interaction as already highlighted. *In vivo*, fibronectin fibrillogenesis is a cell mediated process where integrins stretch fibronectin molecules to reveal FN – FN sites for fibronectin network formation (Mao and Schwarzbauer, 2005) and other cell binding sites important for signalling. A single chain variable antibody fragment screened for specificity for stretched fibronectin over non-stretched fibronectin was used to analyse the fibronectin coatings on the polymers of interest (Figure 16). The highest signal came from analyses of the fibronectin fibrils on C = 2, indicating that fibrils on this polymer are most stretched.

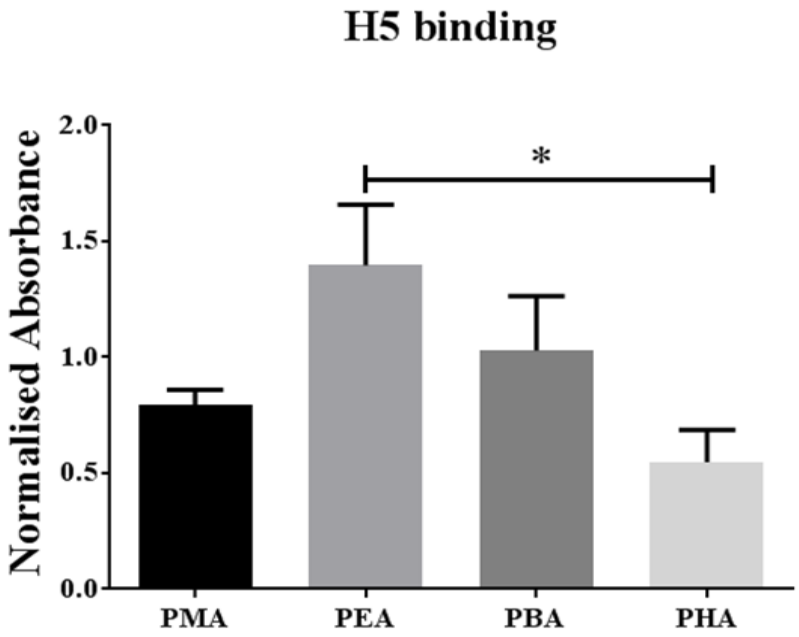

Figure 16 – Fibronectin stretching. ELISA quantification of fibronectin stretching using an antibody fragment which preferentially binds stretched over non – stretched fibronectin (Cao et al., 2012). The highest signal was observed on C = 2. The absorbance readings were normalised with respect to fibronectin availability (See Figure 17 B). Each bar represents an average of 9 readings (3 from each triplicate). Standard deviations are indicated by black error bars. One way Anova analysis revealed statistically significant difference: *$p \leq 0.05$ (GraphPad software, La Jolla, CA).

The relevance of fibronectin conformation and stretch analyses for cell response studies is dependent on whether fibronectin sites (Figure 17A) which allow cells to bind are exposed.

Fibronectin domains exposure by ELISAs for the RGD and Synergy sites

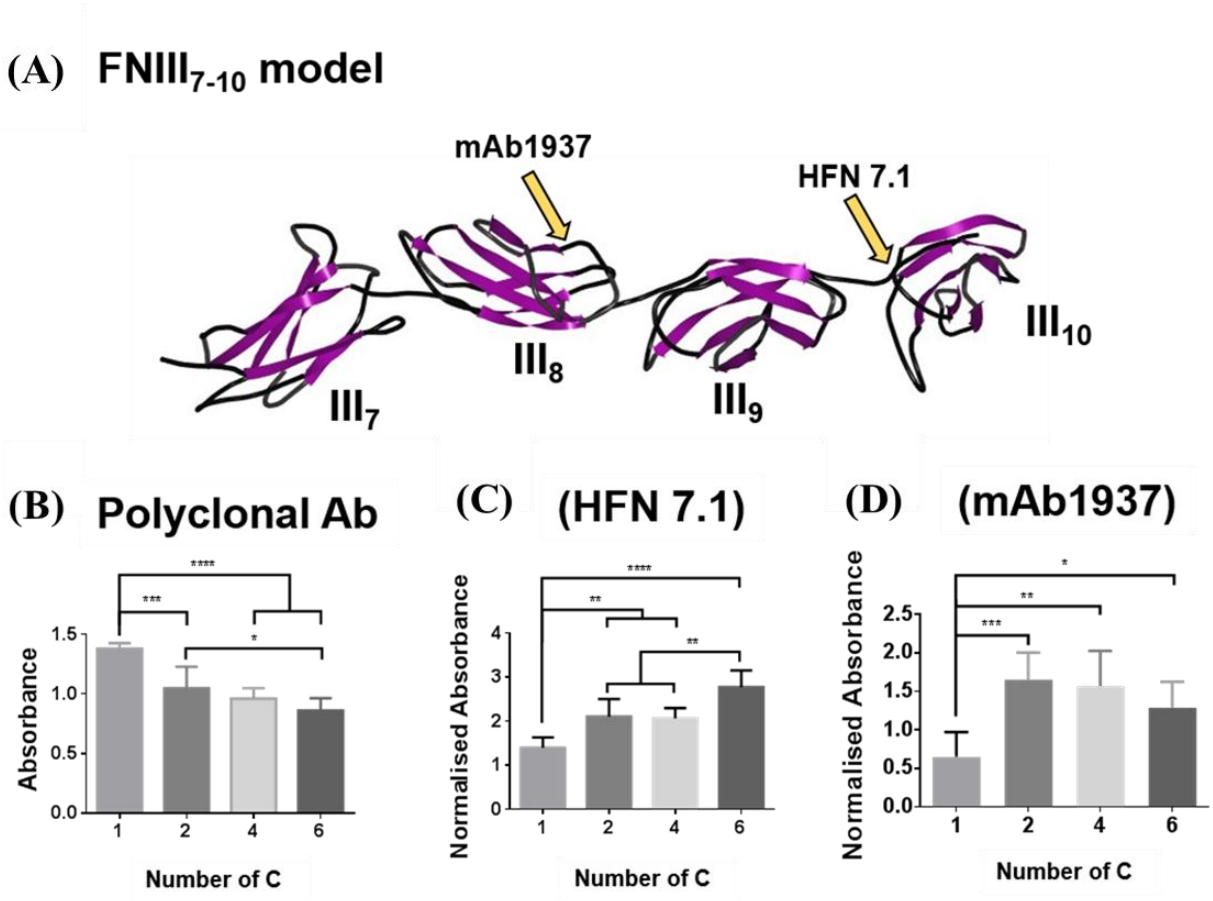

Figure 17 - Indirect analysis of fibronectin conformation using ELISAs. Analyses of the exposure of specific fibronectin structural sites upon adsorption of fibronectin on polymers using 20 μg/ml. (A) A 3D model of 7th – 10th FNIII with Yellow arrows pointing to the binding sites for mAb1937 (Synergy) and HFN 7.1 (RGD). Image adapted from the RCSB PDB (www.rcsb.org) (Leahy et al., 1996) PDB ID 1FNF. (B) Overall availability of fibronectin using a polyclonal antibody. (C) Exposure of cell binding site; RGD using the HFN 7.1 antibody. (D) Synergy site exposure (mAb 1937Ab). Graphs C and D were normalised with respect to fibronectin availability (B). Each bar in the graphs represents an average of 9 readings (3 from each triplicate) and standard deviations are indicated by black error bars. One way Anova analysis revealed statistically significant differences: *$p \leq 0.05$, **$p \leq 0.01$, ***$p \leq 0.001$, and ****$p \leq 0.0001$ (GraphPad software, La Jolla, CA).

Some of the most characterised and most important fibronectin sites for cell interaction include the RGD domain (shown as HFN 7.1) and the synergy site (PHSRN shown as

mAb1937).my ELISA analyses revealed that the exposure of these domains is indiscriminately higher on the fibronectin nanonetwork – forming polymers C > 1 compared to the globular fibronectin on C = 1 (Figure 17C and D).

The network-forming polymers (C = 2, 4 and 6) show similarity in their conformation; as shown by their comparable fractal dimension values (

Figure 12), and in domain exposure (Figure 17C and D). This indicates that the fibronectin conformation on these three polymers would not be a significant contributing factor to any observed differences in cell behaviour. However, the increase in fibronectin stretching observed on C = 2 using the H5 antibody fragment (Figure 16) may cause observable differences in cell behaviour.

Finally, the translation of mobility to the fibronectin layer from the underlying substrate was studied using FRAP analyses of fibronectin-FITC coated polymers (Figure 18). Fibronectin mobility was found to be in agreement with previous results from contact angle hysteresis which also gradually increased with branch chain length for the fibrillar fibronectin (C = 2, 4 and 6). Interfacial mobility however, decreased between C = 1 and C = 2, this is believed to be due to the stabilising conformational change which happens when fibronectin gains a fibrillar conformation on C = 2.

Fibronectin mobility

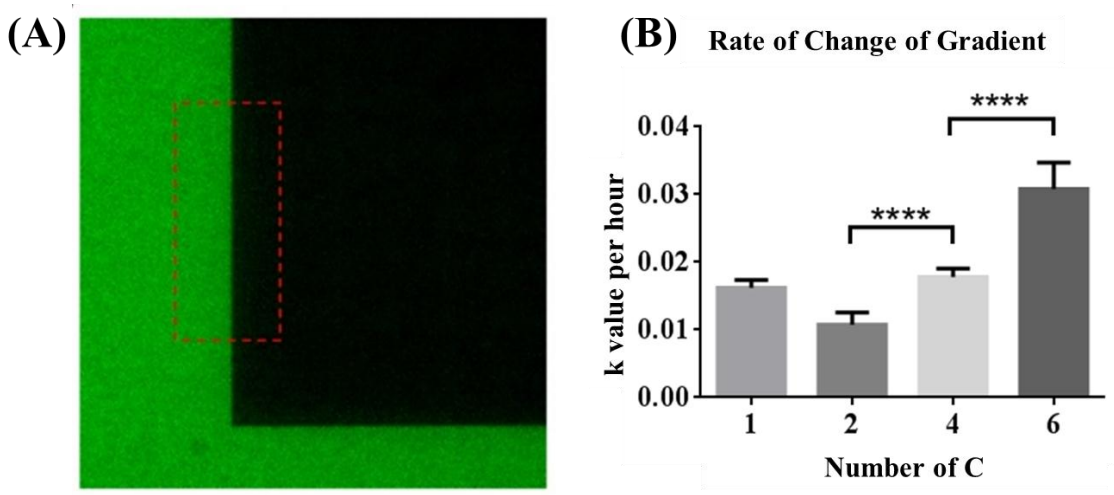

Figure 18 - Interfacial/Protein mobility. A measurement of the rate of change in fluorescence intensity profile indicating protein mobility. (A) Bleach border region, showing a manually area selected for analysis (dotted red box), the fluorescence intensity of the bleached area was compared to the unbleached area which was assumed to be 100% fluorescent. Images were taken every 24 hours for 120 hours. (B) The gradient of the linear region of the bleach border changed over time for each polymer surface. This experiment was carried out in collaboration with Mark Bennet as part of his Masters project (Bathawab et al., 2015). Each bar in the graphs represents an average of 9 readings (3 from each triplicate) and standard deviations are indicated by black error bars. One way Anova analysis revealed statistically significant differences: ****$p \leq 0.0001$ (GraphPad software, La Jolla, CA).

The interaction of fibronectin molecules with the polymers C = 2, C = 4 and C = 6 is likely followed by the exposure of the 1^{st}-5^{th} FNI repeats which are responsible for fibronectin-fibronectin interaction and leads to fibrillogenesis on these polymers (Salmeron-Sanchez et al., 2011). As fibronectin is extended on C = 2 compared with C = 1 and the fibronectin – fibronectin binding sites are exposed leading to the assembly of individual molecules into a network, the fibronectin layer is seen to exhibit lower mobility. While further increasing polymer mobility (C = 4 and C = 6) then translates to the protein layer and compensates for the initial reduction in mobility due to fibronectin network formation.

Conclusion

The four poly(alkyl acrylates) selected for this study differed merely in the length of their side chains, and is indicated as the number of carbon atoms (C) in the side chain throughout this report. The Tg of these polymers decreases with increasing side chain length, indicating increasing polymer mobility from C = 1 to C = 6. Characterization of these surfaces for physical properties known to influence cell behaviour revealed that they would all be perceived as too stiff by cells (Young's moduli > 40kPa (Balaban et al., 2001)), with negligible topographical cues (RMS roughness of ~$37.5 \pm 5.5 \times 101$ pm) and similar in their hydrophibicity (static contact angle). However, water contact angle hysteresis increased with mobility only on polymers coated with fibronectin or fibronectin - FITC. This assured us of

the similarity of my fibronectin and fibronectin – FITC fibrils, this is crucial as it enabled us to analyse the mobility of the fibronectin layer using FRAP.

It was believed that cells would perceive C = 2, C = 4 and C = 6 as similar surfaces since the exposure of the RGD and Synergy sites on these polymers was comparable. However, FRAP analyses revealed that the interfacial protein exhibited different levels of mobility on these polymers. These findings made it possible for us to attribute differences in my functional studies using cells on interfacial mobility.

Chapter 3

Introduction - Effect of Polymer Chain Mobility on Cell Behaviour

To study cell behaviour, 3 cell lines were used; C2C12 cells which are mouse premyoblasts, human fetal foreskin fibroblasts and mouse fibroblasts derived from connective tissue. C2C12 mouse muscle pre myoblasts are an established subclone initially produced by Blau et al. (Blau et al., 1983) and established by Yaffe et al. (Yaffe and Saxel, 1977). This cell line is frequently used to assess the differentiation potential of experimental conditions, as they easily differentiate to form myotubes containing characteristic muscle proteins when cultured in low serum. C2C12 pre myoblast cells retain the potential to differentiate to other cell lines including adipocytes (Ryan et al., 2013) and osteoblasts; where upon stimulation with BMP-2 the expression of osteogenic markers alkaline phosphatase and osteocalcin can be observed and the formation of myotubes expressing troponin and myosin heavy chain are inhibited (Katagiri et al., 1994).

The tuneable differentiation potential of C2C12 cells and their rapid doubling time make them an excellent cell line to use for initial proof of concept differentiation experiments. Moreover, similar to MSCs, the adhesion and differentiation of this pre myoblastic cell line has been shown to respond to physical cues such as adhesion surface shape (Bajaj et al., 2011) and topography (Wang et al., 2012). Unlike the osteogenic differentiation of MSCs whose markers such as osteocalcin can be observed after approximately 21 days of culture, the easily observable myogenic differentiation of C2C12 cells into myotubes requires only 4 days. C2C12 cells are therefore an excellent cell model for preliminary experiments to investigate how cells respond to surfaces of interest, for example in terms of their adhesion and differentiation.

There are different but similar protocols to induce the myogenic differentiation of C2C12 cells, most involve switching their state from proliferation to differentiation through serum starvation. This is done by culturing them with low serum. Undifferentiated C2C12 cells express sarcomeric actin and myosin; however, upon induction of differentiation, the cells fuse to form myotubes. Within the myotubes, the sarcomeric actin and myosin acquire a structured pattern, and this is followed by the appearance of sarcomeres and myofibrils at 4

days (Bajaj et al., 2011). Staining for sarcomeric myosin is therefore an extremely straightforward way to analyse C2C12 differentiation.

Fibroblasts are another well characterised cell type that is robust to culture and sensitive to external cues. For (non – differentiation) analyses; adhesion and cell shape I utilised human fetal foreskin fibroblasts (HFFF2 cells, Sigma - Aldrich) and mouse fibroblasts derived from connective tissue (L929 cells, ATCC). Cells adhere to surfaces via focal adhesions. Some focal adhesion parameters e.g. area and major axis length have been linked to certain cell behaviours (Kim and Wirtz, 2013), I, therefore, analysed focal adhesion major axes and studied their link with cell behaviour.

Fibronectin which is the protein used in this study to create an ECM-like environment for cells contains several sites for integrin binding, including sites specifically bound by $\alpha_v\beta_3$ and $\alpha_5\beta_1$ (Figure 19) (Roumen, 2002). However, integrin expression has also been linked to differentiation, with C2C12 differentiating to myotubes to high levels only when the fibronectin site for $\alpha_5\beta_1$ was available; the availability of the fibronectin binding site (PHSRN) for $\alpha_5\beta_1$ has been shown to vary with conformation, unlike the $\alpha_v\beta_3$ binding site (RGD). I, therefore, set out to analyse the differential expression of these two integrin heterodimers in C2C12 cells cultured on my fibronectin-coated polymers.

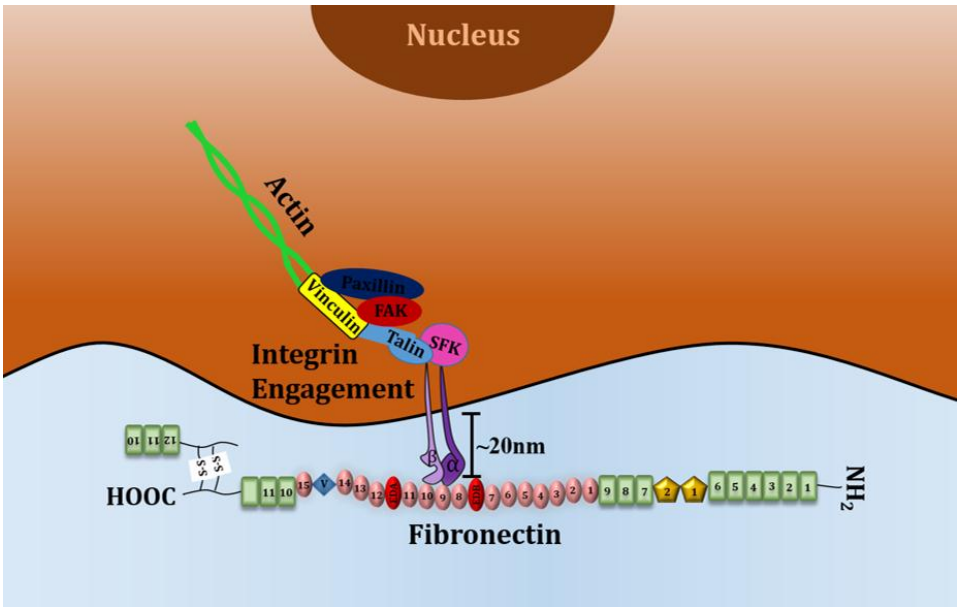

Figure 19 – Cell anchorage and signalling via integrins. Focal adhesions are dynamic complexes made up of several cytosolic proteins including talin, Src family kinases (SFK)

and vinculin which interact directly or indirectly with integrins. Integrin heads have been shown to protrude from the plasma membrane by approximately 20 nm (Nermut 1988) and to anchor cells by interacting with structural peptide sequences within ECM proteins such as fibronectin. Activated integrins may also cluster to produce amplified signalling and it has been shown that integrin interaction with fibronectin fibrils stimulate cytoskeletal contractility through a Rho-dependent mechanism (Hocking et al., 2000). Integrin signalling is reviewed in (Harburger and Calderwood 2009).

Integrins link with actin via cytosolic adhesion proteins such as talin, vinculin and paxillin (Figure 19) some of which interact directly with the actin cytoskeleton. Cytoskeletal contractility which is medicated by actin and myosin has been shown to play a key role in both the differentiation of C2C12 and the perception of mechanical cues. Blebbistatin (Straight et al., 2003) was thus used to inhibit myosin II which is required for contractile fibres, this was to test whether cells cultured on surfaces exhibiting interfacial mobility relied on contractility - related signalling to differentiate into myotubes.

Materials and Methods

Protein coating for cell culture

Collagen I coating

Control slides were wetted with 1 mg/ml collagen I (BD biosciences, USA) diluted in milliQ water. A drop of collagen I solution was placed on samples, allowed to spread and then removed, leaving a thin layer of COL I solution on the sample. Samples were covered and incubated for 1 hour and then uncovered to aid evaporation.

Fibronectin Coating

A 20 μg/ml solution of human fibronectin from plasma (Sigma - Aldrich) was prepared with DPBS++. Samples were then incubated with 200 μl fibronectin solution for 1 hour. Samples were then placed inside 24 well plates, washed with DPBS++ twice and were ready to use for cell culture.

C2C12 cell culture

Mouse premyoblasts (C2C12 cells, ATCC) were thawed and cultured for 48 hours in DMEM (4196, Gibco) with 1% penicillin – streptomycin (Gibco) and 20% FBS (Heat inactivated, Gibco). In a laminar flow hood, samples (prepared by spin coating polymer solutions onto coverslips as described in chapter 2) and control glass coverslips were sterilised using ultraviolet light for 20 minutes prior to use. Protein coating with fibronectin or collagen I (differentiation positive control) was performed on samples, this is described below. The positive control is based on the proven finding that collagen I coated glass reliably induces myogenic differentiation of C2C12 (Heino and Massague, 1990).

Cell harvesting: The medium was removed and the C2C12 cells were washed with 10 ml DPBS--/ 75cm^2 flask, 2 ml of Trypsin/EDTA solution was distributed to detach the cells, then 4 ml of 20% FBS in DMEM was added to neutralise the trypsin. The suspension was then centrifuged at 1300rpm and the supernatant was discarded. Fresh DMEM was used to resuspend the cell pellet and the cells were then counted using a hemocytometer. Cells were passaged when they reached ~80 % confluence, and only cells at passages lower than 10 were used for experimental purposes.

Cell morphology and fibronectin reorganization on polymer surfaces – L929 cells

L929 fibroblasts (ATCC) were cultured in DMEM (4196, Gibco), with 1% penicillin-streptomycin (Gibco) and 10% FBS (Heat inactivated, Gibco). Cell - mediated reorganisation

of the interfacial protein layer was studied by seeding cells on surfaces coated with fibronectin – FITC with ~5000 cells/cm^2 in the presence of 10% FBS. After a 3-hour incubation, cells were fixed with 4% formaldehyde for 20 minutes at 4°C and subsequently permeabilized with 0.1% Triton X-100 for 5 minutes. A blocking with 1% BSA for 20 minutes was carried out followed by actin staining for 1 h with rhodamine phallotoxin R415 (Life Technologies) used at 1:40 dilution. The actin stain was used as a mask for the reorganisation of the underlying fibronectin layer within the cell areas and determination of cell morphology.

Focal adhesion Immunofluorescence staining

For cell adhesion analyses C2C12 cells were seeded on fibronectin – coated polymers at 5000 cells/cm^2 without FBS and left to adhere in the incubator for 3 hours. Samples were then washed twice with DPBS++ and fixed for 30 minutes with 3.7 % formaldehyde at 4 ºC and finally washed with 1 ml DPBS. A permeabilization solution (10.3 g saccharose, 0.292 g NaCl, 0.06 g MgCl2, 0.476 g Hepes Buffer, 0.5 ml Triton X-100 was made up to 100ml, adjusted to pH 7.2 and filtered) for 4 minutes, this was then removed and samples were blocked with 1% BSA in DPBS for 30 minutes at room temperature on rotation. The blocking solution was removed and samples were incubated with mouse monoclonal anti-vinculin antibody at 1:400 in 1% BSA for 1 hour, at room temperature and rotation. Samples were washed twice with 0.5 % Tween 20 in DPBS which was then removed and the samples were incubated with Cy3 Anti-mouse at 1:100 and phalloidin at 1:100 for 1 hour at room temperature. This step was carried out in the absence of light. Samples were washed twice with wash buffer and mounted onto glass slides with Vectashield containing DAPI. Images were taken with a wide field fluorescence microscope, using DAPI, Cy3 and GFP filters.

Analysis:

The analysis of focal adhesions was performed using the online focal adhesion analysis server (ME and SM, 2013) which was instructed to produce a binary image (Figure 20B) of the vinculin staining (Figure 20A) with intensity over a given threshold within the cell mask (actin staining) to eliminate noise. The program then extracts parameters of interest such as cell size from the actin staining, the area of focal adhesions and their major axis lengths. This data was then used to produce the graphical analyses.

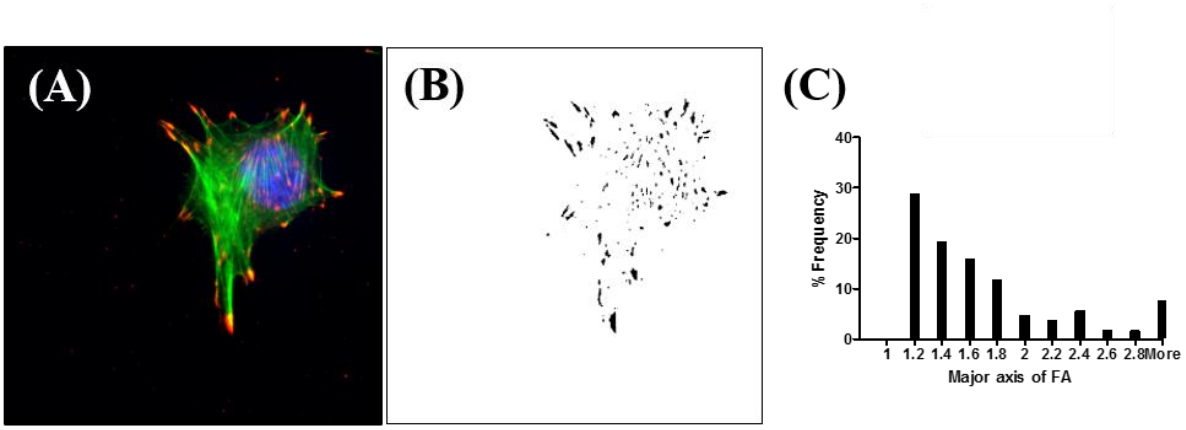

Figure 20: Focal adhesion analysis steps. Major axis lengths of the focal adhesions were analysed by first generating a binary image (B) from (A) the vinculin stain (Red). (C) A histogram of this data was then plotted, showing a major axis length profile. The actin staining (Green, image A) was used as a mask within which vinculin staining was analysed.

Integrin staining

HFFF2 cells were cultured using 10% FBS in DMEM without pyruvate (D5796, Sigma - Aldrich). The HFFF2 cells were seeded at 5000 cells/cm^2 with serum-free medium and then the medium was removed after 3 hours, cells were washed once with ice-cold PBS ++ at pH 7.4 and fixed using 4% formaldehyde (MeOH-free) in PBS for 10 minutes at room temperature. Samples were then rinsed 3 times with PBS, permeabilized with 0.2% TX-100

for 5 minutes at room temperature and rinsed twice with PBS. Samples were then blocked using 5% normal goat serum (Sigma - Aldrich) in PBS for 1 hour at room temperature and the incubated face down with primary antibodies in 5% normal goat serum for 1 hour at room temperature. Samples were then washed 3 times with PBS for 5 minutes each, and incubated with 1:1500 AlexaFluor secondaries (Thermo Fisher Scientific) in 5% normal goat serum in PBS for 1 hour at room temperature. They were then moved to 6-well plates, incubated with 1:1000 Hoechst for 1 minute, washed 3 times (5 minutes each wash) with PBS and rinsed once with deionised Water. Samples were then mounted with ProLong Gold (Invitrogen) and sealed with nail polish.

- Primary antibodies: Rat anti-beta1 (9EG7, BD Pharmingen) used at 1:200, mouse anti-αvβ3 (LM609, Millipore) at 1:300 dilution and rabbit anti-paxillin at 1:300 dilution
- Secondary Antibodies: AlexaFluors 488 (anti-mouse), 546 (anti-rat), and 633 (anti-rabbit).

Analysis

The analysis of fluorescence microscopy images was carried out using a Matlab program which created a mask using the Paxillin image and read intensity values from the β1 and β3 staining within this mask, the program then produced an intensity ratio (Figure 24B and C). The results are shown as heat maps. The original code (See Appendix B) was kindly offered by Vince Fiore at the Matrix Biology and Engineering Laboratory, Georgia Tech Atlanta.

C2C12 differentiation in the presence and absence of blebbistatin

C2C12 cells were thawed and cultured for 48 hours in DMEM (41965, Gibco) with 1% Penicillin-Streptomycin (Gibco) and 20% FBS (Heat inactivated, Gibco). Cell culture, cell harvesting and fibronectin coating, were performed on samples as previously described.

For the differentiation experiment, cell seeding was carried out at 18,500 cells/cm^2. Cells were diluted in DMEM (41965, Gibco) with 1% Penicillin - Streptomycin (Gibco) and 1%

Insulin-Transferrin-Selenium-Ethanolamine (ITS-X, Gibco), FBS was not added to this medium. After 3 hours, the media was refreshed and blebbistatin (Sigma - Aldrich) was added to experimental samples at a 10µM concentration. The differentiation experiment was carried out for a total of 96 hours and medium changed after 24 hours.

Fixation and immunostaining of differentiated C2C12 (4 days after seeding)

The medium was removed from the wells and samples were washed 3 times with DPBS++, fixed and permeabilized with (20:2:1 ETOH 70 %: Formaldehyde 37 %: Acetic acid) for 10 minutes at 4 º C, washed 3 times with DPBS, blocked with 5 % Normal goat serum (Sigma - Aldrich) in PBS for 1 hour at room temperature and washed 3 times with DPBS++. Samples were then incubated at 37 º C for 1 hour with MF20 anti-sarcomeric myosin (Developmental Studies Hybridoma Bank) diluted in 5 % Goat serum at 1:250. Samples were then washed 3 times with DPBS ++, blocked for 10 minutes at room temperature and washed again 3 times with DPBS++. The samples were then incubated for 1 hour at 37ºC with the secondary antibody Cy3 anti-mouse at 1:200 in 5 % Goat serum. This procedure was carried out in the absence of light. The samples were then washed 3 times with DPBS++ and then mounted with Vectashield mounting medium with DAPI (Vectorlabs). A wide-field fluorescent microscope was used to take the pictures using DAPI and Cy3 filters.

Results and Discussion

Fibronectin adsorbed on my polymers of interest, C = 1, 2, 4 and 6, in a globular conformation on C = 1 and in a fibrillar network conformation on C = 2, 4 and 6. Functional/ cell response studies on these polymers included analyses of the cell morphology, cell - mediated fibronectin reorganization on the polymers, focal adhesion formation, integrin recruitment and cell differentiation. These studies were carried out to characterise cell response to interfacial mobility of the fibronectin layer.

Cell morphology and cell - mediated fibronectin reorganization

L929 fibroblasts cultured on fibronectin – FITC coated samples showed no significant differences in their morphology (Figure 21) and were well spread with well-developed actin cytoskeletons.

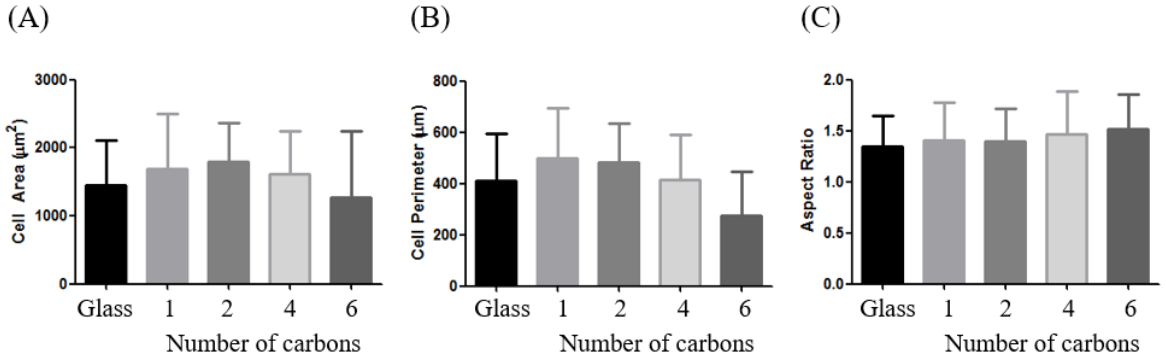

Figure 21: Characteristic cell morphology on the four polymer surfaces. (A) Cell area, (B) cell perimeter and (C) aspect ratio. This demonstrates that L929 cells have no significant morphological differences on each surface. This experiment was carried out in collaboration with Mark Bennet as part of his Masters project (Bathawab et al., 2015). Each bar in the graphs represents values derived from 9 images (3 from each triplicate), the standard deviations are indicated by black error bars.

However, reorganization of the fluorescently labelled fibronectin interfacial layer by L929 fibroblasts (Figure 22) was found to follow a similar non-monotonic trend as interfacial mobility observed from FRAP analyses (Figure 18).

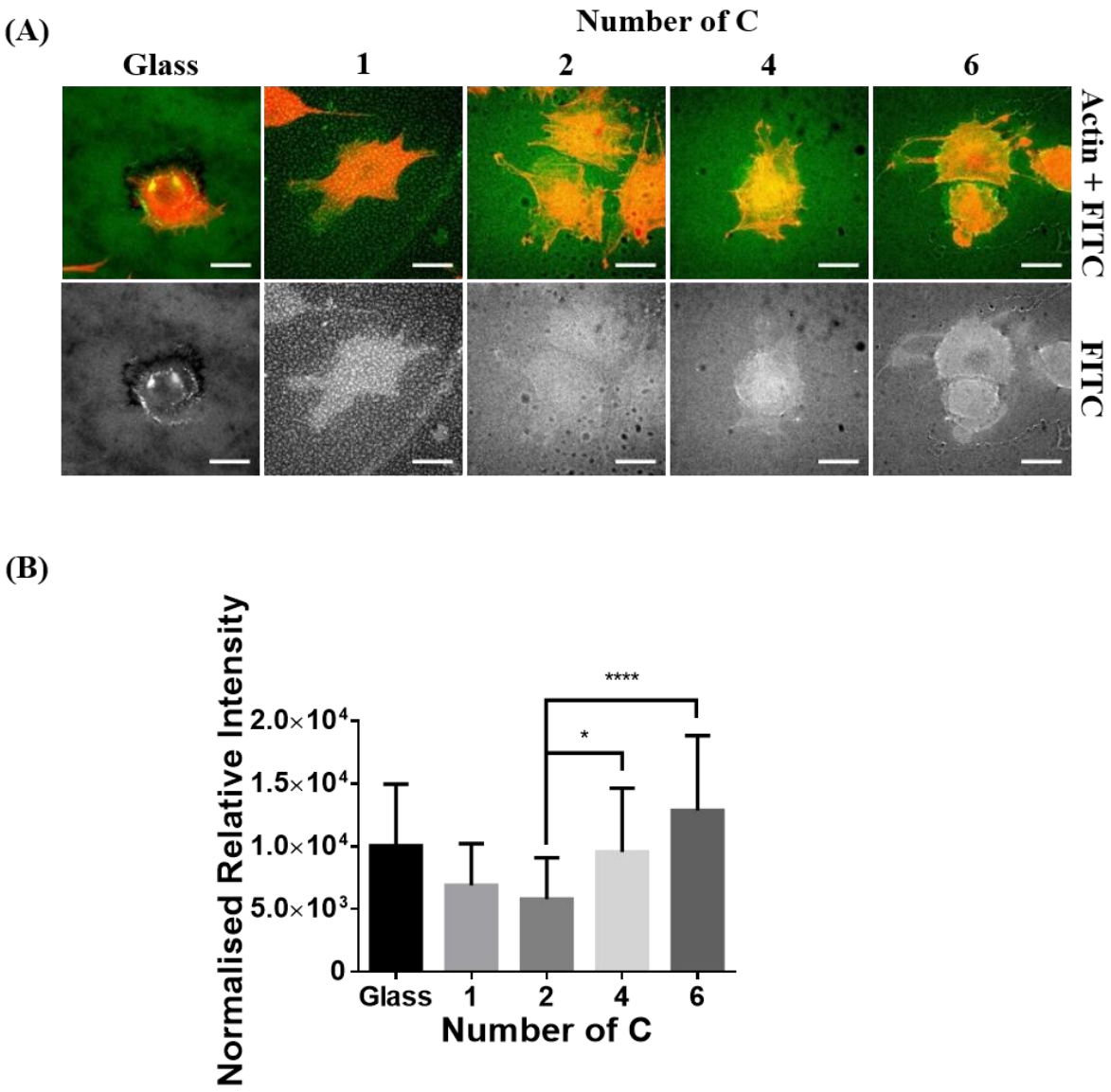

Figure 22 - Cell – mediated reorganisation of fibronectin-FITC on a glass control and four polymers of interest. (A) Cell area (Top panel) and corresponding fibronectin layer (Bottom panel). Scale bar; 25 µm), (B) Relative differences in fluorescence within the area of the cell (Actin mask) compared to outside the cell. This experiment was carried out in collaboration with Mark Bennet as part of his Masters project (Bathawab et al., 2015). Each bar in the graph represents values derived from 9 images (3 from each triplicate), the standard deviations are indicated by black error bars. One way Anova analysis revealed statistically significant differences: *$p \leq 0.05$ and ****$p \leq 0.0001$ (GraphPad software, La Jolla, CA).

The use of labelled fibronectin in the analyses of cell mediated reorganization eliminated the confusion caused by secreted fibronectin, and by comparing the difference in intensity between the inside / underneath the cell and around the cell (Figure 23 A). This semi-quantitative approach enabled us to determine the extent of fibronectin re-organization on the polymer surfaces. Fibronectin reorganization on the polymers was lowest on C = 1 and C = 2 and then rose with polymer mobility (increasing from C = 2 to C = 6), similar to the trend observed for interfacial mobility.

Adhesion of C2C12 cells on fibronectin coated polymers

The adhesion and differentiation of C2C12 cells cultured on the polymers were analysed. My surfaces differed in their polymer chain mobility, which has previously been shown to have a profound effect on cellular attachment (Liu et al., 2012), morphology (Seo and Yui, 2013) and cell differentiation (Gonzalez-Garcia et al., 2012). Results from this work indicate the translation of surface mobility to the interfacial protein layer (Chapter 2, Figure 18). I sought to relate this difference in fibronectin mobility to cell behaviour and hence analysed both the adhesion and differentiation of C2C12 cells.

Focal adhesions are dynamic and complex structures, constantly being assembled and disassembled. By fixing cells at a certain time point, a static photograph of this process is captured, and since focal adhesions are the first reaction of the cell to a surface, I analysed the adhesion of C2C12 cells only 3 hours after seeding.

The focal adhesion major axis length has been used to categorise and quantify adhesion data (Geiger et al., 2001), and studies show that it is directly affected by physical surface properties. It is, therefore, a reliable and accepted method for focal adhesion analysis (Balaban et al., 2001) (Riveline et al., 2001). As previously described the characterization of these polymers showed high similarity in their topography, hydrophobicity (Figure 11B) and stiffness (Figure 10), all of which influence cell behaviour including focal adhesion formation and cell differentiation (McBeath et al., 2004a) (Wang et al., 2012) (Engler et al., 2006).

Surface stiffness affects cell behaviour; however cells have been reported to exert stresses and respond to stiffnesses in the 1-40kPa range (Engler et al., 2006) while the stiffness of

these polymer films as determined by nanoindentation (Figure 10) are all in the MPa range, which is above the threshold detectable by cells.

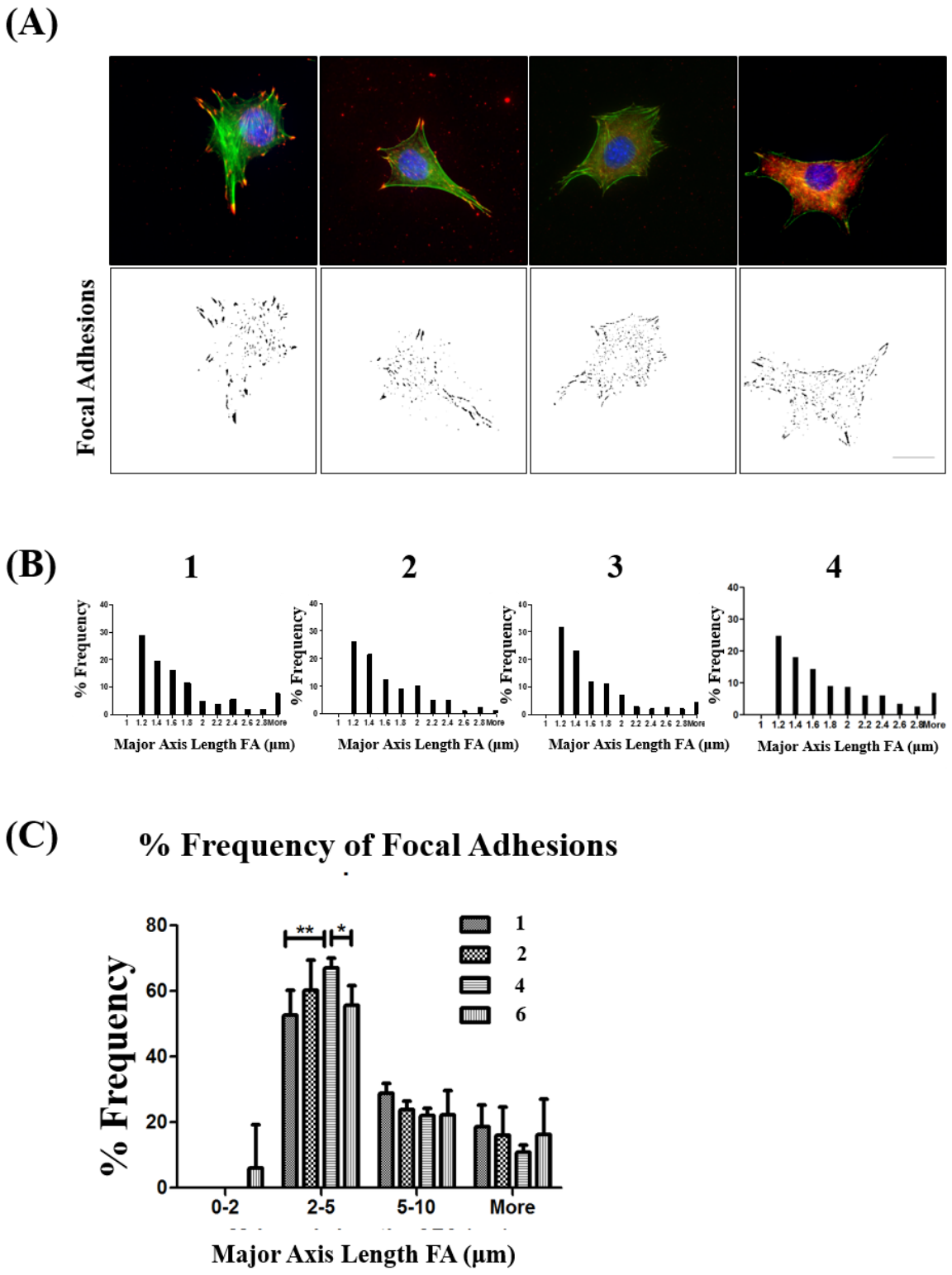

Figure 23 – Adhesion analyses of C2C12 cells (3 hours). (A) Immunostaining, top panel: vinculin (Red), actin (Green) and Dapi (Blue) and bottom panel: inverted focal adhesion

images. (B) Distributions of focal adhesion major axis lengths with their corresponding frequency, finally (C) normalised focal adhesions (in percentage) in relation to major axis length categories. (Bathawab et al., 2015). Each bar in the graph represents values derived from 9 images (3 from each triplicate), the standard deviations are indicated by black error bars. Focal contacts (major axis < 1µm) were filtered out. One way Anova analysis revealed statistically significant differences: *$p \leq 0.05$, **$p \leq 0.01$ (GraphPad software, La Jolla, CA).

Cell morphology, the arrangement of the actin cytoskeleton and traction forces, which vary with focal adhesion sizes, are all properties influenced by changes in stiffness (Discher et al., 2005) (Han et al., 2012). The lack of dependence of the behaviour of these cells on stiffness is supported by the observed lack of variation in their morphology (Figure 21) and in their focal adhesion profiles (Figure 23).

Integrin recruitment analysis

Integrins are used by cells to interact with ECM proteins. While each cell type may express a distinct set of integrins and the binding of some integrins to their ligand is redundant or overlap (Hynes, 1992), the availability of specific integrin ligands within ECM fibrils also dictates the choice of integrins recruited by cells on a substrate. Garcia et al., (1999) for example, utilised fibronectin conformation to bind and activate specific integrins in C2C12 cells thus modulating their differentiation. Using my surfaces which exhibit increasing mobility and fibrillar fibronectin (C = 2, 4 and 6), the recruitment of β1 and β3 integrin subunits by HFFF2 (fibroblast) cells 3 hours after seeding was analysed. This was done by quantifying the fluorescence intensity ratio between β1 and β3 images within a paxillin mask (Figure 24A), however, no differences were found between the polymers (graph in Figure 24B).

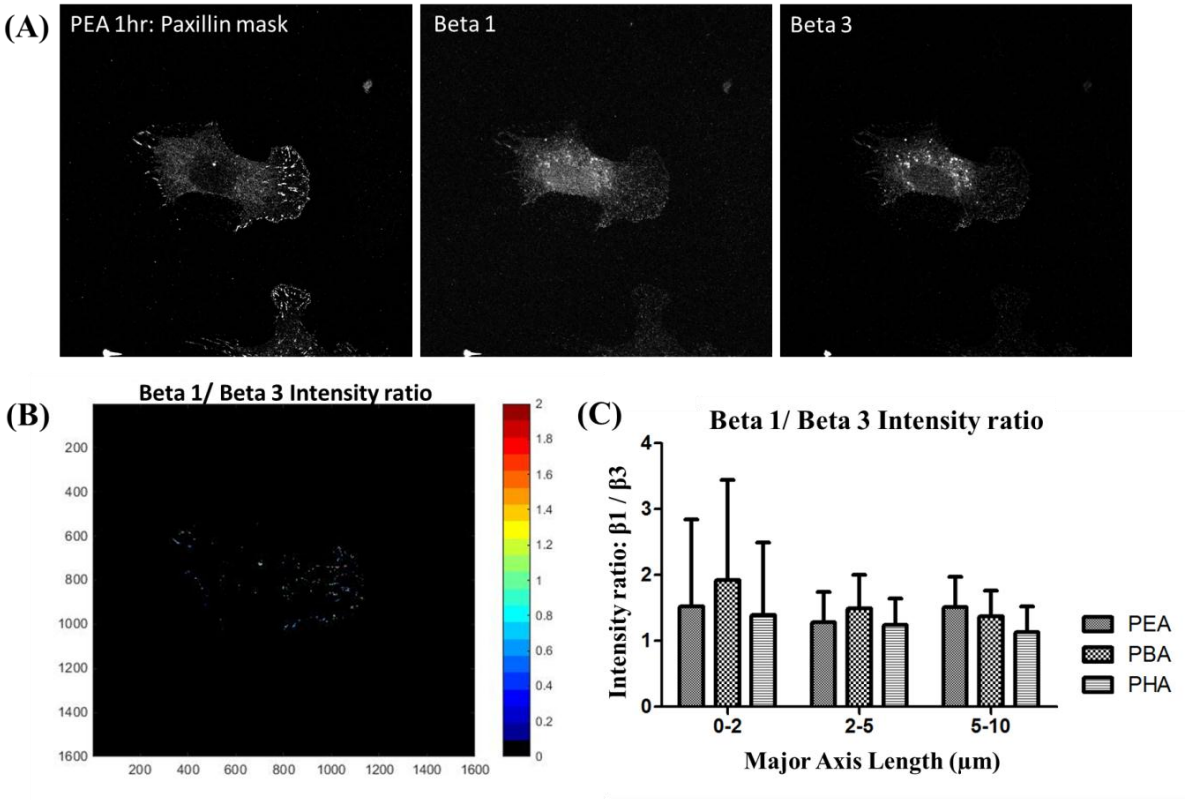

Figure 24 – Integrin recruitment analysis in human foreskin fibroblasts cultured for 3 hours on fibronectin-coated polymers. As example, images of the analysis on PEA are shown here, where a Matlab programme was used to calculate the ratio between the size of staining for (A) β_1 and β_3 integrin subunits within a paxillin stain which was used as a mask for focal adhesions. (B) A heat map of the ratios and (C) A graph of the intensity ratios. Each bar in the graphs represents an average of 9 readings (3 from each triplicate) and standard deviations are indicated by black error bars.

The image in Figure 24 B is an example of a heat map produced to represent the intensity ratios, as the differences were minimal, so are the ratios represented (lack of definition in the heatmap). The lack of difference in the recruitment of these subunits by HFFF2 cells suggests that any resulting differences in cell behaviour between the polymers would not be due to signalling via the β1 and β3 subunits. β1 and β3 subunits were analysed as they are known to interact with the RGD and Synergy sites within the structure of fibronectin (Plow et al., 2000).

C2C12 myogenic differentiation

C2C12 myogenic differentiation was used as another functional assay to analyse the effect of surface mobility on cell behaviour (Figure 25).

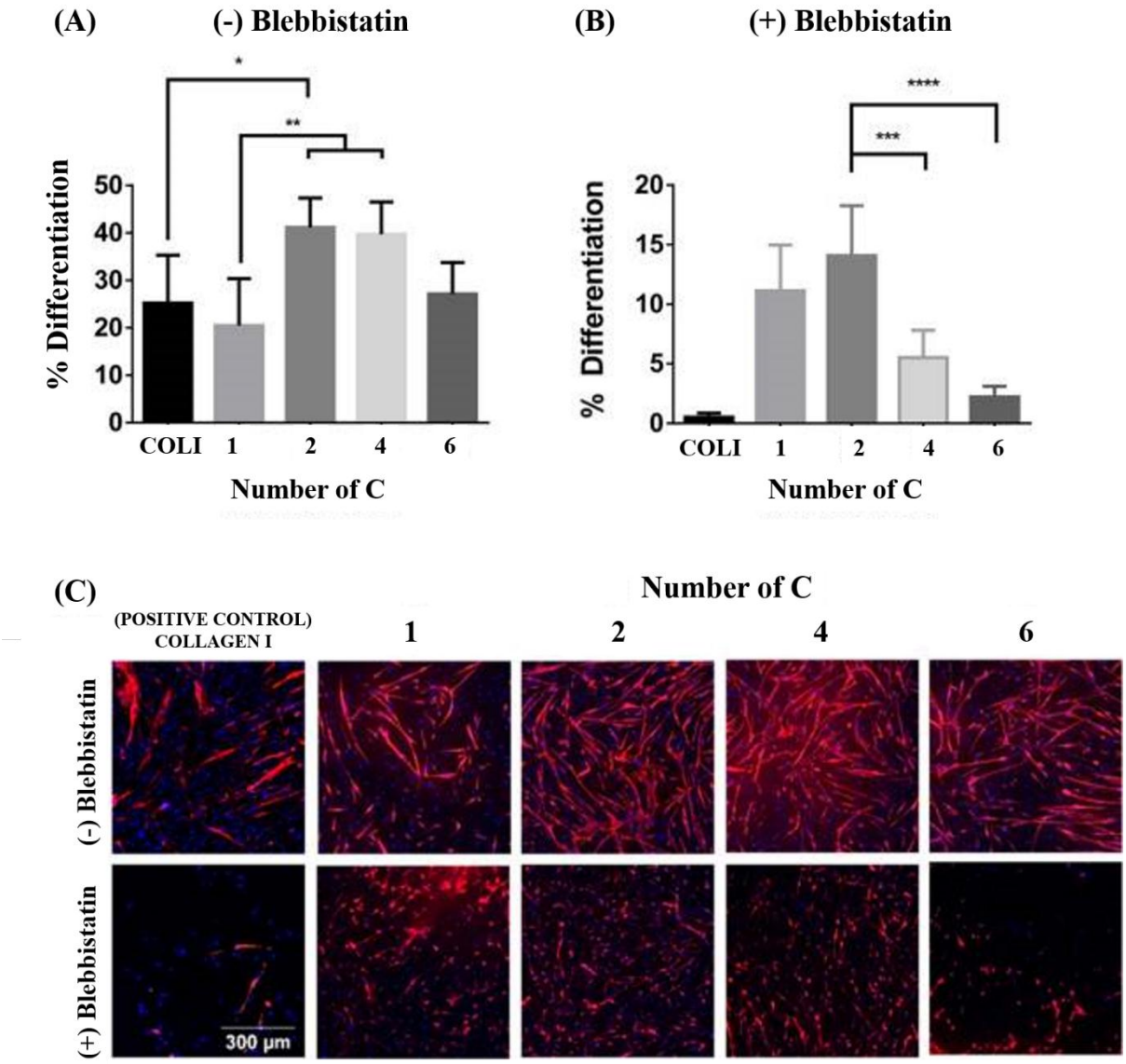

Figure 25 – C2C12 myogenic differentiation. In (C – Top panel) absence and (C – bottom panel) presence of the myosin II inhibitor; Blebbistatin. Myogenic differentiation as quantified by myosin II staining (RED) shows high differentiation on C = 2 and C = 4, however, in the presence of Blebbistatin this increase is abolished on C = 4 and maintained on C = 2. Therefore, suggesting that myogenic differentiation on mobile polymers is contractility dependent. Each bar in the graph represents values derived from 9 images (3 from each triplicate), the standard deviations are indicated by black error bars. One way

Anova analysis revealed statistically significant differences: *$p \leq 0.05$, **$p \leq 0.01$, ***$p \leq 0.001$, and ****$p \leq 0.0001$ (GraphPad software, La Jolla, CA).

When cultured in low serum (differentiation medium), C2C12 cells differentiated to different degrees on the four surfaces, with significantly higher differentiation on C = 2 and C = 4 compared with the collagen coated sample (positive control), C = 1 and C = 6 surfaces (Figure 25A and C top panel).

This difference in myogenic differentiation was enhanced by the presence of the myosin II inhibitor, blebbistatin (Figure 25B and C bottom panel). With minimal differences between the conformation of fibronectin nanonetworks and domain exposure on C = 2, 4 and 6 (

Figure 12 and Figure 17), the difference in myogenic differentiation of C2C12 cells can be attributed to the mobility of the interfacial protein layer (Figure 18).

Blebbistatin is a highly selective inhibitor with a high affinity for ADP (Adenosine diphosphate) and phosphate bound myosin II thus slowing down their release and effectively reducing myosin II affinity for actin binding (Straight et al., 2003). My results (Figure 25B and C bottom panel) show that contractility mediated by actin and myosin II filament bundles plays an essential role in mobility-dependent myogenesis, and when it is inhibited the less mobile surfaces produced greater levels of differentiation. The role of contractility in mobility - dependent myogenesis needs further investigation as contractility itself has been linked to both promotion (Dhawan, 2004) and reduction (Castellani et al., 2006) of myogenic differentiation. Therefore, better understanding of the relationship between C2C12 differentiation and contractility in general, is required, as studies using selective inhibitors of different components of the contractility pathway may yield contradicting results.

Conclusions

Four polymers (C = 1, 2, 4 and 6) with increasing mobility were used in this study to investigate the effect of mobility on cell behaviour. Three of these polymers induce cell independent fibronectin network formation, whose analysis revealed minimal differences in the fibronectin conformation and domain exposure, however, results from FRAP analyses showed that the mobility of the fibronectin networks on C $\geq$2 polymer surfaces, increased with the underlying polymer mobility.

Cell studies on these surfaces revealed that reorganization followed a similar trend as the mobility of the interfacial protein layer, while other morphological parameters including cell shape and focal adhesions remained similar between the polymers. No significant differences were observed for the cellular recruitment of integrin subunits β1 and β3, while cytoskeletal contractility played a role in the mobility - dependent myogenic differentiation of C2C12 cells.

Chapter 4 – hMSCs for Osteogenic differentiation

Introduction

Cells including MSCs have been shown to be responsive to their environment; relevant to this work is their responsiveness to physical cues (McNamara et al., 2010) (Engler et al., 2006) (McBeath et al., 2004b) (Tsimbouri et al., 2014). This study focuses on polymer mobility; an intrinsic physical property of polymers inversely proportional to the Tg (See Chapter 1 - Introduction).

As previously discussed, MSCs hold great potential in the development of regenerative therapies for different tissues, due to their multipotency (Becker, 1963) and ability to respond to differentiation cues *in vitro* (Gimble et al., 2008). Conventionally, biochemical supplements including animal products, nucleic acids and recombinant growth factors have been used to modulate stem cell differentiation (Li and WJiang, 2013), however it is now established that inherent factors which are always present in the environment of the cell can be fine - tuned to elicit desired cellular responses including stem cell differentiation with a potency that rivals biochemical signals (Murphy et al., 2014). This has provided material scientists and stem cell biologists with a platform to work together to create inductive surfaces for applications in tissue engineering and biomaterial design.

The biomimetic approach involves the incorporation of biological molecules onto biomaterial surfaces in ways that enables specific and desirable interactions to occur between cells and biomaterial, and consequently elicit desired cell responses (Shin et al., 2003). Incorporation of these bioactive molecules into the biomaterial is preferred over their addition into the environment in soluble form, as low doses can be used at the desired location for a more targeted approach (Lee et al., 2013) with reduced side effects (Carragee et al., 2011). A useful property of my four polymers of interest is that they readily adsorb the ECM protein fibronectin without any surface modification, thus providing a biomimetic surface. Furthermore, we utilised the fibronectin growth factor binding site to incorporate the BMP-2 onto the surface, hence creating a potentially inductive biomaterial for use in osteogenic differentiation of MSCs. Mymain aim was to study the four surfaces which are very similar in their chemistry, to find out if their varied mobility enhanced MSC osteogenic differentiation, using a fibronectin coating and a very low dose of surface bound BMP-2.

One area of huge demand for cell-based regenerative therapies is the rising global burden of musculoskeletal problems caused by injury, age or disease. Bone grafts are currently the gold standard treatment for bone deficiency. In Europe alone approximately one million patients undergo reconstructive bone surgery every year, this number is increasing due to an ageing population, and many of these surgeries require grafting. A bone graft can be an autograft, an allograft or a synthetic material (Pryor, 2009) for example hydroxyapatite. Autografts are preferred as they are safest and most effective since the patient's own bone is used to provide cells with a natural substrate on which to grow while allografts pose the risk of rejection and infection, and are therefore used in non - viable decellularised format. The drawback with autografts is that an extra surgical site is added for the patient increasing their pain and other complications e.g. infection, and the bone volume that can be acquired is limited to ~20cm^3 (Burchardt et al., 1987).

Multipotent MSCs are present in bone and researchers have long searched for biomaterials other than allografts and autografts to use for bone regeneration (De Groot, 1983) (Daculsi, 1998) (Laurencin et al., 2006). Perhaps to develop tissue engineered bone grafts, the process of tissue engineering using biomaterials would involve extraction of MSCs from the bone marrow (autologous – preferred), expansion of the MSCs *in vitro*, MSC seeding onto biomaterial scaffold and grafting the scaffold in the injury site to regenerate bone over time (Figure 26).

MSC isolation and use in tissue engineering

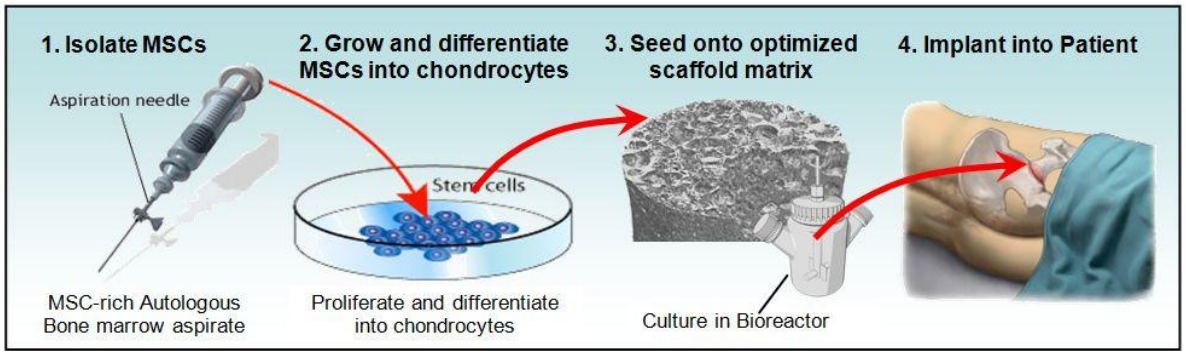

Figure 26 – The classical process of tissue engineering (grafts). Where MSCs are harvested from the body (autologous cells are preferred), cultured and proliferated *in vitro*

then placed onto biomaterials with inductive features for the differentiation of hMSCs to the desired cell type. The setup is then implanted into the patient's injury site to start the regenerative process. Figure sourced with permission (Oseni et al., 2011).

Biomaterials may be incorporated with growth factors to encourage MSC proliferation, differentiation and crucial processes, for example vascularization (Lee et al., 2011). For grafts, biodegradable biomaterial scaffolds are preferred to eliminate the need for their removal post initial surgery. As previously discussed, biomaterials for use in bone may also be decorated with physical surface properties shown to improve osteointegration e.g. chemistry (Morris et al., 2000), topography (McNamara et al., 2010) and coatings of ECM proteins/ protein fragments (Rammelt et al., 2004).

Reconstruction of large bone defects presents a great orthopaedic challenge, as conventionally used materials (calcium phosphate based) fail to act as bone substitutes or to induce the formation of new bone (Bohner and Galea, 2012). Very few bone substitutes have been trialled at the clinical stage and are mainly restricted to defects of a small size; reasons include lack of adequate vascularization, the high cost of isolation, culture and osteogenic differentiation of autologous stem cells. There are also numerous variables determining the success of these trials, including cell source, usage of growth factors, dosage for each biomaterial and timing.

Apart from complete tissue regeneration at an injury site, biomaterials for bone are also highly sought after to be used as implant coatings for improved implant osteointegration and to discourage undesirable processes e.g. bacterial colonisation of the implant surface.

Cell signalling during bone formation

The most potent growth factor used in conjunction with biomaterials for bone is BMP-2 (Agrawal and Sinha, 2016). BMPs are secreted ECM-associated proteins which belong to the Transforming Growth Factor-β (TGF-β) superfamily (Bragdon, 2011). The TGF-β signalling pathway is essential for development such that mouse knockouts of its components result in

embryonic lethality (Zhang and Bradley, 1996) or serious defects. Moreover several human clinical disorders including bone disorders, vascular diseases and cancers are associated with the dysregulation of BMP signalling, also reviewed in (Salazar and Rosen, 2016).

The TGF-β pathway has several layers of regulation including agonistic and antagonistic ligands, phosphorylation of cytoplasmic receptor substrate proteins or R-Smads (versus the existence of inhibitory Smads). The interaction of the R-Smads with a Co-Smad (Smad 4) to form complexes which translocate to the nucleus and recruit DNA binding co-factors for gene selectivity and further interaction of gene activators or repressors (Schmierer, 2007). In this way, the TGF-β pathway regulates hundreds of genes and plays a crucial role in the cell's ability to translate complex inputs into distinct behaviour as reviewed in (Schmierer, 2007). Spatiotemporal control of the activation of this pathway plays a key role in development.

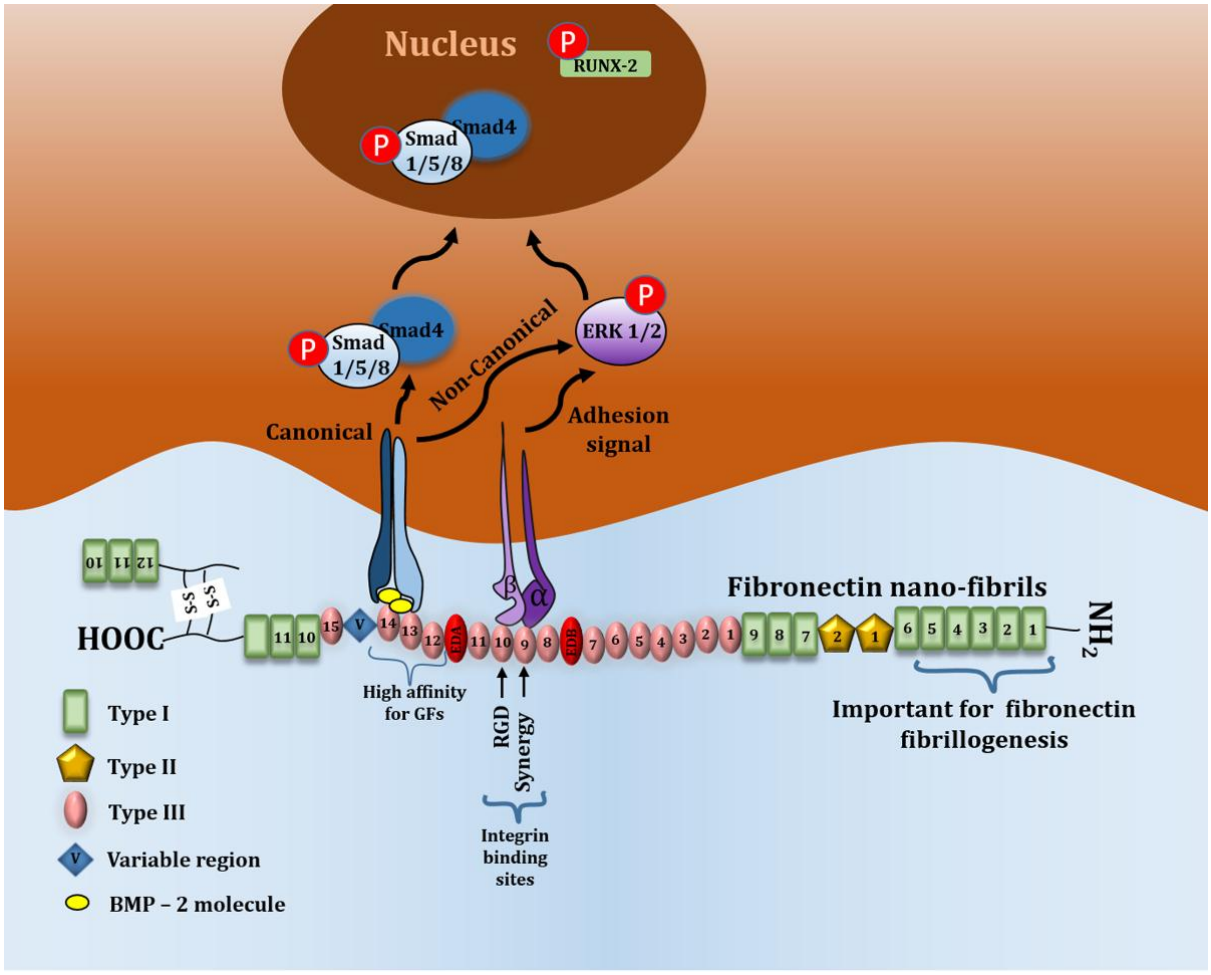

Figure 27 – The TGF-β pathway. Canonical and non-canonical signalling pathways for osteogenic differentiation. Showing the BMP-2 growth factor presented on the fibronectin

growth factor binding site. In the canonical TGF-β/BMP signalling, receptor regulated smads are phosphorylated by activated receptors, they then form a complex with smad4 (a co-smad). This complex is translocated to the nucleus where it induces the expression and phosphorylation of Runx-2. Runx-2 binds a promoter region in several osteoblast specific genes, thus regulating the expression of alkaline phosphatase, osteopontin and osteocalcin. The canonical and non - canonical pathways converge in the nucleus both resulting in increased Runx-2 expression with Erk1/2 activation (non - canonical) enhancing Runx-2 stabilization and transcriptional activity. The adhesion signal from integrin receptors also activates Erk.

In the 1980s BMPs were first characterised and cloned and this was followed by efforts to characterise them biochemically. The ability of some BMPs to induce MSCs to differentiate into bone and cartilage has now been established, with BMP-2, 4, 6, 7 and 9 known for their bone inducing activity (Bigham-Sadegh, 2014) (Luu et al., 2007). Other BMPs, for example, BMP-3 and BMP-13 negatively regulate bone formation (Shen et al., 2009) (Daluiski et al., 2001).

Signalling by BMPs can be canonical or non-canonical. In canonical signalling, BMPs bind a type I and type II serine/threonine kinase heterodimeric receptors. These receptors have a short extracellular domain, a single transmembrane domain and an intracellular domain with serine/threonine kinase activity. Three out of the seven type I TGF receptors and three out of the four type II receptors bind BMPs. BMP-2 and BMP-4 first bind type I receptors and recruit type II receptors while BMP-6 and BMP-7 bind type II receptors first and recruit type I receptors (De Caestecker, 2004). Some BMP-2 receptors are dimerized prior to ligand binding, and variation in the oligomerization process of these proteins determines which signalling pathways are activated (Nohe, 2002). However, another protein; noggin acts antagonistically to BMP-2 (Figure 28).

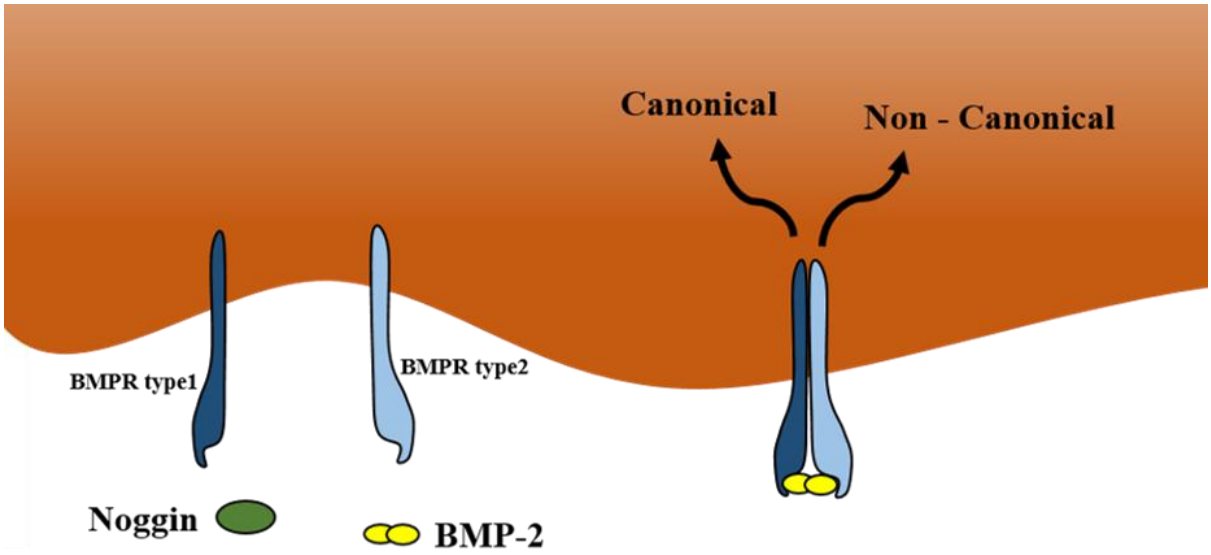

Figure 28- Agonist and antagonist of the BMP receptor. Upon BMP-2 binding the type I and type II BMP receptors dimerise. The growth factor BMP-2 activates the canonical and non-canonical TGF-β pathways. Noggin is able to bind the BMP-2 receptor binding site, therefore effectively blocking BMP-2 activation.

BMPs signal via the canonical (Smad - dependent) and (other) non – canonical pathways (Hayrapetyan et al., 2014). The canonical pathway begins with the BMP ligand binding to the constitutively active type II BMP receptor which then dimerizes and phosphorylates the type I receptor activating it (Figure 28) (Massague and Chen, 2000) (De Caestecker, 2004). The type I receptor then phosphorylates the downstream receptor-regulated Smads (Smad 1/5/8 or R-Smads) (Horbelt, 2012), and the phosphorylated R-smads then associate with Smad4 (a Co-Smad) to form a transcriptional regulatory complex which then translocates to the nucleus where it activates the transcription of specific genes (Attisano and Wrana, 2000).

The activated Smad1/5/8/Smad4 transcription complex interacts with several transcription factors and co-activators including Dlx5 (Distal-Less Homeobox 5), Runx2 and Osx (Osterix) (Ross and Hill, 2008). Runx-2 is a member of the Runt-domain gene family (Kania, 1990) and an essential gene transcription factor for osteoblastogenesis (Komori, 1997) (Enomoto, 2000). It is used as an early marker of osteogenesis as the expression and phosphorylation of

this transcription factor increases immediately upon induction of osteogenic differentiation (Ducy et al., 1997).

BMP/TGFβ also activates the non – canonical signalling pathway (Smad - independent), in which the mitogen-activated protein kinase [MAPK] pathway is activated (Hayrapetyan et al., 2014). Both the smad - dependent and smad - independent pathways (Erk1/2) converge at the nucleus with the upregulation and phosphorylation of Runx - 2 (Lee et al., 2002). Erk1/2 activation has been shown to stabilize and increase the transcriptional activity of Runx-2 (Liu and Lee, 2012). Runx-2 regulates the expression of several osteoblast specific genes, it does this by binding their promoter region (Ducy et al., 1997), consequently high levels of Runx - 2 mRNA enhances osteoblastic differentiation (Zhang et al., 2006).

Role of surface physical properties in MSC differentiation

The cytoskeleton is made up of dynamic structures and several surface physical properties have been found to influence cytoskeletal organization. MSCs cultured on stiff surfaces exhibit high cytoskeletal tension (contractility) and differentiate to the osteoblastic lineage (Engler et al., 2006). Certain topographies (Dalby et al., 2007) and chemistries (Li and WJiang, 2013) have also been identified for different differentiation paths for example osteogenic differentiation (Kingham, 2011). Furthermore, it was realised that the cell shape, which is dependent on contractility of the cytoskeleton, is a key driver of the cellular decision to differentiate down a certain path (McBeath et al., 2004b). Such that round cells achieved by modification of substrates with cell - adhesive islands led to cells differentiating to the adipogenic lineage, in contrast with highly spread cells which preferred the osteoblastic lineage (McBeath et al., 2004b). These studies on spreadability of cells also correlate high contractility in highly spread cells with increased expression of the small GTPase RhoA and its downstream effector Rho-associated protein kinase (ROCK) driving osteogenesis (McBeath et al., 2004b) (Bhadriraju K et al., 2007) (Kilian et al., 2010).

Figure 29 illustrates the role of RhoA and its downstream effector Rho-associated coiled-coil forming protein serine/threonine kinase (ROCK) which are components of the mitogen-activated protein kinase (MAPK) pathway in actomyosin contractility. This pathway can be

activated by diverse extracellular signals (*Yan* et al., 2012) (Plotkin, 2005). Erk1/2 is also activated by RhoA, and both this protein and ROCK are known to induce higher expression and phosphorylation of the osteogenic transcription factor, Runx-2(Castellani et al., 2006). The concept of cells perceiving physical cues and translating them into biochemical signals is known as mechanotransduction (Ingber, 1997).

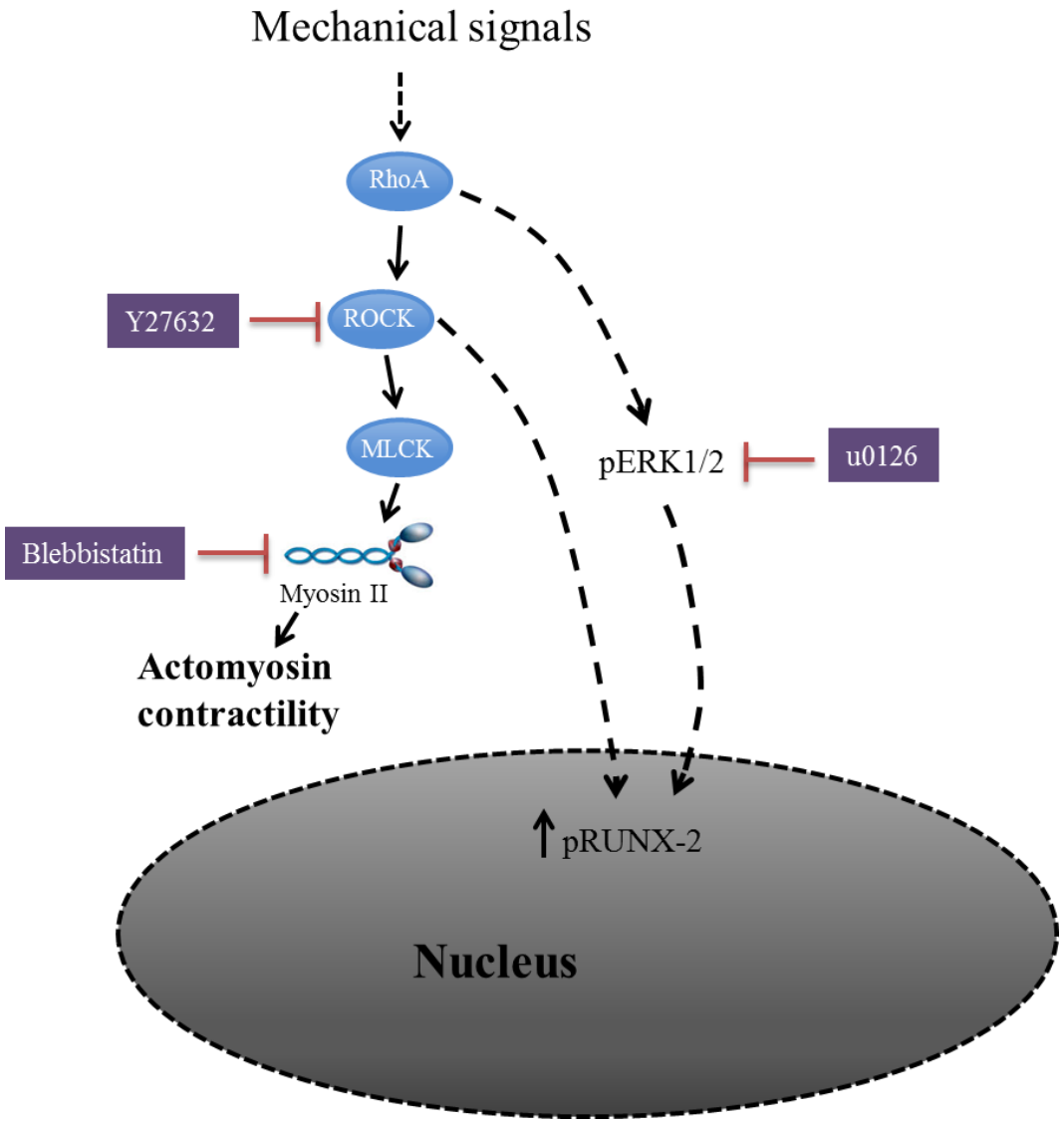

Figure 29 – Schematic showing pathways activated by Physical cues. Such as stiffness and topography, affecting differentiation of hMSCs. Inhibitors used in this work to study these pathways are highlighted in purple boxes. RhoA signalling in implicated in Actomyosin contractility via ROCK and myosin light - chain kinase and the activation of Erk1/2. This figure illustrates how mechanical cues can induce Runx-2 expression and phosphorylation via ROCK and Erk1/2 signalling.

Cells perceive mechanical and biochemical cues in an interdependent manner, such that their response to biological ligands is not only dependent on the cell type, but also the location/environment of the cells. For example, even though BMPs are known for their ability to induce osteogenesis, they play an essential role in the development of the heart (Zhang and Bradley, 1996), lung (El-Bizri et al., 2008) and kidney (Cain et al., 2008) and prior to that, BMP4 gradients mediate the dorsal-ventral patterning of the body (Schmidt et al., 1995).

Conjugation of biomaterials with BMP-2 for research and therapeutics

BMPs have revolutionised treatments of bone disorders. However, regrettably, their increasing use has left behind a profile of side effects, which can be serious and their frequency higher (20-50% of cases) than previously indicated by the original industry-backed publications (Carragee et al., 2011). Carragee's critical review (2011) also highlighted the link between higher doses of rhBMP-2 and a greater apparent risk of new malignancy. It is, therefore, preferable to deliver low doses of BMP-2 directly to the site of interest, and biomaterials offer a means of their delivery (Martino et al., 2011).

Inductive biomaterials for tissue engineering are highly sought after, in this work I utilise polymer surfaces of varied molecular mobility, coated with fibronectin to test whether MSCs respond to molecular mobility. As my results show the translation of surface mobility to the interfacial protein layer, I sought to understand if MSCs are able to detect this mobility of the interfacial layer. I also utilised the fibronectin growth factor binding site (Martino and Hubbell, 2010a) (Roumen, 2002) to present BMP-2 to the cells in conjunction with the integrin binding sites.

Aims, hypotheses and outline

The main aim of this part of the project was to assess MSC response to my materials. To begin with, I analysed MSC behaviour when cultured on fibronectin coatings with varied

mobility, after 21 days there was higher expression of osteocalcin on C = 2 than on the rest of the surfaces. I therefore, used specific inhibitors to study the role of Erk1/2 (Liu and Lee, 2012) and components of the adhesion - related contractility pathway (Arnsdorf et al., 2009); myosin II and ROCK in this observation. Moreover, I analysed my fibronectin samples for the exposure of the promiscuous growth factor binding site (Martino and Hubbell, 2010a) and BMP-2 binding, I then incubated my samples with a BMP-2 solution to create surfaces conjugated with BMP-2. Finally, I analysed osteocalcin expression by MSCs cultured on my BMP-2 conjugated surfaces compared with soluble BMP-2 in culture medium. My experiments revealed higher expression of osteocalcin on the polymer with a fibrillar network and the least interfacial fibronectin mobility. To understand this phenomenon at the molecular level, I quantified the phosphorylation of smad1/5/8 (canonical pathway (Chen et al., 2012)), Erk1/2 (non - canonical (Liu and Lee, 2012)) which are both implicated in increasing the osteogenic transcription factor; Runx-2 (Lee et al., 2002).

Materials and Methods

hMSC cell culture and osteogenic differentiation

Proliferating hMSCs from adult bone marrow were acquired from Promocell (Cat C-12975, Germany). These cells are positively selected for the following surface proteins; the presence of CD44 and CD105 (Endoglin) and the absence of CD31, and CD45.

The medium used for cell culture and experiments was DMEM (D5671, Sigma - Aldrich) with 10 % FBS (Gibco), 0.1 µM Sodium pyruvate (Gibco) and 1% antibiotic mix (0.6 ml of Fungizone (Gibco), 7.5 ml of 200mM L-glutamine (Sigma - Aldrich) and 5 ml of 10,000 U/ml Penicillin-Streptomycin (Gibco). Except when BMP-2 (R&D Systems) was added, then 1% FBS was used, to limit the effects of FBS components on cell behaviour.

MSCs cultured as described above were harvested for experimental purposes in their 1st – 4th passage and seeded on experimental samples coated with fibronectin (cell harvesting and fibronectin coating was carried out as previously described in Chapter 3 - Materials and Methods). Cell seeding was performed at 2500 cells/cm^2 for all experiments.

As a positive control for osteogenic differentiation, cells were cultured in osteoinductive medium (DMEM with 10 % FBS, 1% antibiotic mix, 0.1 µM Dexamethasone, 25 µg/ml L-ascorbic acid, 3mM NaH_2PO_4). This medium recipe will be from here on referred to as osteogenic medium. hMSCs were cryopreserved in 70 % FBS, 10%DMSO and 20 % DMEM (Zuk and Katz 2001).

Immunostaining of osteogenic markers osteocalcin and osteopontin

Samples were washed with DPBS once and then fixed for 15 minutes at room temperature with 4 % Formaldehyde. The fixative was removed and cells were permeabilised with a solution of 10.3 g saccharose, 0.292 g NaCl, 0.06 g MgCl2, 0.476 g Hepes Buffer, 0.5 ml Triton X-100 which was then made up to 100ml and pH adjusted to 7.2. The permeabilization was carried out at 4°C for 4 minutes. Samples were then blocked with 1% BSA solution and incubated at 37°C for 5 minutes. The primary antibody (specific against osteocalcin or osteopontin, both from Santa Cruz Biotechnology) diluted at 1:50 in 1 % BSA was then added and incubated for 1 hour at 37 °C. The samples were washed 3 times with 0.5% Tween20 (5 minutes each wash) and a solution of biotinylated anti – mouse antibody was then added at a dilution of 1:50. Samples were wrapped in foil and incubated at 37 °C for 1 hour and then washed thrice with 0.5% Tween20. This was followed by the incubation of samples with Streptavidin-FITC (1:50, Vectorlabs) and the actin stain phalloidin (1:500, Life Technologies) for 30 minutes at 37 °C after which the samples were washed thrice with 0.5% Tween20 and mounted with mounting medium with DAPI (Vectorlabs) ready for fluorescent imaging.

Mechanistic studies using inhibitors of Erk1/2, ROCK and myosin II

Erk1/2 inhibitor (u0126, Promega madison WI USA), Y27632 ROCK inhibitor (dihydrochloride) (Y0503, Sigma - Aldrich) and Blebbistatin (B0560, Sigma - Aldrich) were

each used at 10μM final concentration in medium. This experiment consisted of the three experimental conditions (using each inhibitor) and a control condition where MSCs were cultured on fibronectin samples without any inhibitor in the medium. This experiment was carried out for 21 days with 10% FBS in DMEM, after which the cells on samples were stained for osteocalcin.

Preparation of samples with surface bound BMP-2

Samples coated for 1 hour with 20 μg/ml fibronectin as previously described, were washed with DPBS++ and subsequently incubated for 1 hour with 100 ng/ml recombinant human BMP-2 from Chinese hamster ovary cells (R&D Systems).

Growth factor binding site exposure on fibronectin coatings - direct ELISA

A specific antibody was used to investigate the availability of the heparin II domain of fibronectin adhered on different materials. Sample triplicates were incubated with 20 μg/ml fibronectin in DPBS++ and another 3 samples were incubated only with DPBS (0 μg/ml) for 1 hour on the bench. They were then washed twice with DPBS ++, transferred into 24 well plated and blocked for 30 minutes using 1% BSA solution (Sigma - Aldrich). The samples were then incubated at 37°C with a monoclonal mouse primary antibody solution (P5F3, Santa Cruz Biotechnology) against the heparin II domain at 1: 30 in 1% BSA. The samples were then washed twice with 0.5% Tween20 and incubated for 1 hour with a goat anti-mouse HRP-tagged secondary antibody (R&D systems) used at 1:2000 at room temperature. Samples were then washed twice with 0.5% Tween20 and transferred into new 24 well plates. 300 μl/well of the substrate solution was added to each sample in the absence of light and incubated for 20 minutes. Finally, 150 μl/well of stop solution was added to each well. Absorbance was measured at 450 nm and 540 nm (Blank reading) using a plate reader. The

substrate solution and stop solution from the ELISA kit by R&D Systems from Minneapolis, USA.

Density of bound BMP-2 on fibronectin coatings - sandwich ELISA

The human BMP-2 DuoSet ELISA kit (R&D Systems) was used to measure BMP-2 bound onto fibronectin - coated samples. Samples were either unblocked or blocked with a heparin II domain antibody (P5F3, Santa Cruz Biotechnology). All samples were first coated with fibronectin as previously described. For the blocked samples; the growth factor site (Heparin II domain) antibody was used 1:1 molar ratio with fibronectin coating, to ensure complete blocking of the growth factor site. All samples were then incubated with 100 ng/ml human BMP-2 (R&D Systems). The ELISA plate was prepared (Overnight with capture antibody) as per product instructions, and the unbound BMP-2 (after incubation on the samples) was analysed by the sandwich ELISA method as detailed in the product manual. The amount of unbound BMP-2 was calculated from the optical density readings against a standard curve and the initial incubation volume, and subtracted from the initial amount used for adsorption on each sample.

MSC differentiation in the presence of BMP – 2 stimulation

For this experiment, I used three conditions;

- BMP-2 in medium (100 ng/ml human BMP-2 (R&D Systems). in 1% FBS DMEM)
- BMP-2 (R&D Systems) bound on fibronectin coated polymers (initial adsorption concentration of 100 ng/ml) and basal BMP-2 stimulation in medium at 25 ng/ml.
- Noggin, a BMP-2 antagonist was used at 50 ng/ml in 1% FBS DMEM with added 100ng/ml BMP-2.

I selected this conditions to compare the effect of BMP-2 freely available in solution with BMP-2 bound on fibronectin coatings. I also used noggin as a negative control and to establish if any osteogenic differentiation observed was indeed due to BMP-2 stimulation.

MSC culture on these conditions was maintained for 21 days, after which the samples were stained for osteocalcin.

Analysis of the phosphorylation of Smad 1/5/8, Erk1/2 and Runx-2 using the In-Cell Western™ Assay

Cells seeded n C = 2 and C = 6 samples were left to adhere for 1.5 hours. They were then washed once with DPBS and fixed with 4% Formaldehyde for 15 mins at room temperature; they were then permeabilized with (a solution of 10.3 g saccharose, 0.292 g NaCl, 0.06 g $MgCl_2$, 0.476 g Hepes Buffer, 0.5 ml Triton X-100 made up to 100ml, adjusted to pH 7.2 and filtered) at 4ºC for 4 minutes. This was directly followed with a blocking using the blocking buffer provided by *LI-COR* for 1.5 hours on rotation. The blocking was then removed and the primary antibody diluted at 1:50 in *LI-COR* blocking buffer was added and incubated for 2.5 hours on rotation. The samples were then washed with 0.1% Tween20, and incubated with a *LI-COR* labelled secondary antibody (1:800) and CellTag (1:500). Samples were then washed 5 times for 5 minutes each time with 0.1% Tween20. The samples were imaged using the ODYSSEY® Sa Infrared Imaging System.

In this experiment 2 sets of monoclonal antibodies; against total proteins and their phosphorylated version were used at a dilution of 1:50 in *LI-COR* blocking buffer.

- Smad antibodies (Rabbit, Cell Signalling Technology); Smad1 (mAb 6944), Smad5 (mAb 12534) and specific antibodies against phospho - Smad1/5 Ser463/465 (Rabbit mAb 9516).
- Erk1/2 antibody (Rabbit mAb 9154, Cell Signalling Technology) and phospho-specific Phospho-p44/42 Erk1/2 (Rabbit mAb 4370, Cell Signalling Technology).
- Antibody against Runx-2 (M-70, sc-10758) and phospho-Runx-2 antibody from Santa Cruz Biotechnology

Calcium Assay

Deposition of calcium by cells was assayed using the o-cresolphthalein complexone method (Sharp, 2011) after 21 days of culture in experimental and control conditions. This method is based on the reaction of calcium ions with o-cresolphthalein complexone in alkaline solution to form an intensely violet coloured complex, whose maximum absorbance occurs at 577 nm. The absorbance levels are directly proportional to the initial calcium concentration.

Samples were prepared by incubation with 1M hydrochloric acid for 8 hours at room temperature; this was to ensure that all deposited calcium was solubilised. Dibasic calcium phosphate $CaHPO_4$ (Sigma - Aldrich) was used to make up solutions of 1600, 800, 400, 200, 100, 50, 25, 12.5, 6.25 and 0µg/ml in 1 M HCl for standard curve measurements.

A colour reagent was prepared using 0.1 mg/ml o-cresolphthalein complexone (Sigma – Aldrich) and 1 mg/ml 8-hydroxyquinoline (Sigma – Aldrich) in 0.2 M HCl. Equal volumes of alkaline buffer solution (Sigma - Aldrich) and the colour reagent were mixed together. 5 µl of standard or test sample was then added to 200 µl of this mixture. 100 µl of the final mixture for each sample was transferred into a 96 well plate and the optical density was read using a spectrophotometer at 577nm. The calcium concentration per sample was calculated using the standard curve.

Results and Discussion

Behaviour of mesenchymal stem cells on biomaterials

As described in Chapter 2, four poly(alkyl acrylates) with increasing mobility were selected for this study, three of which induce the spontaneous formation of fibronectin fibrils upon adsorption. The fibronectin structure contains a region in its structure with high affinity for several growth factors (Martino and Hubbell, 2010a) and if this site is exposed then incubation with a solution of BMP-2 on fibronectin-coated polymers would encourage specific and strong binding of BMP-2 molecules on the fibronectin sites. It was thus

hypothesised that the availability of BMP-2 (bound to fibronectin at the growth factor site (Martino and Hubbell, 2010a)) close to the integrin binding synergy site (PHSRN), would encourage their simultaneous binding leading to a synergistic effect on the activated signalling pathways.

Previous characterization of the polymer surfaces revealed that they exhibit comparable hydrophobicity (static contact angle) and that fibronectin adsorption led to the assembly of physiological-like fibrillar nanonetworks on C = 2, C = 4 and C = 6. In addition, the mobility of adsorbed fibronectin was lower on C = 2 than C = 1 and then increased gradually with increasing mobility of the underlying surface (Figure 18). The decrease in interfacial mobility between C = 1 and C = 2 is thought to be due to the stabilising change in fibronectin conformation from globular to fibrillar, as discussed in Chapter 2.

In this part of the study, I focused on studying the effect of this observed fibronectin interfacial mobility (Figure 18) (Bathawab et al., 2015) on the behaviour of hMSCs, in conjunction with and without bound and soluble BMP-2. hMSC osteogenic differentiation was quantified after 21 days of culture in two ways; the expression of extracellular osteogenic markers; osteocalcin or osteopontin and the deposition of calcium otherwise referred to as mineralisation.

Osteogenic differentiation of MSCs in the absence of differentiating stimuli

Analyses of 21-day MSC cultures on samples in the absence of differentiation cues revealed that there was higher expression of the osteogenic markers; osteopontin and osteocalcin on C = 2 compared with the other three polymer surfaces (Figure 30A and B). Significantly higher expression of osteocalcin (One way Anova) was observed on C = 2 compared with the rest of the polymers; however, it was much lower than the osteogenic control (Figure 30B). This is also the case for the amount of calcium deposited by the samples (Figure 31). These observations are not in agreement with results from a previous study by Gonzalez-Garcia, et al. (Gonzalez-Garcia et al., 2012) which found for similar experimental conditions but on C = 1, 2 and 4, the lowest expression of osteocalcin and osteopontin on C = 2.

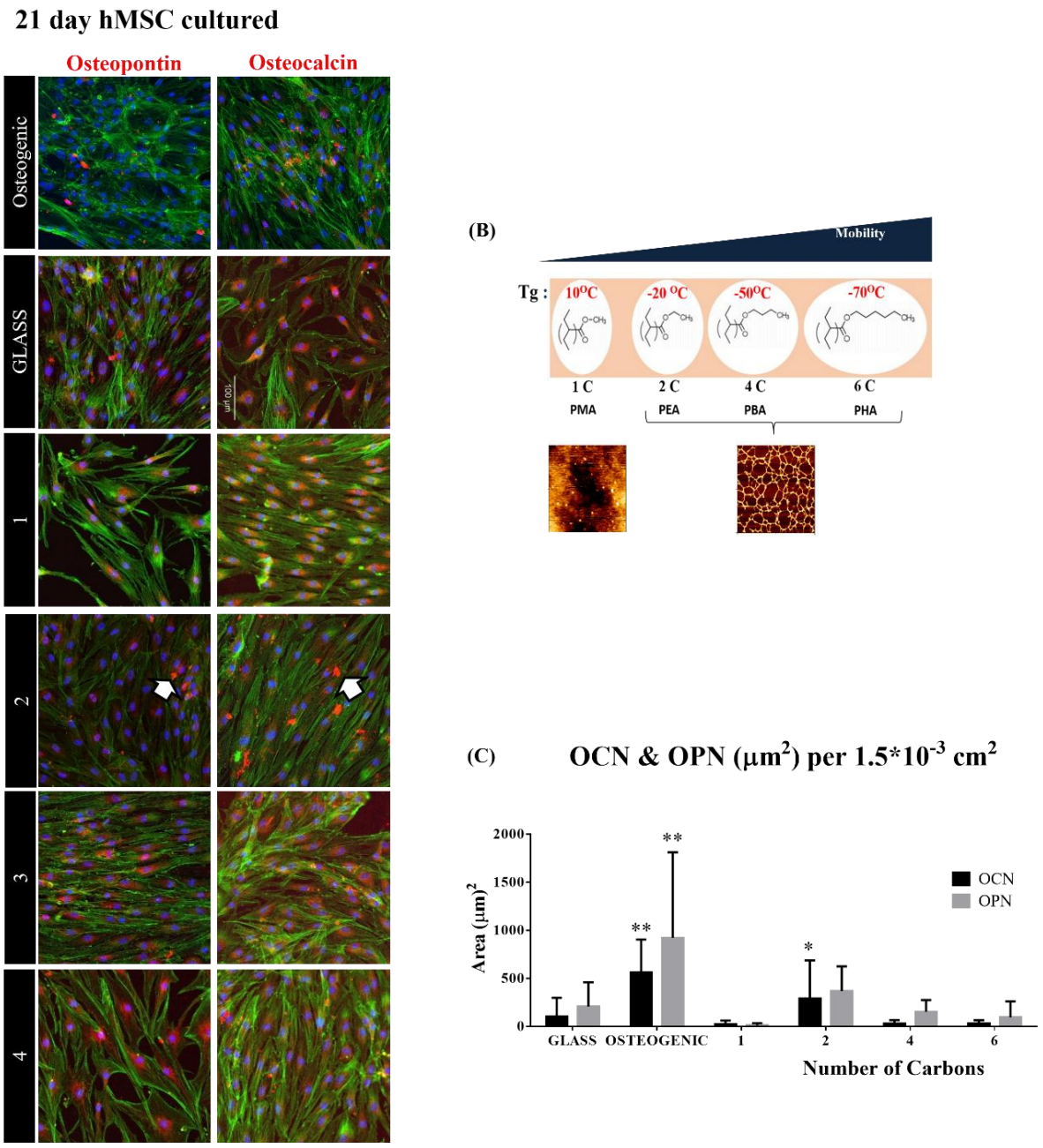

Figure 30 – Osteocalcin expression on the polymer surfaces in the absence of differentiating stimuli. (A) Images showing fluorescently labelled OCN and OPN in a 21-day culture on fibronectin coated polymers, (B) Schematic showing the relationship between polymer mobility, Tg, free volume and the fibronectin conformation formed and (C) Graph of quantification of OCN and OPN nodule sizes. Each bar in the graphs represents results from 9 images (3 from each triplicate) and standard deviations are indicated by black error bars. One way Anova analysis revealed statistically significant differences: *$p \leq 0.05$ and **$p \leq 0.01$ (GraphPad software, La Jolla, CA).

Calcium deposited by the newly formed osteoblasts is also used to assay osteogenic differentiation of cells. Calcium was quantified using a colorimetric method based on the reaction of o-Cresolphthalein Complexone in Alkaline solution with calcium ions which yields a violet solution. The optical density is used against a standard curve to estimate the amount of deposited calcium (Sharp, 2011). Deposited calcium on the polymers was found to be highest on C = 2 compared with the rest of the polymers (Figure 31).

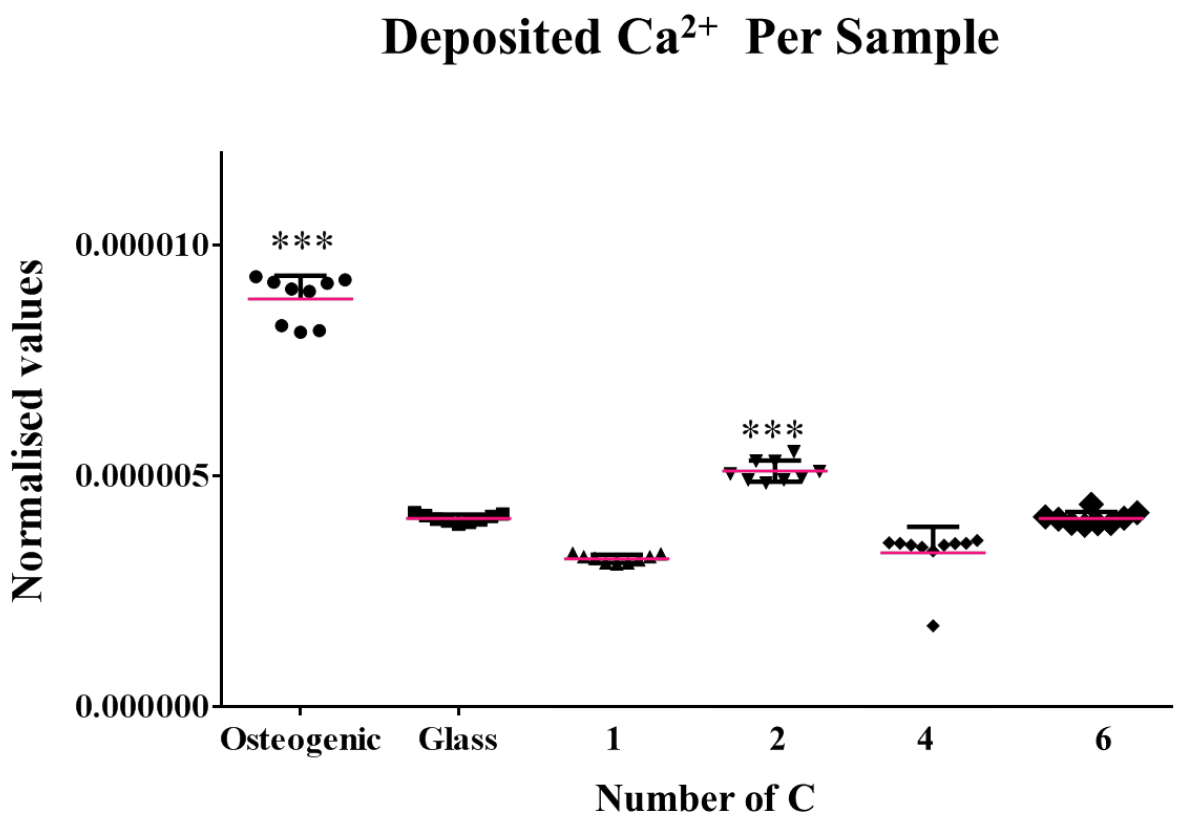

Figure 31 – Calcium deposition by hMSCs cultured without differentiating stimuli. Graph showing the quantification of the deposited calcium as measured by the O-cresolphthalein complexone method. Calcium ions were found to be higher on C = 2 compared with the rest of the polymers. The optical density was read at 577 nm and values were normalised with respect to the cell growth area (1.13 cm^2). Each cluster in the graph represents an average of 9 readings (3 from each triplicate) and standard deviations are indicated by black error bars. One way Anova analysis revealed statistically significant differences: ***$p \leq 0.001$ (GraphPad software, La Jolla, CA).

Erk1/2 but not contractility is involved in osteogenic differentiation on C = 2

Osteogenic differentiation as a response to specific mechanical cues e.g. stiffness is mediated by adhesion - mediated signalling which modulates contractility (Arnsdorf et al., 2009) , and Erk1/2 related signalling (Figure 32A) (Kilian et al., 2010; *Yan* et al., 2012).

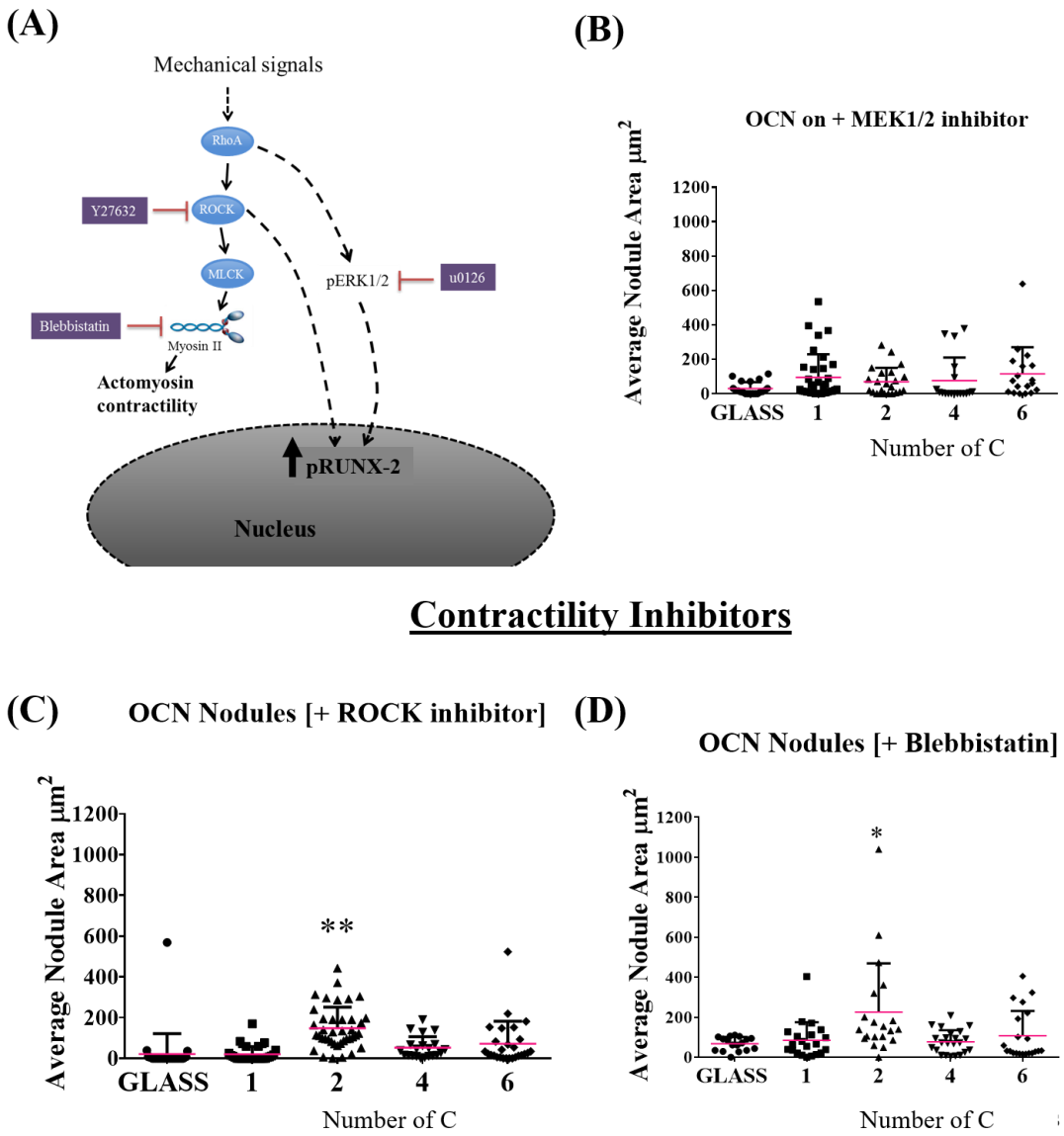

Figure 32 – Mechanistic study to deduce pathways involved in the increased osteogenic differentiation observed for C = 2. (A) A flow diagram of how mechanical signals are transduced through contractility (Arnsdorf et al., 2009) or Erk1/2 (Kanno et al., 2007) to lead to increased osteogenic differentiation. (B) Inhibition of Erk1/2 resulting in the disappearance of the increase previously observed in osteocalcin expression on C = 2, (C) and (D) show

graphs of OCN quantification for samples cultured in the presence of the inhibitors of ROCK and Myosin II respectively, both of which do not inhibit the increase in osteocalcin levels on C = 2. Each cluster in the graphs represents results from analysis of images from each sample triplicate and standard deviations are indicated by black error bars. One way Anova analysis revealed statistically significant differences: *$p \leq 0.05$ and **$p \leq 0.01$ (GraphPad software, La Jolla, CA).

To test whether these two pathways were involved, osteocalcin expression was studied in hMSC 21 day cultures carried out with specific contractility inhibitors; Y27632 against ROCK (Figure 32C) and Blebbistatin against myosin II (Straight et al., 2003). On the other hand, Erk1/2 was also inhibited using a MEK1/2 inhibitor (Figure 32B). Erk1/2 signalling has proven to be essential in the osteogenic differentiation of hMSCs (Lee et al., 2002) and its inhibition was performed as a positive control to make sure that my use of inhibitors successfully disabled osteogenic differentiation of the hMSCs on my substrates.

Results from this mechanistic study using inhibitors (Figure 32) indicate that contractility does not play a major role in the osteogenic differentiation of MSCs on these polymer surfaces, as ROCK and myosin II inhibition (Figure 32C and D) do not abolish the increased osteogenic differentiation on C = 2. Osteogenic differentiation remains low on the other polymers in the absence and presence of inhibitors. However, Erk1/2 inhibition abolishes the increased differentiation previously observed on C = 2 (Figure 30), indicating its involvement in the differentiation of hMSCs on this surface towards the osteogenic lineage.

In conclusion, in the absence of differentiating stimuli Erk1/2 activation plays a role in the osteocalcin expression observed on C = 2. This polymer supports a fibronectin network with the lowest interfacial protein mobility, while previous studies have shown mobility as a favourable property for the osteogenic differentiation of MSCs (Gonzalez-Garcia et al., 2012).

Moreover, my study of C2C12 cells revealed that their myogenic differentiation which was relatively high on C = 2 and C = 4, was negatively affected by myosin II inhibition only on C=4 and C = 6 (Chapter 3 - Figure 25). MSCs showed no notable reliance on contractility, as osteocalcin, osteopontin and calcium deposition (Figure 30 and Figure 31 respectively) remained low; similar levels between Glass, C = 1, C = 4 and C = 6) and this trend was

maintained in the presence of contractility inhibitors. This suggests that unlike the myogenic differentiation of C2C12 cells, MSC osteogenic differentiation on more mobile polymers C = 4 and C = 6, is not contractility dependent, and that it is promoted on a surface with low interfacial protein mobility.

Surface analysis

ELISAs were carried out to measure the level of exposure of the growth factor binding site on fibronectin (Martino and Hubbell, 2010a) (Figure 33) and the density of bound BMP-2 (Figure 34).

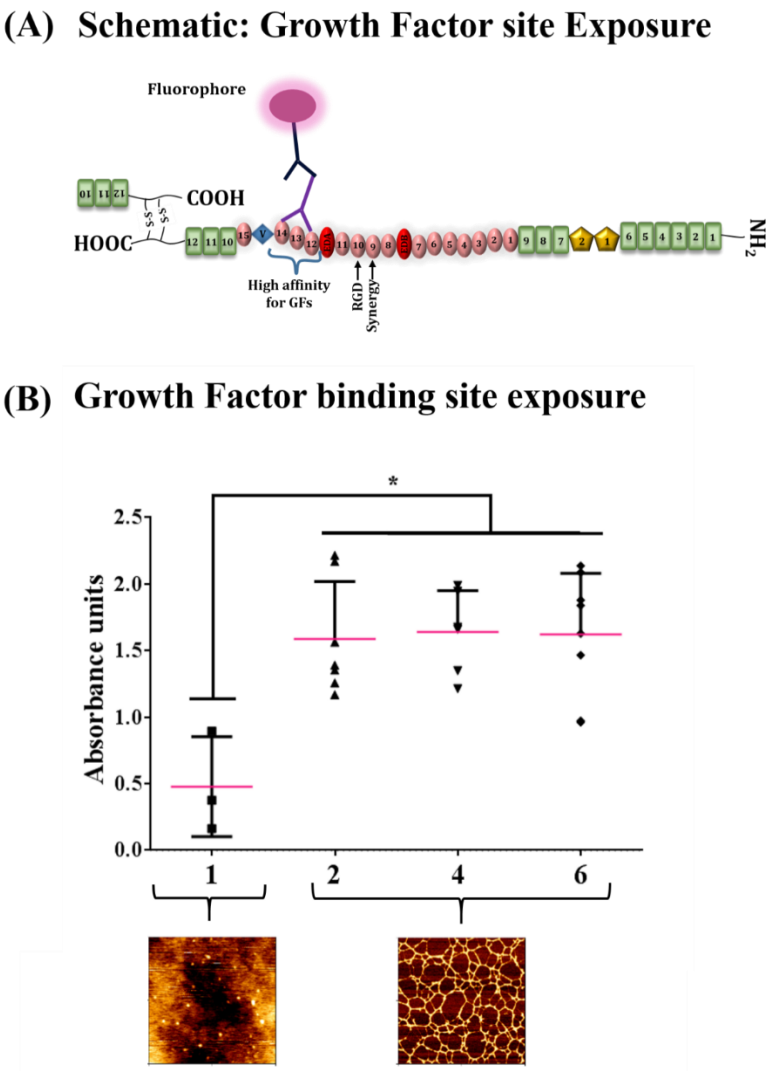

Figure 33 – ELISA analyses for the exposure of the growth factor site on fibronectin also known as the heparin II domain. Fibronectin fibrils on polymers C = 2, C = 4 and C =

6 were bound by the specific antibody to higher levels than the globular fibronectin on C = 1. (A) A schematic of fibronectin bound at the growth factor site during the ELISA analysis of its exposure. (B) Plotted are the results of analysis of n = 6, standard deviations are indicated by black error bars. One way Anova analysis revealed statistically significant differences: *p ≤ 0.05, **p ≤ 0.01, ***p ≤ 0.001, and ****p ≤ 0.0001 (GraphPad software, La Jolla, CA).

This characterization was carried out for the next step; to use surface bound BMP-2 on my fibronectin - coated polymers to drive MSC osteogenesis. It can be deduced from Figure 33B that the growth factor binding site exposure is higher in the fibrillar conformation of fibronectin than in the globular one, following a similar trend as the exposure of the RGD and Synergy sites (Chapter 2 - Figure 17) and is in agreement with the findings of Llopis-Hernández, et al. (Virginia Llopis-Hernández et al., 2016).

The actual binding of BMP-2 was also analysed, to assess whether the high availability of this site on the fibronectin networks also led to higher BMP-2 binding/presentation. This was done by quantifying bound BMP-2 when the growth factor site (Martino and Hubbell, 2010a) was unblocked and blocked using an antibody (Figure 34A and B) respectively.

Figure 34C is a graph of the quantification of bound BMP-2. The density of bound growth factor on the unblocked samples was similar between the surfaces, however, when the growth factor site was blocked with a specific antibody; only the density of growth factor on C = 2 was reduced.

Analyses of fibronectin structure directly by AFM (Chapter 2 - Figure 13) and indirectly by ELISAs (Figure 17 and Figure 33) for the exposure of specific structural sites (RGD, Syrnergy and Heparin II/ Growth factor site) revealed minimal differences between the fibronectin fibrils on C = 2, 4 and 6. However, my FRAP analysis revealed differences in the mobility of the fibronectin layer between these three fibronectin network forming polymers, where it followed a non - monotonic trend, lowering between C = 1 and C = 2 and then increasing with the underlying surface mobility.

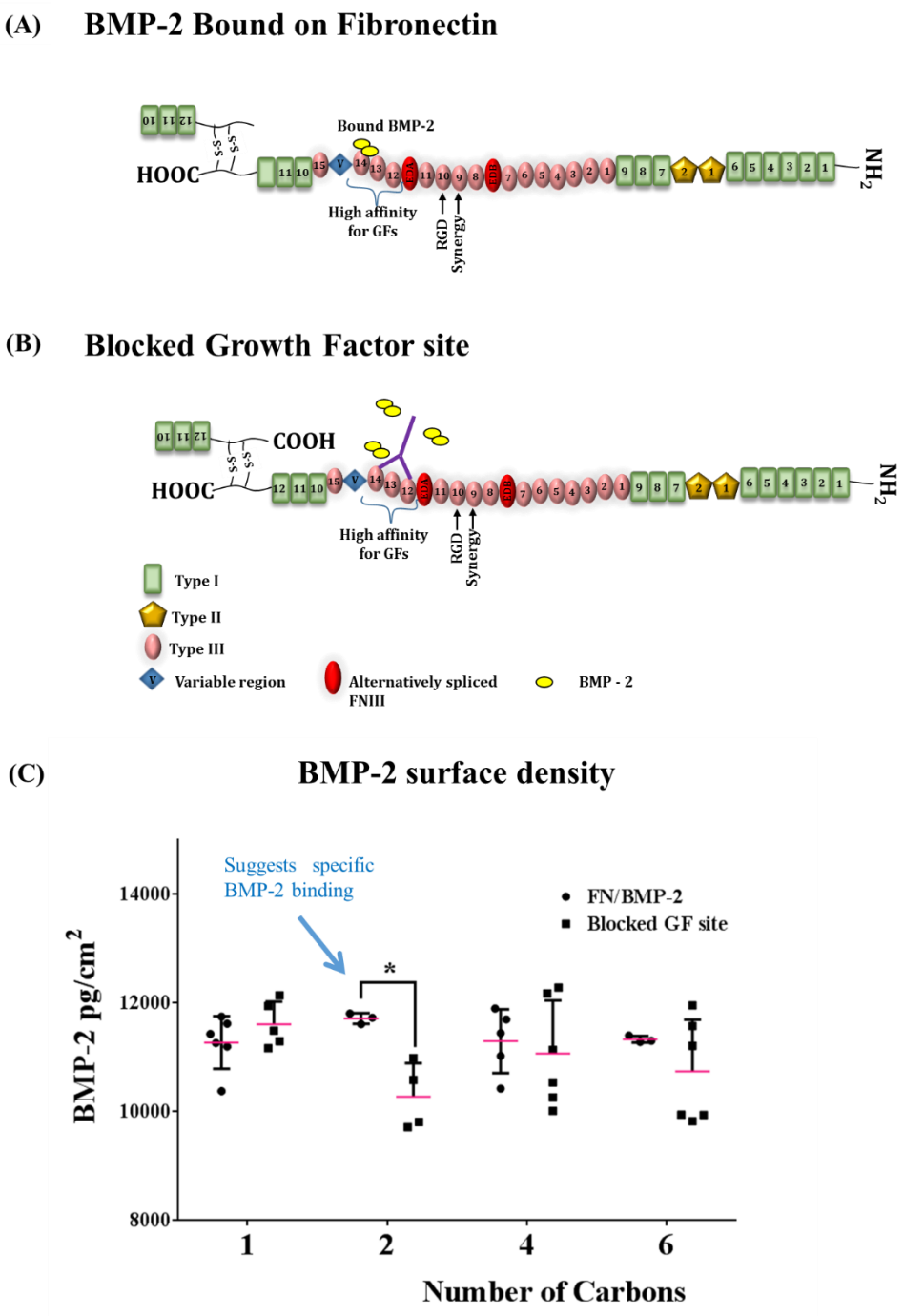

Figure 34 – Bound BMP-2 density. Sandwich ELISAs used to quantify bound BMP-2 on fibronectin – coated polymers incubated with 100 ng/ml solution of BMP-2. Schematics illustrate (A) a freely accessible growth factor binding site (Martino and Hubbell, 2010a) and (B) a growth factor binding site blocked with a specific antibody. (C) Graph comparing BMP-2 surface density on fibronectin-coated polymers with and without blocking the growth factor site. Plotted are the results of analysis of n = 6, standard deviations are indicated by

black error bars. One way Anova analysis revealed statistically significant differences: *$p \leq 0.05$ (GraphPad software, La Jolla, CA).

These results therefore suggest that low interfacial fibronectin mobility (on C = 2) may allow for more specific binding of BMP-2. Which we expect will have an effect on how BMP-2 is presented to MSCs, as when BMP-2 is specifically bound on fibronectin, it would be positioned in close proximity to integrin receptors (Roumen, 2002).

Presentation of BMP-2 on fibronectin-coated surfaces enhances osteocalcin expression

Finally, we used the fibronectin coatings on the four polymers to present BMP-2 to hMSCs and then analyse their differentiation (Figure 35). We also speculated that the specific binding of BMP-2 on fibronectin-coated C = 2 illustrated by the graph (Figure 34C), may result in a synergistic effect due to the activation of BMP receptors and integrins at close proximity, leading to an increased (synergistic) effect on the osteogenic differentiation of hMSCs on this material.

The expression of the osteogenic differentiation marker – osteocalcin was compared between three experimental conditions;

- BMP-2 added to the culture medium (conventional approach)
- BMP-2 bound on the fibronectin-coated surfaces
- Noggin (an inhibitor of the BMP-2 receptor) added to the medium

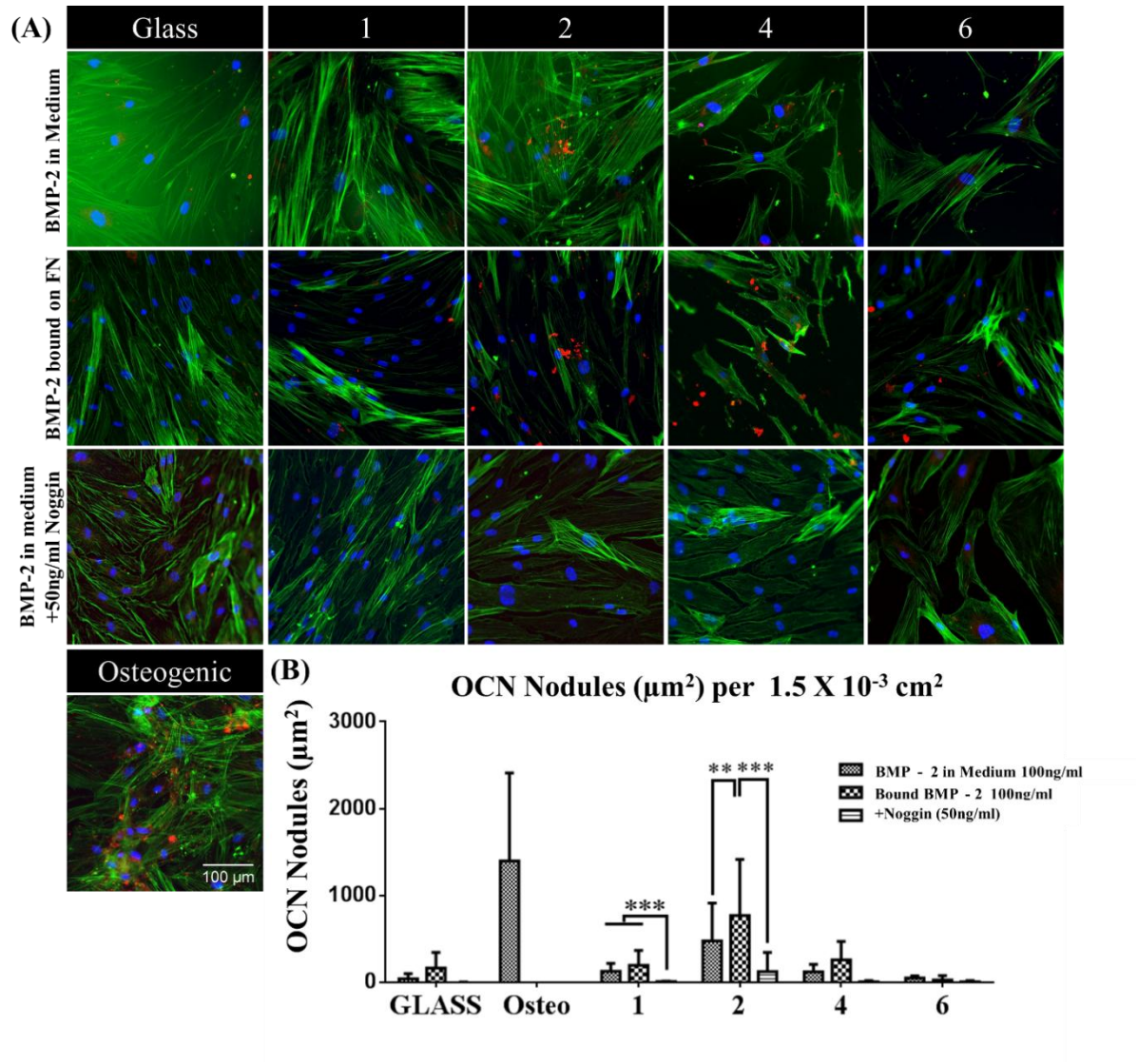

Figure 35 – Osteogenic differentiation of BMP-2 stimulated hMSCs. Representative images of MSCs cultured for 21 days using three different conditions (A) 1st row - BMP-2 in medium, 2nd row - BMP-2 bound onto fibronectin and 3rd row - fibronectin bound BMP-2 and the presence of soluble Noggin. The image in the 4th row is representative for the osteogenic control. (B) Quantification of the osteocalcin in the fluorescent images. Osteocalcin – Red, Actin – Green and Dapi – Blue. The graph shows the highest osteocalcin expression on the C = 2 polymer with surface - bound BMP-2 in contrast with when BMP-2 is added in the medium, there is also a marked decrease in osteocalcin expression upon BMP-2 inhibition with noggin. Plotted are the results of analysis of ~17 images from triplicate samples, standard deviations are indicated by black error bars. One way Anova analysis revealed statistically significant differences: $^{**}p \leq 0.01$ and $^{***}p \leq 0.001$ (GraphPad software, La Jolla, CA).

Figure 35B shows that the surface C = 2 with BMP-2 bound on fibronectin induced significantly higher osteogenic differentiation of hMSCs compared with the rest of the samples ($p \leq 0.01$), including on C = 2 with BMP-2 present in the culture medium. This result illustrates that when MSCs are cultured on C=2 samples with fibronectin bound BMP-2, they are more strongly induced to express the osteogenic marker osteocalcin than when they are cultured on fibronectin bound BMP-2 on C = 1, 4 or 6. Even though C = 4 and C = 6, adsorb fibronectin in a similar conformation to C = 2. My previous observation of more specific binding on C = 2 (Figure 34C) strongly supports this finding, which is also reinforced by the highly significant reduction in osteocalcin expression in the presence of noggin. The correlation between more specific binding of BMP-2 on C = 2 and the high expression of osteocalcin on the same sample when bound with BMP-2, may indicate that the specific binding of BMP-2 on this surface leads to better presentation of BMP-2. This consequently drives osteogenic differentiation more strongly. Moreover, the ability of noggin to inhibit osteocalcin expression on the same sample, provides us with compelling evidence for the major role played by BMP-2 stimulation on C = 2.

Interfacial fibronectin mobility was the only parameter found to differ between the fibronectin network inducing polymers (C = 2, 4 and 6). This protein mobility was lowest on C = 2, which when coated with fibronectin was also found to bind BMP-2 in a more specific manner (Figure 34C). The subsequent observations of higher osteocalcin expression when MSCs are cultured on this sample with bound BMP-2, may indicate that the low mobility of fibronectin networks on this polymer favours a more synergistic presentation of BMP-2 on fibronectin (growth factor site), this strongly links low protein mobility with more specific BMP-2 binding.

Phosphorylation of Erk1/2, pSmad 1/5/8 and Runx-2

Osteogenic differentiation is characterised by both increased phosphorylation of Erk1/2 and the phosphorylation of Smad 1/5/8 by the type I BMP receptors, these two pathways of the TGFβ/BMP signalling both lead to higher phosphorylation of Runx-2 (Figure 27) (Lee et al.,

2002). Quantification of the level of phosphorylation of these three proteins (Figure 36) was carried out 1.5 hours after cell seeding (on BMP-2 coated samples) using the In-Cell-Western technique, since the activation of these pathways is immediate following the stimulation of cells with BMP-2.

Furthermore, it should be noted that two polymers C = 2 and C = 6 and not four were utilised in this part of the study. Mainly to decouple which pathway played a major role in producing an increased level of differentiation on C = 2. These two polymers were selected based on previous results, as the most likely (C = 2) and the least likely (C = 6) to induce high osteogenic differentiation.

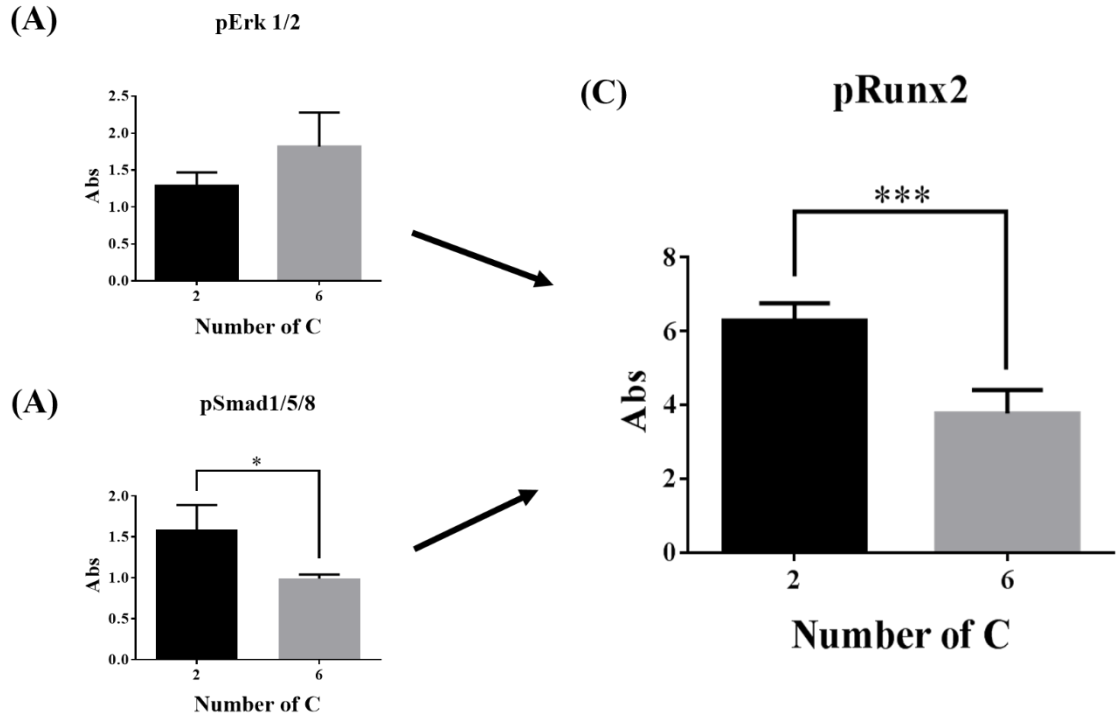

Figure 36 – Quantification of phosphorylation of Erk1/2, Smad1/5/8 and Runx2 in cells adhered to BMP-2 bound to fibronectin coated surfaces. InCell Western analysis of phosphorylated; smad1/5/8 and Erk1/2 and the osteogenic transcription factor Runx2 in hMSCs immediately post adhesion. No significant differences were observed for Erk1/2 phosphorylation, while smad1/5/8 phosphorylation was significantly higher on C = 2. hMSCs on C = 2 samples also exhibited significantly higher Runx2 phosphorylation compared with those on C = 6 samples. Quantification of each phosphorylated protein was normalised with the total protein. Plotted are results from 6 reading (3 from duplicate samples), the standard deviations are indicated by black error bars. One way Anova analysis revealed statistically significant differences: *$p \leq 0.1$ and ***$p \leq 0.001$ (GraphPad software, La Jolla, CA).

The level of phosphorylated protein normalised with total protein in (Figure 36) indicate that Erk1/2 is phosphorylated to similar levels on C = 2 and C= 6, while Smad 1/5/8 is phosphorylated to a significantly higher level on the polymer C = 2 than on C = 6. Since contractility was found not to influence expression of osteocalcin on C = 2, it could be assumed that the Erk1/2 phosphorylation on C = 2 and C = 6 (Figure 36) was due to non – canonical signalling TGFβ/BMP. However, the presence of Erk1/2 signalling in the absence of BMP-2 shown by inhibition (Figure 32) suggests that it is indeed adhesion based signal (Greenblatt et al., 2010) which causes Erk1/2 phosphorylation, while when BMP-2 is added, both adhesion – based and non – canonical TGFβ/BMP signalling may contribute to the phosphorylation Erk 1/2.

The simultaneous activation of smad signalling and Erk1/2 related signalling is understood to induce a much stronger/ synergistic effect on the osteogenic differentiation of hMSCs (Lee et al., 2002), which was apparent when Runx-2 phosphorylation was analysed. Runx-2 is downstream of both Erk1/2 and Smad 1/5/8 phosphorylation, this explains the marked increase in its phosphorylation on the C = 2 polymer on which higher Smad 1/5/8 phosphorylation was observed (Figure 36). My results therefore strongly suggest that the low interfacial fibronectin mobility on C = 2 encourages more specific binding of BMP-2 (Figure 34) thus effectively and efficiently presenting BMP-2 in a manner that supports synergistic signalling.

Conclusion

This work utilised four poly(alkyl acrylates) with similar chemistry; a vinyl backbone and side groups – $COO(CH_2)_xH$ where x = 1, 2, 4, and 6 for poly-methyl, ethyl, butyl, and hexyl acrylates. These polymers were selected due to their gradual increase in polymer surface mobility as previously described in Chapter 1 Intoduction - Polymer surface mobility. Physical characterization (Chapter 2) of these polymer surfaces revealed high similarity between them, in their stiffness, hydrophobicity and WCA hysteresis, which suggests similar surface chemistry.

AFM analyses showed that three of the polymers (C = 2, C = 4 and C = 6) adsorbed fibronectin in similar fibrillar nanonetworks also shown in previous studies (Guerra et al., 2010) (Rico et al., 2009) (Salmeron-Sanchez et al., 2011) . When the mobility of these networks was studied using FRAP, it was clear that although similar in conformation, the interfacial fibronectin layers on the polymers are mobile to different extents; following a non-monotonic trend on the four polymers. Moreover, I found that fibronectin fibrils on C = 2 were bound more by a single chain variable fragment specific for stretched fibronectin. Therefore, mobility of the fibronectin layer and fibronectin stretching were the two properties found to be different between fibronectin - coated C = 2, C = 4 and C = 6 despite their similarity in conformation as observed by AFM. Indirect analysis by ELISA for the exposure of specific domains; RGD, Synergy and heparin II growth factor binding site, within the structure of the fibronectin fibrils, also revealed minimal differences between the fibronectin network forming polymers (C = 2, C = 4 and C = 6).

When BMP-2 binding was quantified (Figure 34C), it was found that even though similar levels of BMP-2 bound the fibronectin networks on C = 2, 4 and 6, only C = 2 binding was hindered by specifically blocking the growth factor site. This strongly suggests more specific binding on C = 2 fibrils compared to those on C = 4 and C = 6.

Moreover, studies on MSC osteogenic differentiation on the four polymers in the absence of BMP-2 stimulation revealed higher osteogenic marker expression (osteocalcin and osteopontin) on C = 2, and this was found to be dependent on Erk1/2 related signalling. While ROCK and myosin II were not influential in the osteogenic differentiation observed on C = 2 (without BMP-2, Figure 32). ROCK and myosin II are important for adhesion based and contractility dependent cellular responses to mechanical cues (Illustrated in Figure 32A) (Bhadriraju K et al., 2007) (Arnsdorf et al., 2009). In the presence of BMP-2, Erk1/2 signalling was still activated on C = 2 (and C = 6) as seen in the quantification of its phosphorylation while smad1/5/8 - dependent signalling (Canonical) was higher on C = 2 than C = 6. Runx - 2 phosphorylation was higher on C = 2, very likely to be a consequence of the increased smad1/5/8 phosphorylation on this surface.

In summary, the lack of influence of signalling due to contractility, equivalent levels of Erk1/2 phosphorylation on C = 2 and C = 6 and significantly higher smad1/5/8 phosphorylation on C = 2, further supports my hypothesis that BMP-2 is adsorbed on C = 2 in a more specific manner allowing for more canonical signalling. Higher phosphorylation of

Runx-2 on C = 2 (Figure 36) is most likely due to a combination of Erk1/2 related signalling (non - canonical (Hayrapetyan et al., 2014) or due to adhesion (Greenblatt et al., 2010)); which is comparable between C = 2 and C = 6 and higher smad1/5/8 phosphorylation (on C = 2, canonical) (Figure 36). The high osteogenic differentiation observed on C = 2 in the presence of BMP-2 (Figure 35) is in agreement with the literature as higher Runx-2 activation also observed on this surface, has been linked to higher osteoblastic differentiation and mineralisation of MSCs (Zhang et al., 2006). Llopis-Hernández, et al. who carried out similar work but on C = 1 and C = 2 alone, found similar trends of increased osteogenic activity on BMP-2 bound C = 2 (Virginia Llopis-Hernández et al., 2016). In this study, I show that polymer mobility should be optimised in the design of polymeric biomaterials as it is translated to the protein layer and hence may play a major role in the biological activity and growth factor presentation capabilities of this layer. This study adds to the increasing evidence (Guerra et al., 2010) (Berglin et al., 2004) (Sabater i Serra et al., 2016) (Virginia Llopis-Hernández et al., 2016) of the role of surface mobility on cell behaviour.

Chapter 5 – Discussion

The ability of cells to respond to a wide range of surface properties is an established fact (Engler et al., 2006) (Dalby et al., 2007) (McNamara et al., 2010) (Resende et al., 2014) (Benoit 2008) (McBeath et al., 2004a). Now researchers from engineering and biology are working together and focusing their efforts on designing functional biomaterials. Several key modifications of the surface including topography and chemistry underlie these efforts (Shin et al., 2003) (Hubbell, 1999). However, the use of polymers in tissue engineering is widespread, while the way an intrinsic property of polymers, known as molecular mobility confounds the effect of polymeric biomaterials on cells is not very well understood. In this work, I explored this question using short term functional studies of cell morphology, focal adhesions and integrin recruitment and cell - driven fibronectin reorganization. I then carried out longer term analyses of the response of human mesenchymal stem cells on my materials, and analysed the intracellular mechanisms involved.

To study mobility, four poly(alkyl acrylates) with a vinyl backbone and side groups – $COO(CH2)_xH$ where x = 1, 2, 4, and 6 represents the number of carbons in the side chains of poly-methyl, ethyl, butyl, and hexyl acrylates, respectively) (Gonzalez-Garcia et al., 2012) (Guerra et al., 2010). In this document, the number of carbons is simply represented as C, such that C = 2 represents poly-ethyl acrylate. My polymers of interest were selected for the similarity in their chemistry and decreasing glass transition temperatures (10°C, -20°C, -50°C and -70°C for C = 1, 2, 4 and 6 respectively). Polymer chain mobility is known to increase in polymers with lower glass transition temperatures, therefore in this set of polymers, chain mobility increases with the number of carbons in the side chains.

Fibronectin strongly interacts with the surfaces of these four polymers (Gugutkov et al., 2010) adsorbing in a globular conformation on C = 1 and spontaneously undergoing fibrillogenesis on C = 2, 4, 6 (Salmeron-Sanchez et al., 2011). My challenge in this work was to analyse whether polymer mobility is a property that should be considered in the design of biomaterials, and if it could be used to modulate stem cell fate. Firstly, I characterized the surface of my polymer films with regards to properties which have been shown to affect cell behaviour including stem cell differentiation (Dalby et al., 2007) (Engler et al., 2006) (McNamara et al., 2010) (Resende et al., 2014). Using water contact angle measurements and atomic force microscopy I found that there was minimal variation in the wettability, stiffness

and topography of my surfaces. This result made it possible to attribute further observations on these polymers to their varied mobility.

Prior to any cell work, I sought to understand the nature of the fibronectin coating which forms the interfacial layer between the polymer and cells. The density and conformation of adsorbed protein are highly influenced by the physical properties of the surfaces onto which they are adsorbed (Arima and Iwata, 2007) (Michael et al., 2003a) and in turn play an essential role in modulating cell behaviour (Watt and Huck, 2013) (Frantz et al., 2010) (Garcia et al., 1999). My results of adsorbed fibronectin density and its conformation, analysed by protein assay, AFM and immunostaining of the fibronectin coating are in agreement with previous observations (Salmeron-Sanchez et al., 2011) (Guerra et al., 2010). The micro BCA protein assay after incubation with 20 µg/ml fibronectin solution showed that a 400 – 600 ng/cm^2 surface density was achieved and my AFM scans post fibronectin adsorption revealed fibrillar networks on C = 2, 4 and 6, and a globular conformation on C = 1. These networks on C = 2, 4 and 6 could also be observed by immunostaining, where a polyclonal antibody against fibronectin was used. With this setup, therefore, I had globular fibronectin on the polymer with the least mobility and fibronectin networks on the other three polymers with gradually increasing mobility.

The interfacial protein layer has been shown to play a crucial role in influencing cell behaviour (Watt and Huck, 2013) (Frantz et al., 2010) (Garcia et al., 1999), as ECM proteins are often decorated with sites in their structure which are important for cellular interaction (Plow et al., 2000). Fibronectin is a major ECM protein and its cell binding sites are well characterized (Roumen, 2002), the main ones being the RGD and PHSRN binding sites also otherwise known as the cell binding site and the synergy site respectively. The RGD site is bound by the $\alpha_v\beta_3$ integrin heterodimer while the close proximity between this site and the synergy site enhances the binding of the $\alpha_5\beta_1$ integrin heterodimer (Krammer et al., 2002) (Mould et al., 1997). I carried out ELISAs with specific antibodies for the RGD and the PHSRN sites to indirectly analyse the conformation of the adsorbed fibronectin. This was mainly to examine whether the fibronectin fibrils on C = 2, 4 and 6 which appeared to be similar on AFM scans actually differed in their domain exposure, in which case they would consequently affect cell behaviour. However, the ELISA results indicated minimal differences in the exposure of the RGD and PHSRN fibronectin sites between the fibrillar fibronectin. The exposure of these sites was lower for the globular fibronectin.

The conformation of adsorbed fibronectin as observed by AFM analysis and as deduced from ELISAs for RGD and Synergy site exposure indicated a difference only between C = 1 and the rest of the polymers. The similarity between the conformation of adsorbed fibronectin on C = 2, 4 and 6 indicates that increasing mobility (by increasing side chain length from C = 2) does not lead to adsorption of fibronectin in a non - network conformation. This is in agreement with recent observations (Sabater i Serra et al., 2016) which showed that reducing mobility by cross - linking C = 2 thus increasing Tg of this polymer and consequently lowering its mobility, hinders the ability of C = 2 to induce fibronectin fibrillogenesis.

Cells perceive the physical cues of surfaces via the interfacial protein layer (Geiger et al., 2001). And there is evidence to suggest that cells can detect polymer mobility (Curran et al., 2011) (Liu et al., 2012) (Seo and Yui, 2013) (Seo et al., 2013) (Liu et al., 2012) (Gonzalez-Garcia et al., 2012), this led us to hypothesize that polymer surface mobility can be translated to the interfacial protein layer. The strong interaction between fibronectin molecules and this set of polymers led us to expect a direct translation of the trend of surface polymer mobility (Figure 4) to the interfacial layer. The Tg of my polymers of interest decrease with the number of carbons in their side chains, hence at 37°C (experimental temperature) the mobility of these polymers increases with side chain length, with the highest mobility on C = 6. Through FRAP analyses using fibronectin – FITC coatings, I demonstrated for the first time a non-monotonic relationship between interfacial mobility and the underlying polymer mobility. I observed that interfacial fibronectin mobility gradually increased replicating the trend from the underlying polymer mobility except for an initial drop between C = 1 and C = 2, this is also where fibronectin gains a network conformation. The formation of fibronectin networks is known to rely on the exposure on the of the 70kDa 1st-5th FNI repeats at the amino terminal of the fibronectin molecule (Hocking et al., 1994) (Aguirre, 1994). This fibronectin – fibronectin binding which leads to network assembly is thought to be the introduction of order in the system, and the reason behind the observed reduction in interfacial fibronectin mobility between C = 1 and C = 2.

This set of polymers varied in their surface and interfacial protein mobility but with fibrils on C = 2, 4 and 6 which did not vary significantly in the exposure of important cell binding sites; RGD and the Synergy. Using this system, I set out to further characterize these surfaces and to understand whether cells would detect and respond to mobility. Fibroblasts (mouse L929 cells and human HFFF2 cells) spread well on the surfaces and did not differ significantly in their morphology and integrin recruitment profiles between the four fibronectin - coated

polymers. However, cell mediated reorganization replicated the trend observed for interfacial fibronectin mobility with low reorganization on C = 1 and C = 2 and highest on C = 6, even though the morphology of cells seemed to be relatively unaffected by mobility. A previous study also linked high mobility with more cell - mediated reorganization (Gonzalez-Garcia et al., 2013). Different levels of myogenic differentiation were observed on the four fibronectin coated polymers, with the highest levels on C = 2 and C = 4 (higher than the positive control; collagen I coating). As C2C12 differentiation has been linked to contractility (Dhawan, 2004), differentiation levels were also analysed in the presence of a specific myosin II inhibitor (blebbistatin (Straight et al., 2003)), this led to the observation that cell contractility is required for mobility dependent myogenic differentiation on these polymers. This is in line with a previous study of MSC differentiation on these polymers (Gonzalez-Garcia et al., 2012).

The main aim of this project was to engineer surface mobility to direct stem cell fate. MSCs have been shown to respond to several physical surface properties, including topography (Dalby et al., 2007; McNamara et al., 2010) (McNamara et al., 2010), stiffness (Engler et al., 2006) and cell shape (McBeath et al., 2004a). C = 1, 2, 4 and 6 were selected due to their similarity in chemistry and their gradual increase in mobility, to investigate the effect of this physical property on cell behaviour. Surface characterization of these polymers revealed minimal differences between the polymers in terms of the properties known to affect stem cell behaviour, apart from a non-monotonic trend in the mobility of the interfacial fibronectin layer and fibronectin stretching as revealed by the specific single chain variable fragment H5 (Chapter 2). My differentiation analysis of hMSC culture on the four polymers only coated with fibronectin, revealed that osteocalcin was expressed more when MSCs were cultured on C = 2 compared to the rest of the polymers, and this was found to be dependent on Erk1/2 related signalling and not contractility due to ROCK or myosin II activation. Calcium deposition, which is characteristic of osteoblasts, was also found to follow the same trend.

To make use of the full potential of the fibronectin coating in the design of an osteogenic biomaterial, I characterised the exposure of the fibronectin growth factor site (Martino and Hubbell, 2010b) and quantified BMP-2 binding on the fibronectin coated polymers. The exposure of this site was higher on the fibrillar fibronectin than the globular one, but showed minimal differences between the networks on C = 2, 4 and 6, a trend similar to that observed for the exposure of RGD and the Synergy site. Quantification of bound BMP-2 revealed equivalent binding between the four fibronectin- coated polymers, these two results; BMP-2

binding and HeprainII domain exposure are in line with a recently published study on C = 1 and C = 2 surfaces (Virginia Llopis-Hernández et al., 2016). However, blocking the growth factor site with a specific antibody led to an unexpected result; where BMP-2 was found to bind more specifically on the fibronectin network of C = 2, the surface with the lowest mobility in its fibronectin network. This suggests that low disorder may encourage a more stable binding of the BMP-2 molecule to the growth factor binding site of fibronectin.

It was immediately realised that the specific binding of BMP-2 achieved on C = 2 is likely to present BMP-2 in close proximity to integrin binding sites, such that the two interactions activate simultaneous signalling, leading to synergistic effects on MSC osteogenic differentiation. To analyse this concept further, the expression of osteocalcin was quantified for MSCS cultured in the presence and absence of BMP-2, as well as in the presence of BMP-2 inhibition by its antagonist, noggin. In line with the previous results of specific BMP-2 binding, C = 2 fibronectin coated surfaces with surface bound BMP-2 induced the highest expression of osteocalcin. This expression was higher than when BMP-2 was only present in the medium, therefore indicating that the surface presentation of BMP-2 on this polymer as a more effective way to present this growth factor. Addition of noggin to the culture resulted in a marked decrease in osteocalcin expression, this is a confirmation that the observed osteocalcin expression is due to BMP-2 signalling (canonical, see Figure 35).

Osteogenic differentiation of MSCs is characterised by the increased expression and phosphorylation of Runx-2 (Liu and Lee, 2012) such that higher activation of Runx-2 enhances osteoblastic differentiation and mineralization and (Zhang et al., 2006). There are several pathways involved in the osteogenic differentiation of MSCs (Hayrapetyan et al., 2014) with considerable crosstalk between them. BMPs are secreted ECM-associated proteins from the TGF-β superfamily (Bragdon, 2011), some of these proteins are known for their ability to induce osteogenesis. Upon binding to cell receptors, they activate two signalling pathways, the canonical (smad-dependent) and non-canonical (Smad-independent/Erk related pathway), both of which lead to the increased expression and phosphorylation of the osteogenic transcription factor Runx-2 in the nucleus of the cell (Lee et al., 2002). I therefore, quantified the phosphorylation of the three proteins; Erka/2, smad1/5/8 and Runx-2, to study whether the observed osteogenic differentiation on C = 2 was due to one or both pathways. The In-Cell Western results indicated that Erk activation was equivalent between C = 2 and C = 6; samples chosen based on previous results as most likely and least likely to induce osteogenic differentiation. However, fibronectin coated C = 2

with bound BMP-2 induced higher smad1/5/8 phosphorylation as well as higher Runx-2 phosphorylation. Therefore, it can be concluded that due to a stronger induction of the canonical signalling pathway on C = 2 upon BMP-2 stimulation compared with the other polymers, higher Runx-2 phosphorylation and higher osteocalcin expression can be achieved on this polymer.

Therefore, the high osteocalcin expression observed on the C = 2 fibronectin coated polymer with bound BMP-2, may be attributed to the fact that these C = 2 fibronectin networks with low mobility are able to bind BMP-2 in a more specific manner, compared with more mobile networks on C = 1, 4 and 6. Thus presenting the BMP-2 molecule to cells in such a way that higher activation of the canonical pathway is achieved, thus resulting in higher Runx-2 phosphorylation. I note that Erk signalling should not be discounted, as although equivalent between the samples, it was shown to be essential in the osteocalcin expression by MSCs on C = 2 cultured in the absence of any differentiating stimuli. And because of this, the Erk1/2 phosphorylation is likely due to adhesion (Greenblatt et al., 2010).

The study of surface properties and their influence on cell behaviour has emerged as a major field in tissue engineering and biomaterial design. Several surface characteristics have been connected with distinct cellular responses e.g. high stiffness is related to high contractility and osteogenic differentiation. The fact that polymers make up a vast proportion of the biomaterials currently used today, raises the need for further study of characteristics typical specifically to polymers; such as polymer mobility. This study, therefore, contributes to that end. It should be emphasised, however, that, as shown in this study, the role of the interfacial protein layer should not be disregarded. The conclusions of this study could in fact only be drawn when the mobility on the fibronectin layer and the exposure of binding sites were analysed.

This study outlines the role of mobility as a subtle polymer property with influential effects on the protein layer, in terms of its own (interfacial) mobility and essential interaction with other proteins such as growth factors. This indicates that mobility should be taken into account in the design of biomaterials as a way to optimise their desired function.

Future Research Avenues

The subject of polymer mobility remains open so long as polymers are used biomaterials. In terms of the scope of this work, some findings need to be further investigated to be established. For example, whether Erk1/2 phosphorylation observed on the fibronectin - coated polymers was due to non-canonical signalling or adhesion. MSC focal adhesions should also be studied to analyse how soon these cells respond to interfacial mobility. Attempts to analyse ligand anchorage on these samples were not very successful for C = 6 as it is an extremely adhesive polymer, therefore optimization of this experiment may yield more information which can be contextualised with the current study. Another avenue for cell response analysis would be to investigate the maintenance of stemness markers by MSCs cultured on these samples, as these samples offer a unique window to study polymer mobility and this experiment is yet to be carried out. Three dimensional constructs also offer an attractive path to study mobility, as most biomaterials ultimately need to acquire a three - dimensional structure for different applications. Currently studies have shown that mobility does exert influence in three dimensional constructs (Andersson et al., 2008) (Sabater i Serra et al., 2016), therefore, coupling the low interfacial mobility of C = 2 with growth factors may yield surfaces with more specific presentation of these growth factors, which may improve their effect and efficiency.

Appendix A

Table: Immunostaining reagents used in this work.

Antibodies	**Company**	**Dilution**
Anti - vinculin (monoclonal mouse)	Sigma - Aldrich	1:200
Anti - osteocalcin - OCN (monoclonal mouse)	Santa Cruz Biotechnology	1:50
Anti - osteopontin - OPN (monoclonal mouse)	Santa Cruz Biotechnology	1:50
Anti - mouse, anti - rabbit antibodies and Streptavidin- FITC	Vactorlabs	1:50
Mounting Medium with DAPI	Vactorlabs	
LI-COR anti-mouse, donkey, rabbit e.t.c (800 nm)	*LI-COR*	1:800
LI-COR CellTag (700 nm)	*LI-COR*	1:500
Monoclonal mouse mAb1937 - For the fibronectin Synergy site (PHRSN)	Sigma - Aldrich	1:20,000
Monoclonal mouse HFN 7.1 - For the fibronectin cell binding site (RGD)	Developmental Studies Hybridoma Bank	1:20,000
Anti - mouse HRP-tagged secondary antibody	R&D systems	1:10 000
Rabbit polyclonal anti - fibronectin antibody	Sigma-Aldrich	1:10 000
Biotinylated horse anti - rabbit antibody	Vectorlabs	1:50
Biotinylated horse anti - mouse antibody	Vectorlabs	1:50
Biotinylated goat anti - rabbit antibody	Millipore Cat: AP132B	1:1000
HRP - streptavidin	R&D Systems	1:200
Rhodamine phallotoxin R415	Life Technologies	1:40
Cy3 anti - mouse	Jackson Immunoresearch	1:200
Anti - sarcomeric myosin antibody	Developmental Studies Hybridoma Bank	1:250
Rat anti - integrin subunit beta1	BD Pharmingen	1:200
Phalloidin	Life Technologies	1:500
mouse anti - integrin αvβ3	Millipore	1:300
Rabbit anti-paxillin	Millipore	1:300
ProLong® Gold Antifade Reagent	Invitrogen	1x
VECTASHIELD Antifade Mounting - Medium	Vectorlabs	1x

With DAPI		
AlexaFluors 488 (anti-mouse), 546 (anti-rat), and 633 (anti-rabbit)	Thermo Fisher Scientific	1:1500
Extravidin-peroxidase	Sigma - Aldrich	1:1000
TMB 1-step™ Ultra TMB-ELISA	Thermo Scientific	1x
heparin II domain antibody	Santa Cruz Biotechnology	14.5 µg/ml

Appendix B

Integrin Ratio Analysis Matlab code

Main Function

```
function out = ratioChan_Fatma(img)
close all

Binary_scale   = 0.7; % The lower this factor the lower the intensity
values included in the mask.

Show_Channels  = 1;    % If 0 you will see less images through the process

Edge_Draw      = 0;    % To be selected to draw in the cells edge for
distance to edge calculation

convf          = 0.11; % Micron to pixel conversion factor

Size_Low       = 5;   % Low end size constraint (pixels)

Size_High      = 1e5;  % High end size constraint (pixels)

Signal2_scale = 1.5;    % Signal 2 scale factor

Signal1_scale = 1;    % Signal 1 scale factor

Open_Close     = 1;    % Watershed on/off

pwr            = 3;    % Watershed Strength

ColormapScale  = 2;   % Sets the colormap max value;

ColormapBins   = 20;   % Sets the number of bins in the colormap
%--------------------------------------------------------------------------
%--------------------------------------------------------------------------

colormap(jet(ColormapBins));
currentMap = colormap;
```

```
newMap = [0 0 0; currentMap];


img1 = mat2gray(imread(img,2));
img2 = mat2gray(imread(img,1));
img3 = mat2gray(imread(img,3));
img4 = mat2gray(imread(img,4));



if Show_Channels == 1;

subplot(1,3,1)
colormap(newMap)

imagesc(img1);
title('Channel "Signal-1"')

subplot(1,3,2)
colormap(newMap)

imagesc(img4);
title('Channel "Signal-2"')

subplot(1,3,3)
colormap(newMap)

imagesc(img3);
title('Channel FA') % Binirization to produce mask image


end

%% A FA Mask

threshold = mean(max(img3));
mask = img3; % Inputs mask image here
mask(mask>threshold.*Binary_scale) = 1;
mask(mask~=1) = 0;

% Code for making a selection with clicks and double clicks

if Open_Close == 1;

    mask = OpenCloseImage(mask,pwr);

    mask = double(mask);

end

figure;
colormap(newMap);
imagesc(mask);


%% Allows choice of ROI (region of interest) for further analysis
```

```
ROIselection = roipoly;

img22 = img4.*mask; %Inputs "Signal-2" image here
img11 = img1.*mask; %Inputs "Signal-1" image here

img22(~ROIselection) = 0;
img11(~ROIselection) = 0;

img22 = img22.*Signal2_scale;      % Scales channels here
img11 = img11.*Signal1_scale;

subplot(1,2,1)
img22(isnan(img22)) = 0;
colormap(newMap);
imagesc(img22);
title('Signal-2 w/ ROI and Mask')

subplot(1,2,2)
img11(isnan(img11))=0;
colormap(newMap);
imagesc(img11);
title('Signal-1 w/ ROI and Mask')

%% Production of Ratios of the two channels and visualization

rat = img11./img22;
rat(isnan(rat)) = 0;
figure;
colormap(newMap);
imagesc(rat);
caxis([0 ColormapScale]);
title('Ratio of Channel Signal 2-to-1 (Selections)')



ratb = rat;
ratb(ratb>0) = 1;
ratb(ratb~=1) = 0;


%% Capture of parameters about the ratioed channels

S = bwconncomp(ratb);
data = regionprops(S,'Area');

% Area Threshold
idx = find([data.Area] > Size_Low & [data.Area]<=Size_High);
aimg = ismember(labelmatrix(S),idx);

S2 = bwconncomp(mat2gray(aimg));
data =
regionprops(S2,rat,'Area','MajorAxis','MinorAxis','Orientation','Solidity',
'MeanIntensity', ...
                    'MaxIntensity');


%% Multiplication of Conversion Factior (Convf)
```

```
for k = 1:numel(data);
      data(k).Area = data(k).Area.*convf.^2;
      data(k).MinorAxisLength = data(k).MinorAxisLength.*convf;
      data(k).MajorAxisLength = data(k).MajorAxisLength.*convf;
end

%% Distance to Edge Calculation


if Edge_Draw == 1;

        zimg = img3;
        figure
        imagesc(zimg);
        [bw] = roipoly;
        zimg(bw) = 1; zimg(~bw) = 0;
        C2=bwconncomp(zimg);
        bounds = bwboundaries(zimg);
        boundsx= bounds{1}(:,2);
        boundsy=bounds{1}(:,1);

     Q = findline(data,boundsx,boundsy,img3);

     for t = 1:numel(Q)
         data(t).DteLoc = Q(t).trueloc;
     end

     Z = finddist(data);

     for t = 1:numel(Z)
         data(t).DTE = Z(t).MinDTE.*convf;
         data(t).LOCE = Z(t).Minloc;
     end

end




out = data;
```

Data file (excel) generator function

```
function ratioXLS(data_in, file_name)
format long g

isPC = 0;

area = [];
majoraxis = [];
minoraxis = [];
```

```
orientation  = [];
solidity = [];
meanintensity = [];
maxintensity = [];
DTE = [];

DTEcheck = 0;

store = NaN.*ones(numel(data_in(1).Area),8);

for i = 1:numel(data_in);

    area = [area data_in(i).Area];
    majoraxis = [majoraxis data_in(i).MajorAxisLength];
    minoraxis = [minoraxis data_in(i).MinorAxisLength];
    orientation = [orientation data_in(i).Orientation];
    solidity    = [solidity data_in(i).Solidity];
    meanintensity = [meanintensity data_in(i).MeanIntensity];
    maxintensity = [maxintensity data_in(i).MaxIntensity];

    if DTEcheck == 1;
       DTE = [DTE data_in(i).DTE];
    end
end


store(1:numel(area),1)             = area';
store(1:numel(majoraxis),2)        = majoraxis';
store(1:numel(minoraxis),3)        = minoraxis';
store(1:numel(orientation),4)      = orientation';
store(1:numel(solidity),5)         = solidity';
store(1:numel(meanintensity),6)    = meanintensity';
store(1:numel(maxintensity),7)     = maxintensity';
store(1:numel(DTE),8)              = DTE';


xlswrite(file_name,store);

if isPC == 1

xlswrite(file_name,['area',
'majoraxis','minoraxis','orientation','solidity','meanintensity','maxintens
ity','DTE'],'a1')

end
```

References

Abraham, C.M. (2014). A Brief Historical Perspective on Dental Implants, Their Surface Coatings and Treatments. The open dentistry journal *8*, 50–55.

AC, D., Weng, S., Feil, G., Schäfer, J., Baumann, S., Kanz, L., Sievert, K., Stenzl, A., and Möhle, R. (2009). In vitro myogenic differentiation of human bone marrow-derived mesenchymal stem cells as a potential treatment for urethral sphincter muscle repair. Annals of the New York Academy of sciences *1176*, 135-143.

Adam, G., and Gibbs, J.H. (1965). On the Temperature Dependence of Cooperative Relaxation Properties in Glass-Forming Liquids. Journal of Chemical Physics *43*, 139-146.

Agrawal, V., and Sinha, M. (2016). A review on carrier systems for bone morphogenetic protein-2. Journal of Biomedical Materials Research, Part B; Applied Biomaterials.

Aguirre, K.M., R. JSchwarzbauer, J. E (1994). Fibronectin self-association is mediated by complementary sites within the amino-terminal one-third of the molecule. The Journal of Biological Chemistry, 27863-27868.

Aguzzi, A.O.C., T (2010). Protein aggregation diseases: pathogenicity and therapeutic perspectives. Nature Reviews Drug Discovery *9*, 237-248

Andersson, M., Suska, F., Johansson, A., Berglin, M., Emanuelsson, L., Elwing, H., and Thomsen, P. (2008). Effect of molecular mobility of polymeric implants on soft tissue reactions: An in vivo study in rats. Journal of Biomedical Materials Research Part A *84A*, 652-660.

Aota, S., Nomizu, M., and Yamada, K. (1994). The short amino acid sequence Pro-His-Ser-Arg-Asn in human fibronectin enhances cell-adhesive function. Journal of Biological Chemistry *269*, 24756-24761.

Arima, Y., and Iwata, H. (2007). Effects of surface functional groups on proteinadsorption and subsequent cell adhesion using self-assembled monolayers. Journal of Materials Chemistry *17*, 4079-4087

Arnsdorf , E.J., Tummala , P., Kwon , R.Y., and Jacobs, C.R. (2009). Mechanically induced osteogenic differentiation – the role of RhoA, ROCKII and cytoskeletal dynamics. Journal of Cell Science *122*, 546-553.

Atherton, P.S., Ben Jethwa, Devina Ballestrem, Christoph (2016). Mechanosensitive components of integrin adhesions: Role of vinculin. Experimental Cell Research *343*, 21-27.

Attisano, L., and Wrana, J.L. (2000). Smads as transcriptional co-modulators Current Opinion in Cell Biology *12*, 235–243

Axelrod, D., Koppel, D.E., Schlessinger, J., Elson, E.L., and Webb, W.W. (1976). Mobility measurement by analysis of fluorescence photobleaching recovery kinetics. Biophysical Journal *16*, 1315 – 1329.

Bajaj, P., Reddy, B.J., Millet, L., Wei, C., Zorlutuna, Pinar, Bao, G., and Bashir, R. (2011). Patterning the differentiation of C2C12 skeletal myoblasts. Integrative Biology *3*, 897-909.

Balaban, N.Q., Schwarz, U.S., Riveline, D., Goichberg, P., Tzur, G., Sabanay, I., Mahalu, D., Safran, S., Bershadsky, A., Addadi, *et al.* (2001). Force and focal adhesion assembly: a close relationship studied using elastic micropatterned substrates. Nature Cell Biology *3*, 466−472.

Bathawab, F., Bennett, M., Cantini, M., Reboud, J., Dalby, M., and Salmerón-Sánchez, M. (2015). Lateral Chain Length in Polyalkyl Acrylates Determines the Mobility of Fibronectin at the Cell/Material Interface. Langmuir, 800-809.

Becker, A.J., McCulloch, E.A., and Till, J.E. (1963). Cytological demonstration of the clonal nature of spleen colonies derived from transplanted mouse marrow cells. Nature, 452.

Benoit , D.S.W.S., Michael P. Durney , Andrew R. Anseth , Kristi S. (2008). Small functional groups for controlled differentiation of hydrogel-encapsulated human mesenchymal stem cells. Nature Materials *7*, 816 - 823.

Berglin, M., Andersson, M., Sellborn, A., and Elwing, H. (2004). The effect of substrate molecular mobility on surface induced immune complement activation and blood plasma coagulation. Biomaterials *25*, 4581-4590

Bhadriraju K, Yang M, Alom Ruiz S, Pirone D, Tan J, and CS, C. (2007). Activation of ROCK by RhoA is regulated by cell adhesion, shape, and cytoskeletal tension. Experimental Cell Research *313*, 3616-3623.

Bigham-Sadegh, O.A.M. (2014). Bone morphogenetic proteins: a powerful osteoinductive compound with non-negligible side effects and limitations. Biofactors *40*, 459-481.

Blau, H.M., Pavlath, G.K., Hardeman, E.C., Chiu, C.-P., Silberstein, L., Webster, S.G., Miller, S.C., and Webster, C. (1983). Plasticity of the Differentiated State. Science *230*, 758-766.

Bohner, M., and Galea, L.D., Nicola (2012). Calcium phosphate bone graft substitutes: Failures and hopes. Journal of the European Ceramic Society *32*, 2663–2671.

Bonfiglio, G.M., Jeter, W., and Smith, C. (1955). The immune concept: its relation to bone transplantation. In Immune Reactions in Tissue Homotransplants (The NewYork academy of sciences).

Bouvard, D.B., Cord, and , G., Erika Aszódi, Attila Bengtsson, Therese Berna, Alejandro Fässler, Reinhard (2001). Functional consequences of Integrin gene mutations in mice. Circulation research *89*.

Bradshaw, M.J., and Smith, M.L. (2014). Multiscale relationships between fibronectin structure and functional properties. Acta Biomaterialia *10*, 1524–1531.

Bragdon, B.M., OSaldanha, SKing, DJulian, J Nohe, A (2011). Bone Morphogenetic Proteins: A critical review. Cellular Signalling *23*, 609–620.

Brew, S.A.I., K. C (1994). Purification of human plasma fibronectin. Journal of Tissue Culture Methods *16*, 197.

Brockman, H.L., Law, J.H., and Kezdy, F.J. (1973). The hydrolysis of tripropionin by pancreatic lipase adsorbed to siliconized glassbeads. The journal of Biological Chemistry *248, 14*, 4965-4970.

Burchardt, H., Apr, O.C.N.A., and 18(2):187-96. (1987). Biology of bone transplantation. The Orthopedics Clinics of North America *18*, 187-196.

Cain, J., Hartwig, S., Bertram, J., and Rosenblum, N. (2008). Bone morphogenetic protein signaling in the developing kidney: present and future. Differentiation *76*, 831–842

Calmar, E.A.V., R. J (2002). The anatomy and physiology of bone fracture and healing. In Clinical Pediatric Emergency Medicine (Boston Medical Center, Boston, MA, USA), pp. 85–93.

Cantini, M., Sousa, M., Moratal, D., Mano, J., and Salmeron-Sanchez, M. (2013). Non-monotonic cell differentiation pattern on extreme wettability gradients. Biomaterials Science *1*, 202-212.

Cao, L., Zeller, M.K., Fiore, V.F., Strane, P., Bermudez, H., and Barker, T.H. (2012). Phage-based molecular probes that discriminate force-induced structural states of fibronectin in vivo. Proceedings of the National Academy of Sciences of the United States of America *109*, 7251-7256.

Caplan, A. (1991). Mesenchymal stem cells. Journal of Orthopaedic research *5*, 641-650.

Carragee , E.J., Hurwitz, E.L., and Weiner, B.K. (2011). A critical review of recombinant human bone morphogenetic protein-2 trials in spinal surgery: emerging safety concerns and lessons learned . The Spine Journal *11*, 471.

Carragee, E.J., Hurwitz, E.L., and Weiner, B.K. (2011). A critical review of recombinant human bone morphogenetic protein-2 trials in spinal surgery: emerging safety concerns and lessons learned. . Spine Journal, 471.

Castellani, L., Salvati, E., Alemà, S., and Falcone, G. (2006). Fine Regulation of RhoA and Rock Is Required for Skeletal Muscle Differentiation. The journal of Biological Chemistry, 15249-15257.

Castro-Malaspina, H.G., RE Resnick , G Kapoor , N Meyers , P Chiarieri , D McKenzie , S Broxmeyer, HE Moore, MA (1980). Characterization of human bone marrow fibroblast colony-forming cells (CFU-F) and their progeny. Blood *56*, 289-301.

Chaudhuri, O., Koshy, S.T., Branco da Cunha, C., Shin, J.-W., Verbeke, C.S., Allison, K.H., and Mooney, D.J. (2014). Extracellular matrix stiffness and composition jointly regulate the induction of malignant phenotypes in mammary epithelium. Nature Materials *13*, 970–978.

Chen, G., Deng, C., and Li, Y.P. (2012). TGF-b and BMP signaling in osteoblast differentiation and bone formation. International Journal of Biological science *8*.

Cohen, M.H., and Turnbull, D. (1959). Molecular Transport in Liquids and Glasses. Journal of Chemical Physics *31*.

Cohnheim, J. (1867). Ueber entzündung und eiterung. Path Anat Physiol Klin Med.

Coppé , J.-P., Desprez , P.-Y., Krtolica , A., and Campisi, J. (2014). The Senescence-Associated Secretory Phenotype: The Dark Side of Tumor Suppression. Annual Review in Pathology *5*, 99-118.

Curran , J.M., Pu , F., Chen , R., and Hunt , J. (2011). The use of dynamic surface chemistries to control msc isolation and function. Biomaterials *32*, 4753 – 4760.

da Silva, M.L., Chagastelles, P., and Nardi, N. (2006). Journal of Cell Science *119(Pt 11)*, 2204-2213.

Daculsi, G. (1998). Biphasic calcium phosphate concept applied to artificial bone, implant coating and injectable bone substitute. Biomaterials *19*, 1473–1478.

Dalby, M., Childs, S., Riehle, M., Johnstone, H., Affrossman, S., and Curtis, A. (2003). Fibroblast reaction to island topography: changes in cytoskeleton and morphology with time. Biomaterials *24*, 927–935.

Dalby , M.J., Gadegaard , N., Tare , R., Andar , A., Riehle , M.O., Herzyk , P., Wilkinson , C.D.W., and Oreffo, R.O.C. (2007). The control of human mesenchymal cell differentiation using nanoscale symmetry and disorder. Nature Materials *6*, 997 - 1003.

Daluiski, A., Engstrand, T., Bahamonde, M., Gamer, L., Agius, E., Stevenson, S., Cox, K., Rosen, V., and Lyons, K. (2001). Bone morphogenetic protein-3 is a negative regulator of bone density. Nature Genetics *27*, 84-88.

Damsky, C., Librach, C., Lim, K., Fitzgerald, M., McMaster, M., Janatpour, M., Zhou, Y., Logan, S., and Fisher, S. (1994). Integrin switching regulates normal trophoblast invasion. Development *120(12)*, 3657-3666.

De Caestecker, M. (2004). The transforming growth factor-beta superfamily of receptors. Cytokine Growth Factor Review *15*, 1–11.

De Groot, K. (1983). Ceramics of calcium phosphates: preparation and properties. In Bioceramics of calcium phosphate (Raton, Florida: CRC Press).

Dhawan, J., D. M (2004). Modulation of acto-myosin contractility in skeletal muscle myoblasts uncouples growth arrest from differentiation. Journal of Cell Science *117*, 3735-3748.

Discher, D.E., Janmey, P., and I, W.Y. (2005). Tissue Cells Feel and Respond to the Stiffness of Their Substrate. Science *310*, 1139-1143.

Dominici, M., Le Blanc, K., Mueller, I., Slaper-Cortenbach, I., Marini, F., Krause, D., Deans, R., Keating, A., Prockop, D., and Horwitz, E. (2006). Minimal criteria for defining multipotent mesenchymal stromal cells. The International Society for Cellular Therapy position statement. Cytotherapy *4*, 315-317.

Ducy, P., Zhang, R., Geoffroy, V., Ridall, A.L., and Karsenty, G. (1997). Osf2/Cbfa1: a transcriptional activator of osteoblast differentiation. Cell *89*, 747.

El-Bizri, N., Guignabert, C., Wang, L., Cheng, A., Stankunas, K., Chang, C., Mishina, Y., and M, R. (2008). SM22alpha-targeted deletion of bone morphogenetic protein receptor 1A in mice impairs cardiac and vascular development, and influences organogenesis. Development *135*, 2981–2991.

Elias, D., and Poloukhtine, A., VTsourkas, A (2013,). Effect of ligand density, receptor density, and nanoparticle size on cell targeting Nanomedicine: Nanotechnology, Biology and Medicine *9*, 194–201.

Ellison, C.J., and Torkelson, J.M. (2003). The distribution of glass-transition temperatures in nanoscopically confined glass formers. Nature Materials *2*, 2 695-700.

Engler, A.J., Sen, S., Sweeney, H.L., and Discher, D.E. (2006). Matrix elasticity directs stem cell lineage specification. Journal of Cell Science *126*, 677–689

Enomoto, H.-I., MIwamoto, M (2000). Cbfa1 is a positive regulatory factor in chondrocyte maturation. Journal of Biological Chemistry, 8695–8702

Eun Yang, K., Kwon, J., Rhim, J.-H., Choi, J., Kim, S.I., Lee, S.-H., Park, J., and Jang, I.-S. (2011). Differential expression of extracellular matrix proteins in senescent and young human fibroblasts: A comparative proteomics and microarray study. Molecules and Cells *32*, 99-106.

Fink, T., and Zachar, V. (2011). Adipogenic differentiation of human mesenchymal stem cells. Methods in Molecular Biology *698*, 243-251.

Frantz, C., Stewart, K., and Weaver, V. (2010). The extracellular matrix at a glance. Journal of Cell Science, 4195-4200.

Friedenstein, A., Chailakhjan, R., and Lalykina, K. (1970). The development of fibroblast colonies in monolayer cultures of guinea-pig bone marrow and spleen cells. Cell and Tissue kinetics *4*, 393-403.

Friedenstein, A., Gorskaja, J., and Kulagina, N. (1976). Fibroblast precursors in normal and irradiated mouse hematopoietic organs. Experimental Hematology *4*, 267-274.

Ganguly , K.K., Pal , S., Moulik , S., and Chatterjee , A. (2013). Integrins and Metastasis. Cell Adhesion and Migration *7*, 251–261.

Gao, F.C., S. M Motan, D. A. L Zhang, Z Chen, L Ji , H-L Tse, H-F, and Fu, Q.-L.L., Q (2016). Mesenchymal stem cells and immunomodulation: current status and future prospects. Nature: Cell Death and Disease *7*.

Garcia, A., Vega, M., and Boettiger, D. (1999). Modulation of cell proliferation and differentiation through substrate-dependent changes in fibronectin conformation. Molecular Biology of the Cell *10*, 785-798.

Gartner, S.K., HS (1980). Long-term culture of human bone marrow cells. Proceedings of the National Academy of Sciences *77*, 4756-4759.

Geiger, B., Bershadsky, A., Pankov, R., and Yamada, K.M. (2001). Transmembrane Extracellular Matrix - Cytoskeleton Crosstalk. Nature Reviews: Molecular Cell Biology *2*, 793-805.

George, E., Georges-Labouesse, E., Patel-King, R., Rayburn, H., and Hynes, R. (1993). Defects in mesoderm, neural tube and vascular development in mouse embryos lacking fibronectin. Development, 1079-1091.

Gimble , J.M., Guilak , F., Nuttall , M.E., Sathishkumar , S., Vidal , M., and Bunnell, B. (2008). In vitro Differentiation Potential of Mesenchymal Stem Cells. Transfusion medicine and Hemotherapy *35*, 228–238.

Gonzalez-Garcia, C., Cantini, M., Moratal, D., Altankov, G., and Salmeron-Sanchez, M. (2013). Vitronectin alters fibronectin organization at the cell-material interface. Colloids Surfaces.

Gonzalez-Garcia, C., Moratal, D., Oreffo, R.O.C., Dalby, M.J., and Salmeron-Sanchez, M. (2012). Surface mobility regulates skeletal stem cell differentiation. Integrative Biology *4*, 531-539.

Greenblatt, Shim, Zou, Sitara, Schweitzer, Hu, Lotinun, Sano, Baron, Park, *et al.* (2010). The p38 MAPK pathway is essential for skeletogenesis and bone homeostasis in mice. Journal of Clinical Investigation *120*, 2457–2473.

Guerra, N.B., Gonzalez-Garcia, C., Llopis, V., Rodriguez-Hernandez, J.C., Moratal, D., Rico, P., and Salmeron-Sanchez, M. (2010). Subtle variations in polymer chemistry modulate substrate stiffness and fibronectin activity. Soft Matter *6*, 4748-4755.

Gugutkov, D., Altankov, G., Rodríguez Hernández, J.C., Monleón Pradas, M., and Salmerón-Sánchez, M. (2010). Fibronectin activity on substrates with controlled -OH density. Journal of Biomedical Materials Research Part A *92A*, 322-331.

Han, S.J., Bielawski, K.S., Ting, L.H., Rodriguez, M.L., and Sniadecki, N.J. (2012). Decoupling Substrate Stiffness, Spread Area, and Micropost Density: A Close Spatial Relationship between Traction Forces and Focal Adhesions. Biophysical Journal *103*, 640-648.

Harburger, D.S., and Calderwood , D.A. (2009). Integrin signalling at a glance. Journal of Cell Science *122(2): 159–163.*

Hass, R., C, Böhm , S., and Jacobs, R. (2011). Different populations and sources of human mesenchymal stem cells (MSC): A comparison of adult and neonatal tissue-derived MSC. Cell communication and signalling, 1-14.

Hayrapetyan, A., Jansen, J., Jeroen, J.J.P., and Beucken, V. (2014). Signaling Pathways Involved in Osteogenesis and Their Application for Bone Regenerative Medicine. Tissue Engineering, Part B.

Healy, K.E. (1999). Molecular engineering of materials for bioreactivity. Current Opinion in Solid State Material Science *4*, 381–387.

Heino, J., and Massague, J. (1990). Cell Adhesion to

Collagen and Decreased Myogenic Gene Expression Implicated in the Control of

Myogenesis by Transforming Growth Factor β. Journal of Biological Chemistry *265.18*, 10181-10184.

Hirsh, J. (1991). Oral Anticoagulant Drugs. The New England Journal of Medicine *324*, 1865-1875

Hocking, D., Sottile, J., and Langenbach, K. (2000). Stimulation of integrin-mediated cell contractility by fibronectin polymerization. Journal of Biological Chemistry *275*, 10673-10682.

Hocking, D.C., Sottile, J., and McKeown-Longo, P.J. (1994). Fibronectin's III-1 module contains a conformation-dependent binding

site for the amino-terminal region of fibronectin. The Journal of Biological Chemistry *269*, 19183-19187.

Horbelt, D., AKnaus, A (2012). A portrait of transforming growth factor β superfamily signalling: background matters. International Journal of Biochemistry *44*, 469–474.

Hoshino , A.C.-S., Bruno Shen, Tang-Long, Rodrigues , G.A.H., Mark, M.T., Molina, H., Shinji Kohsaka , Giannatale, A.D., Ceder, S., Singh, S., Williams, C., Nadine Soplop , *et al.* (2015). Tumour exosome integrins determine organotropic metastasis. Nature *527*, 329–335. .

Hubbell, J.A. (1999). Bioactive biomaterials. Current Opinion in Biotechnology *10*, 123–129.

Humby, P. (2016). February 2016. In Overview of the UK population: (Office for National Statistics, UK).

Humphrey, J.D., Dufresne, E.R., and Schwartz, M.A. (2014). Mechanotransduction and extracellular matrix homeostasis. Nature Reviews Molecular Cell Biology *15*, 802–812.

Humphries, J., Byron, A., and Humphries, M. (2006). Integrin ligands at a glance. Journal of Cell Science *119(Pt 19)* 3901-3903.

Hynes, R. (2002). Integrins: bidirectional, allosteric signaling machines. Journal of Cell Science *110(6)*, 673-687. .

Hynes, R.O. (1992). Integrins: Versatility, Modulation and Signalling in Cell Adhesion. Cell *69*, 11-25.

Hynes, R.O. (2004). The emergence of integrins: a personal and historical perspective. Matrix Biology *23*, 333–340.

Hynes, R.O., and Naba, A. (2012). Overview of the matrisome—an inventory of extracellular matrix constituents and functions. . Cold Spring Harbour Perspectives in Biology *4*, a004903.

Ingber, D. (1997). Integrins, tensegrity, and mechanotransduction. Gravitational and Space Biology Bulletin *10*, 49-55.

Irish, J. (2004). A 5,500 year old artificial human tooth from Egypt: a historical note. The international journal of oral and maxillofacial implants *19*, 645-647.

Jiang , Y., Jahagirdar, B.N., Reinhardt, R.L., Schwartz, R.E., Keene, C.D., Ortiz-Gonzalez, X.R., Reyes, M., Lenvik, T., Lund, T., Blackstad, M., *et al.* (2002). Pluripotency of mesenchymal stem cells derived from adult marrow. Nature *418*, 41-49.

Jin-Young, B.-H., Byung-Young, Seoung-Ho, Shi-Jiang,, and Jae-Hyung (2005). Critical size defect in the canine mandible Oral Surgery, Oral Medicine, Oral Pathology, Oral Radiology, and Endodontology *100*, 296–301.

Johnell, O., and Kanis, J. (2006). An estimate of the worldwide prevalence and disability associated with osteoporotic fractures. . Osteoporos International *17*, 1726.

Jones, D.L., and Wagers, A.J. (2008). No place like

home: anatomy and function of the stem cell niche. Nature Reviews Molecular Cell Biology *9*, 11-21.

Juopperia, chulerc, Yuanc, Collectorc, Danga, and Sharkisc (2007). Isolation

of Bone Marrow–Derived Stem Cells using Density-Gradient Separation. Experimental Hematology *35*, 335–341.

Kania, M.A.B., A.S.Duffy, J.B. (1990). The Drosophila segmentation gene runt encodes a novel nuclear regulatory protein that is also expressed in the developing nervous system. Genes and Development, 1701–1713

Kanno, T., Takahashi, T., Tsujisawa, T., Ariyoshi, W., and Nishihara, T. (2007). Mechanical stress-mediated Runx2 activation is dependent on Ras/ERK1/2 MAPK signaling in osteoblasts. Journal of Cellular Biochemistry *101*, 1266.

Katagiri, T., Yamaguchi, A., Komaki, M., Abe, E., Takahashi, N., Ikeda, T., Rosen, V., Wozney, J.M., Fujisawa-Sehara, A., and Suda, T. (1994). Bone Morphogenetic Protein-2 Converts the Differentiation Pathway of C2C12 Myoblasts into the Osteoblast Lineage. The Journal of Cell Biology, 1755-1176.

Keselowsky, B., Collard, D., and Garcia, A. (2003). Surface chemistry modulates fibronectin conformation and directs integrin binding and specificity to control cell adhesion. Journal of Biomedical Materials Research Part a *66A*, 247-259.

Kfoury, Y., and Scadden, D.T. (2015). Mesenchymal cell contribution to the stem cell niche. Cell stem cell *16*, 239–253.

Kilian , K.A., Bugarija , B., Lahn , B., and Mrksich, M. (2010). Geometric cues for directing the differentiation of mesenchymal stem cells. Proceedings of the National Academy of Sciences of the United States of America *107*, 4872–4877.

Kim, D.-H., and Wirtz, D. (2013). Focal adhesion size uniquely predicts cell migration. FASEB Journal *27*, 1351–1361.

Kim, S.-H., Turnbull, J., and Guimond, S. (2011). Extracellular matrix and cell signalling: the dynamic cooperation of integrin, proteoglycan and growth factor receptor. Journal of Endocrinology *209*, 139–151.

Kingham, E.J., P.MGadegaard, NDalby, M.JOreffo, R.O.C (2011). Nanotopography induced osteogenic differentiation of human stem cells Bone *48*, S108-S109.

Komori, T., HNomura,S (1997). Targeted disruption of Cbfa1 results in a complete lack of bone formation owing to maturational arrest of osteoblasts. Journal of Cell Science *89*, 755–764.

Koo, L., Irvine, D., Mayes, A., Lauffenburger, D., and Griffith, L. (2002). Co-regulation of cell adhesion by nanoscale RGD organization and mechanical stimulus. Journal of Cell Science *7*, 1423-1433.

Kosmehl, H., Berndt, A., and ., K.D. (1996). Molecular variants of fibronectin and laminin: structure, physiological occurrence and histopathological aspects. Virchows Archives, 311-322. .

Krammer, A., Craig, D., Thomas, W., Schulten, K., and Vogel, V. (2002). A structural model for force regulated integrin binding to fibronectin's RGD-synergy site. Matrix biology, 139-147.

Kuo, B.A., Uporova, T.M., Liang, H., Bennet, V.D., Tuan, R.S., and Norton, P.A. (2002). Alternative splicing during chondrogenesis: Modulation of fibronectin exon EIIIA splicing by SR proteins. Journal of Cellular Biochemistry *86*, 45–55.

Kuo, J., Han, X., Yates, J.r., and Waterman, C. (2012). Isolation of focal adhesion proteins for biochemical and proteomic analysis. Methods in Molecular Biology *757*, 297-323.

Laurencin, C., Khan, Y., and El-Amin, S. (2006). Bone graft substitutes. Expert Rev Med Devices *3*, 49–57.

Leahy, D.J., Aukhil, I., and Erickson, H.P. (1996). A crystal structure of a four-domain segment of human fibronectin encompassing the RGD loop and synergy region. . Cell *84*, 155−164.

Lee , K., Silva , E.A., and Mooney, D.J. (2011). Growth factor delivery-based tissue engineering: general approaches and a review of recent developments. The Royal Society of Chemistry: Interface *8*, 153–170.

Lee, K.S., Hong, S.H., and Bae, S.C. (2002). Both the Smad and p38 MAPK pathways play a crucial role in Runx2 expression following induction by transforming growth factor-beta and bone morphogenetic protein. Oncogene *21*, 7156-7163.

Lee, S.S., Huang, B.J., Kaltz, S.R., Christina, S.S.J., Newcomb, S.R., Stock, R.N., Shah, and I, S.S. (2013). Bone Regeneration with Low Dose BMP-2 Amplified by Biomimetic Supramolecular Nanofibers within Collagen Scaffolds. Biomaterials *34*, 452-459.

Li, and WJiang, K., W Shi, YDing, S (2013). Chemical approaches to studying stem cell biology. Cell Research *23*, 81–91.

Lindholm , R., Lindholm , S., Liukko , P., Paasimaki , J., Isokääntä , S., Rossi , R., Auti0 , E., and Tamminen, E. (1969). The Mast cell as a component of callus in healing fractures. The bone and joint journal *1;51*, 148-155.

Liu, R., Masters, K.S., and Gellman, S.H. (2012). Polymer Chain Length Effects on Fibroblast Attachment on Nylon-3-Modified Surfaces. Biomacromolecules *13*, 1100-1105.

Liu , R., Masters , K.S., and Gellman , S.H. (2012). Polymer Chain Length Effects on Fibroblast Attachment on Nylon-3-Modified Surfaces. Biomacromolecules *13*, 1100 – 1105.

Liu, T.M., and Lee, E.H. (2012). Transcriptional regulatory cascades in Runx2-dependent bone development Tissue Engineering Part B Review *19*, 254.

Lu, P., Weaver, V.M., and Werb, Z. (2012). The extracellular matrix: A dynamic niche in cancer progression The Journal of Cell Biology *196*, 395–406

Luu, H., Song, W., Luo, X., Manning, D., Luo, J., Deng, Z., Sharff, K., Montag, A., Haydon, R., and He, T. (2007). Distinct roles of bone morphogenetic proteins in osteogenic differentiation of mesenchymal stem cells. Journal of Orthopedic research *25*, 665-677.

Macewen, W. (1881). Observations concerning Transplantation of bone. Illustrated by a case of inter-human osseous transplantation, whereby over two-thirds of a humerus was restored. Proceedings of the Royal society of London *32*, 232-247.

Main , A.L., Harvey , T.S., Baron , B., and Campbell, I.D. (1992). The three-dimensional structure of the tenth type III module of fibronectin: An insight into RGD-mediated interactions. Journal of cell science *71*, Pages 671-678.

Mao, Y., and Schwarzbauer, J. (2005). Fibronectin fibrillogenesis, a cell-mediated matrix assembly process. Matrix Biology *6*, 389-399.

Mardon, H., and Grant, K. (1994). The role of the ninth and tenth type III domains of human fibronectin in cell adhesion. FEBS letters, 197-201.

Martino, M., and Hubbell, J. (2010a). The 12th–14th type III repeats of fibronectin function as a highly promiscuous growth factor-binding domain. The FASEB journal *24*, 4711 - 4721.

Martino, M., Mochizuki, M., Rothenfluh, D., Rempel, S., Hubbell, J., and Barker, T. (2009). Controlling integrin specificity and stem cell differentiation in 2D and 3D environments through regulation of fibronectin domain stability. Biomaterials *30*, 1089-1097.

Martino, M.M., and Hubbell, J.A. (2010b). The 12th-14th type III repeats of fibronectin function as a highly promiscuous growth factor-binding domain. FASEB *24*, 12 4711-4721.

Martino, M.M., Tortelli, F., Mochizuki, M., Traub, S., Ben-David, D., Kuhn, G.A., Muller, R., Livne, E., Eming, S.A., and Hubbell, J.A. (2011). Engineering the Growth Factor Microenvironment with Fibronectin Domains to Promote Wound and Bone Tissue Healing. Science Translational Medicine *3*, 89.

Massague, J., and Chen, Y.G. (2000). Controlling TGF-beta signaling. Science Signalling *14*, 627.

McBeath, R., Pirone, D., Nelson, C., Bhadriraju, K., and Chen, C. (2004a). Cell shape, cytoskeletal tension, and RhoA regulate stem cell lineage commitment. Developmental cell ***6***, 483-495.

McBeath, R., Pirone, D., Nelson, C., Bhadriraju, K., and Chen, C. (2004b). Cell shape, cytoskeletal tension, and RhoA regulate stem cell lineage commitment. Developmental cell *6*, 483-495.

McNamara, L., McMurray, R., Biggs, M., Kantawong, F., Oreffo, R., and Dalby, M. (2010). Nanotopographical Control of Stem Cell Differentiation. Journal of Tissue engineering *2010*.

ME, B., and SM, G. (2013). The Focal Adhesion Analysis Server: a web tool for analyzing focal adhesion dynamics. *2* 68

Mecham, R. (2012). Overview of extracellular matrix. Current Protocols in Cell Biology *10*.

Meekeren, J. (1668). Heel en geneeskonstige aanmerkingen (Amsterdam Commelijn).

Michael, K., Vernekar, V., Keselowsky, B., Meredith, J., Latour, R., and Garcia, A. (2003a). Adsorption-induced conformational changes in fibronectin due to interactions with well-defined surface chemistries. Langmuir *19*, 8033-8040.

Michael, K.E., Vernekar , V.N., Keselowsky , B.G., Meredith , J.C., Latour, R.A., style="text-align:justify, p.c.M., text-justify:inter-ideograph, and line-height:150%">García, A.J. (2003b). Adsorption-Induced Conformational Changes in Fibronectin Due to Interactions with Well-Defined Surface Chemistries. Langmuir *19*, 8033–8040.

Milanesi , A.L., Jang-Won Li , Zhenhua Da Sacco , Stefano Villani , Valentina Cervantes , Vanessa Perin, Laura Yu, John S. (2012). β-Cell Regeneration Mediated by Human Bone Marrow Mesenchymal Stem Cells. PLoS One *7*.

Minton, A. (2000). Effect of Excluded surface area and adsorbate clustering on surface adsorption of proteins I. Equilibrium models.

. Biophysical chemistry, 239-247.

Minton, A. (2001). Effects of excluded surface area and adsorbate clustering on surface adsorption of proteins. II. Kinetic models. *80*, 1641-1648.

Montarras, D., Morgan, J., Collins, C., Zaffran, S., Cumano, A., T, P., and Buckingham, M. (2005). Direct isolation of satellite cells for skeletal muscle regeneration. Science *309*, 2064-2067

Morris, H.F., Ochi, S., Spray, J.R., and Olson, J.W. (2000). Periodontal-type measurements associated with hydroxyapatite-coated and non-HA-coated implants : uncovering to 36 months. Annals of Periodontology/the American Academy of Periodontology 56 – 67.

Mould, A., Askari, J., Aota, S., Yamada, K., Irie, A., Takada, Y., Mardon, H., and Humphries, M. (1997). Defining the topology of integrin alpha5beta1-fibronectin interactions using inhibitory anti-alpha5 and anti-beta1 monoclonal antibodies. Evidence that the synergy sequence of fibronectin is recognized by the amino-terminal repeats of the alpha5 subunit. Journal of Biological Chemistry, 17283-17292.

Murphy , W.L., McDevitt, T.C., and Engler, A.J. (2014). Materials as stem cell regulators. Nature Materials *13*, 547–557.

Méndez-Ferrer, S.M., Tatyana V., Ferraro , F., Mazloom , A.R., MacArthur , B.D., Lira , S.A., Scadden , D.T., Ma'ayan , A., Enikolopov , G.N., and Frenette, P.S. (2010). Mesenchymal and haematopoietic stem cells form a unique bone marrow niche. Nature *466*, 829–834. .

Nakanishi, K., Sakiyama, T., and Imamura, K. (2001). On the adsorption of proteins on solid surfaces , a common but very complicated phenomenon. Bioscience and Bioengineering *3*, 233-244.

Nasser, M., Tibi, A., and Savage-Smith, E. (2009). Ibn Sina's *Canon of Medicine*: 11th century rules for assessing the effects of drugsIbn Sina's Canon of Medicine: 11th century rules for assessing the effects of drugs. In Journal of Royal Society of Medicine, pp. 78–80.

Nermut , M.V.G., N.M Eason , P Yamada , S.S Yamada , K.M (1988). Electron microscopy and structural model of human fibronectin receptor. EMBO Journal *7*, 4093–4099.

Nohe, A.H., SEhrlich, MNeubauer, FSebald, WHenis, YIKnaus, P (2002). The mode of bone morphogenetic protein (BMP) receptor oligomerization determines different BMP-2 signaling pathways. Journal of Biological Chemistry *277*, 5330–5338.

Nuss, K.M.R., and von Rechenberg, B. (2008). Biocompatibility Issues with Modern Implants in Bone - A Review for Clinical Orthopedics. Open Orthopaedics journal, 66–78.

Oseni, A.O., Crowley, C., Boland, M.Z., Butler, P., and Seifalian, A. (2011). the Application of Nanomaterials and Stem Cell Technology, Tissue Engineering for Tissue and Organ Regeneration. In Cartilage Tissue Engineering, D. Eberli, ed. (http://www.intechopen.com/books/tissue-engineering-for-tissue-and-organ-regeneration/cartilage-tissue-engineering-the-application-of-nanomaterials-and-stem-cell-technology: InTech).

Ouberai, M., M., Xu, K., Welland, and E., M. (2014). Effect of the interplay between protein and surface on the properties of adsorbed protein layers. Biomaterials *35*, 6157–6163.

Pierre, J.M. (2013). Targeting integrins to promote bone formation and repair. Nature Reviews Endocrinology, 288-295

Pittenger, M.F.M., Alistair M Beck, Stephen C Jaiswal, Rama K Douglas, Robin Mosca, Joseph D Moorman, Mark A Simonetti, Donald W Craig, Stewart Marshak, Daniel R (1999). Multilineage Potential of Adult Human Mesenchymal Stem Cells. *284*, 143-147.

Plotkin, L.I., IAguirre, J. IParfitt, A. MManolagas, S. CBellido, T (2005). Mechanical stimulation prevents osteocyte apoptosis: requirement of integrins, Src kinases, and ERKs. Journal of Physiology; Cell Physiology *289*, C633–C643.

Plow , E.F., Haas , T.A., Zhang , L., Loftus , J., and Smith , J.W. (2000). Ligand binding to integrins. The Journal of Biological Chemistry *275*, 21785-21788.

Pompe , T., Glorius , S., Bischoff , T., Uhlmann , I., Kaufmann , M., Brenner , S., and Werner, C. (2009). Dissecting the Impact of Matrix Anchorage and Elasticity in Cell Adhesion. Biophysical Journal *97*, 2154–2163.

Pryor, G., Langevin, Fernando Herrera, Breithaupt, Gordon Afifi, Zins, Meltzer, Gosman, Cohen, Holmes, (2009). Review of Bone Substitutes. Craniomaxillofac Trauma Reconstr *2*, 151–160.

Pytela, R.P., MD Argraves, S Suzuki, S Ruoslahti, E (1987). Arginine-glycine-aspartic

acid adhesion receptors. Methods Enzymology *144* 475-489.

Rabe, M., Verdes, D., and Seeger, S. (2011). Understanding protein adsorption phenomena at solid surfaces. Advances in Colloid and Interface science, 87 – 106.

Raffaini, G.G., Fabio (2013). Surface Topography Effects in Protein Adsorption on Nanostructured Carbon Allotropes. Langmuir *29*, 4883–4893.

Rammelt, S., Schulze, E., Bernhardt, R., Hanisch, U., Scharnweber, D., Worch, H., Zwipp, H., and Biewener, A. (2004). Coating of titanium implants with type-I collagen. Journal of Orthopaedic Research *22*, 1025 – 1034.

Resende, R.R., Fonseca, E.A., Tonelli, F.M.P., Sousa, B.R., Santos, A.K., Gomes, K.N., Guatimosim, S., Kihara, A.H., and Ladeira, L.O. (2014). Scale/Topography of Substrates Surface Resembling Extracellular Matrix for Tissue Engineering. Journal of Biomedical Nanotechnology *10*, 1157-1193.

Rico, P., Hernandez, J., Moratal, D., Altankov, G., Pradas, M., and Salmeron-Sanchez, M. (2009). Substrate-Induced Assembly of Fibronectin into Networks: Influence of Surface Chemistry and Effect on Osteoblast Adhesion. Tissue Engineering Part a *15*, 3271-3281.

Riveline, D., Zamir, E., Balaban, N.Q., Schwarz, U.S., and Ishizaki, T. (2001). Focal contacts as mechanosensors: externally applied local mechanical force induces growth of focal contacts by an mDia1-dependent ROCK-independent mechanism. Journal of Cell Biology *153*, 1175–1185

Riveline, D., Zamir, E., Balaban, N.Q., Schwarz, U.S., and Ishizaki, T. (2001). Focal contacts as mechanosensors: externally applied local mechanical force induces growth of focal contacts by an mDia1-dependent ROCK-independent mechanism. Journal of Cell Biology *153*, 1175–1185

Ross, S., and Hill, C.S. (2008). How the Smads regulate transcription. International Journal of Biochemical Cell Biology *40*, 383.

Roth, C.B., and Dutcher, J.R. (2005a). Glass transition and chain mobility in thin polymer films. Journal of Electroanalytical ChemistryVolume 584, Issue 1 , 1 October 2005, Pages 13–22, 13–22.

Roth, C.B., and Dutcher, J.R. (2005b). Glass transition and chain mobility in thin polymer films. Journal of Electroanalytical chemistry *584*, 584 513-522

Roumen, P., Kenneth M (2002). Fibronectin at a glance. Cell Science, 3861-3863.

Rozario, T., and DeSimone, D.W. (2010). The extracellular matrix in development and morphogenesis: a dynamic view. Developmental Biology *341*, 126-140.

Ryan , K.J.P., Daniel , Z.C.T.R., Craggs , L.J.L., Parr , T., and Brameld, J.M. (2013). Dose-dependent effects of vitamin D on transdifferentiation of skeletal muscle cells to adipose cells. Journal of Endocrinology *217*, 45-58.

Sabater i Serra, R., León-Boigues, L., Sánchez-L, aosaa, A., Gómez-Estrad, L., Gómez Ribelle, J.L., Salmeron-Sanche, M., and Gallego Ferrer, G. (2016). Role of chemical

crosslinking in material-driven assembly of fibronectin (nano)networks: 2D surfaces and 3D scaffolds. Colloids and Surfaces B: Biointerfaces *148*, 324–332.

Sacco, A., Doyonnas, R., Kraft, P., Vitorovic, S., and Blau, H. (2008). Self-renewal and expansion of single transplanted muscle stem cells. Nature *456*, 502-506.

Salazar , V.S.G., Laura W, and Rosen, V. (2016). BMP signalling in skeletal development, disease and repair. Nature Reviews Endocrinology *12*, 203–221.

Salmeron-Sanchez, M., Rico, P., Moratal, D., Lee, T., Schwarzbauer, J., and Garcia, A. (2011). Role of material-driven fibronectin fibrillogenesis in cell differentiation. Biomaterials *32*, 2099-2105.

Schmidt, J., Suzuki, A., Ueno, N., and Kimelman, D. (1995). Localized BMP-4 mediates dorsal/ventral patterning in the early Xenopus embryo. Developmental Biology *169*, 37-50.

Schmierer, B.H., Caroline S. (2007). TGFβ–SMAD signal transduction: molecular specificity and functional flexibility. Nature Reviews Molecular Cell Biology *8*, 970-982.

Schwab, E.H., Pohl, T.L.M., Haraszti, T., Schwaerzer, G.K., Hiepen, C., Spatz, J.P., Knaus, P., and Cavalcanti-Adam, E.A. (2015). Nanoscale control of surface immobilized BMP-2: toward a quantitative assessment of BMP-mediated signaling events. Nano letters, 1526–1534.

Schwarzbauer, J., and DeSimone, D. (2011). Fibronectins, Their Fibrillogenesis, and In Vivo Functions. Cold Spring Harbor Perspectives in Biology *3*.

Seo , J.H., Kakinoki , S., Inoue , Y., Nam , K., Yamaoka , T., Ishihara , K., Kishida , A., and Yui , N. (2013). The significance of hydrated surface molecular mobility in the control of the morphology of adhering fibroblasts. Biomaterials *34*, 3206 – 3214.

Seo, J.H., and Yui, N. (2013). The effect of molecular mobility of supramolecular polymer surfaces on fibroblast adhesion. Biomaterials *34*, 55-63.

Sharp (2011). Bioactive Scaffolds for Potential Bone Regenerative Medical Applications. In Clinical and Surgical Science (University of Edinburgh).

Shen, B., Bhargav, D., Wei, A., A Williams, L., Tao, H., Ma, D.D.F., and D Diwan, A. (2009). BMP-13 Emerges as a Potential Inhibitor of Bone Formation. International Journal of Biological Science *5*, 192–200.

Shin, H., Jo, S., and Mikos, A.G. (2003). Biomimetic materials for tissue engineering. Biomaterials *24*, 4353–4364

Solchaga , L.A.P., Kitsie J. Welter,Jean F. (2011). Chondrogenic Differentiation of Bone Marrow-Derived Mesenchymal Stem Cells: Tips and Tricks. Methods in Molecular Biology *698*, 253–278. .

Straight, A., Cheung, A., Limouze, J., Chen, I., Westwood, N., Sellers, J., and Mitchison, T. (2003). Dissecting temporal and spatial control of cytokinesis with a myosin II Inhibitor. Science *299*, 1743-1747.

Tonna, E.A., and Cronkite, E.P. (1961). Cellular response to fracture studied with tritiated thymidine. Journal of bone and joint surgery *43*, 352 -362

Truong, H.H., Xiong, J., Ghotra, V.P.S., Nirmala, E., Haazen, L., Dévédec1, S.E.L., Balcioğlu, H.E., He, S., Snaar-Jagalska, B.E., Vreugdenhil, E., *et al.* (2014). β_1 Integrin Inhibition Elicits a Prometastatic Switch Through the TGFβ–miR-200–ZEB Network in E-Cadherin–Positive Triple-Negative Breast Cancer. Science signalling *Vol. 7* 15.

Tsimbouri, P., Gadegaard, N., Burgess, K., White, K., Reynolds, P., Herzyk, P., Oreffo, R., and Dalby, M.J. (2014). Nanotopographical Effects on Mesenchymal Stem Cell Morphology and Phenotype. Journal of Cellular Biochemistry *115*, 380-390.

Urist, M.R. (1965). Bone: Formation by Autoinduction. Science *150*, 893-899.

Virginia Llopis-Hernández, V.M.C., M, González-García, C.C., Z. A Yang, J Tsimbouri, P. M, and García, A.J.D., M. J Salmerón-Sánchez, M (2016). Material-driven fibronectin assembly for high-efficiency presentation of growth factors. Science Advances *2*.

Vogel, V., and Baneyx, G. (2003). The Tissue Engineering Puzzle: A Molecular Perspective. Biochemistry *5*, 441-446.

Walcott S, K.D., Wirtz D, and Sun SX (2011). Nucleation and decay initiation are the stiffness-sensitive phases of focal adhesion maturation. Biophysical Journal *101*, 2919-2928

Walko, G., Castañón, M.J., and Wiche, G. (2015). Molecular architecture and function of the hemidesmosome. Cell Tissue Research *360*, 529–544.

Wallace, W.E., Fischer, D.A., Efimenko, K., Wu, W., and Genzer, J. (2000). Polymer Chain Relaxation: Surface Outpaces Bulk. Macromolecules *34*, 5081-5082.

Wang, P., Thissen, H., and Tsai, W. (2012). The roles of RGD and grooved topography in the adhesion, morphology, and differentiation of C2C12 skeletal myoblasts. Biotechnology and Bioengineering *109*, 2104-2115

Watt, F.M., and Huck, W.T.S. (2013). Role of the extracellular matrix in regulating stem cell fate. Nature Reviews Molecular Cell Biology *14*, 467–473.

Wei, X., Yang, X., Han, Z., Qu, F., Shao, L., and Shi, Y. (2013). Mesenchymal stem cells: a new trend for cell therapy. Acta Pharmacologica Sinica *34*, 747-754.

Williams, D.F. (2008). On the mechanisms of biocompatibility. *29*, 2941–2953.

Wray, J.B. (1964). Acute Changes in Femoral Arterial Blood Flow after Closed Tibial Fracture in Dogs. Journal of Bone and Joint Surgery *46*, 1262 -1268.

Yaffe, D., and Saxel, O. (1977). Serial passaging and differentiation of myogenic cells isolated from mouse muscle. Nature *270*, 725-727.

Yan, Y., *Gong, Y.*, *Guo, Y.*, *Lv, Q.*, *Guo, C.*, *Zhuang, Y.*, *Zhang, Y.*, *Li, R.*, and Zhang, X. (2012). Mechanical strain regulates osteoblast proliferation through integrin-mediated ERK activation. PLoS One *7*, 35709.

Yonghui, Y., O. DLenhoff, A. M (2003). Mobility of

Adsorbed Proteins Studied by Fluorescence Recovery after Photobleaching. Langmuir *19*, 3705–3711.

Young, R.W. (1962). Cell proliferation and specialization during endochondral osteogenesis in young rats. Journal of Cell Biology *14*, 7-370.

Young, T. (1805). An Essay on the Cohesion of Fluids. Philosophical Transactions Royal Society London, 66-87.

Zaidel-Bar, R., Cohen, M., Addadi, L., and Geiger, B. (2004). Hierarchical assembly of cell-matrix adhesion complexes. Biochemical society transactions, 416-420.

Zhang, Yang, Lin, Chen, Ma, Zhou, and Ao (2006). Runx2 overexpression enhances osteoblastic differentiation and mineralization in adipose-derived stem cells in vitro and in vivo. calcified Tissue International *79*.

Zhang , H., and Bradley, A. (1996). Mice deficient for BMP2 are nonviable and have defects in amnion/chorion and cardiac development. Development *122*, 2977-2986.

Zhang, H., and Bradley, A. (1996). Mice deficient for BMP2 are nonviable and have defects in amnion/chorion and cardiac development. . Development *122*, 2977–2986.

Zuk , P.Z., M Mizuno , H Huang , J Futrell , JW, and Katz , A.B., P Lorenz , HP Hedrick , MH (2001). Multilineage cells from human adipose tissue: implications for cell-based therapies. Tissue engineering *7*, 211-228.